PLASTIC FLOW AND FRACTURE OF ZINC SINGLE CRYSTALS

Thesis by

Edwin Jule Stofel

In Partial Fulfillment of the Requirements

For the Degree of

Doctor of Philosophy

California Institute of Technology

Pasadena, California

1962

ACKNOWLEDGEMENTS

The author expresses his appreciation to Professor David S. Wood, who directed this research, for his aid and encouragement. Appreciation also is expressed to Professors Donald S. Clark and Thad Vreeland, Jr. for their valuable suggestions during the course of this research. Thanks are extended to Mr. Benjamin Burke, Mr. Martin Conneally, Mr. Stephen Crow, and Mr. James Wooster for their assistance in specimen preparation and to Mr. Donald Forrest and Mr. Robert Hearn for their assistance in preparing many of the figures in this thesis.

The author is indebted to the Shell Oil Company, the Union Carbide and Carbon Corporation, and the Gillette-PaperMate Company for fellowship grants.

The testing program was conducted under a contract with the United States Army Research Office (Durham), formerly the Office of Ordnance Research, United States Army. Appreciation is extended to this agency for supporting this work.

ABSTRACT

Plastic flow and fracture of zinc single crystals subjected to tension parallel to the hexagonal crystallographic axis, torsion about that axis, and combinations of such tension and torsion have been investigated experimentally at 25°C and -77°C. The results show that under tension alone, cleavage fracture on the basal plane is preceded by plastic elongation in the direction of the hexagonal crystallographic axis. Some evidence is presented which indicates that this newly discovered mode of plastic deformation of zinc crystals probably occurs by slip on $\{\bar{1}\bar{1}22\}$ planes in $\langle 11\bar{2}3\rangle$ directions. The temperature dependence of this mode of plastic deformation is anomalous. The tensile stress required to produce a given amount of plastic strain is greater at 25°C than at -77°C.

The critical resolved shear stress for basal slip, as determined from the results of torsional tests, is increased markedly by prior tensile plastic deformation. The tensile stress-strain relation is raised moderately by prior basal slip.

Fracture was always found to occur by cleavage on a basal plane. The observed combinations of tensile stress and shear stress on the basal plane at fracture are not consistent with predictions based upon current dislocation theories for the initiation of cleavage fracture in zinc. The present results indicate that dislocations having Burgers vectors that do not lie in the basal plane may be of crucial importance in the dislocation mechanism of cleavage fracture of zinc. Such dislocations have not been considered in previously proposed theories.

TABLE OF CONTENTS

LIST OF TABLES

LIST OF FIGURES

FIGURE PAGE

I. INTRODUCTION

One of the most important characteristics of metals is their high mechanical strength. This desirable property has made metals useful as structural material. However, there are factors limiting the strength of metals, and these factors must be understood in order to use metals economically.

The practical strength of metals generally is limited either by the inception of plastic flow or by fracture. Most metals behave in a ductile manner, and their proper structural use normally is determined by the yield stress. However, fracture also plays a role in limiting the useful application of some metals and alloys. A few metals, such as beryllium, normally are so brittle that they cannot be fabricated into proper shapes unless special precautions are taken to avoid fracture. Furthermore, some normally ductile alloys behave in a brittle manner when subjected to conditions of low temperature and large stress rate. Mild steel, one of the most useful of all the modern structural materials, is among the alloys having fracture characteristics that strongly depend upon these variables. A sound understanding of the mechanism of fracture is needed for the proper utilization of these metals.

Much work has already been done on the problem of finding an adequate theory to describe the mechanism of fracture

in metals, but the problem is still far from being satisfactorily solved. Two different approaches to this problem are being tried. The first approach is to study experimentally the existing structural alloys in order to determine the effect different variables have upon the stress required to cause the fracture of these materials. The recent recognition of the importance of brittle fracture phenomena, especially in steel, has made this approach to the general problem of understanding fracture an immediate engineering necessity. The dramatic brittle fracture of steel ships during World War II and the subsequent efforts to provide better ships is only one example of how an increased understanding of the properties of existing structural materials can prevent serious economic loss.

The second approach to the problem of understanding fracture is to search for the basic atomic mechanisms by which cracks are initiated and propagated through metallic crystals. Single crystals often are used as specimens for the experimental study of the atomic mechanisms of fracture. This eliminates the effect of grain boundaries and makes it possible to apply stress along known crystallographic directions. Bicrystals may be used for studying the effects of grain boundaries. The study of the basic atomic mechanisms is less useful for solving immediate engineering problems, but it offers a greater possibility of forming a complete understanding of fracture. The two methods of

studying this problem, therefore, complement one another. This thesis is concerned with the second method and deals with the atomic mechanisms involved in initiating cracks in metallic single crystals.

The first theoretical estimate of the tensile stress required to fracture crystalline solids was based upon the assumption that all atoms within any crystal are always arranged in a precisely regular three-dimensional space lattice. All atoms within such a perfect crystal would contribute equally to the binding energy. Seitz and Read (1) have considered the energy needed to separate two planes of atoms and have derived an expression for the tensile stress required to produce fracture of a perfect crystalline solid. This theoretical fracture stress is expressed by:

$$\sigma_{th} = \sqrt{\frac{E\gamma}{\alpha}} \qquad (1)$$

where σ_{th} is the theoretical fracture stress, E is Young's modulus, γ is the specific energy of the fracture surface, and α is the equilibrium spacing of the atomic centers. Typical values of E, γ , and α are 10^{12} dynes/cm^2, 10^3 ergs/cm^2, and 3×10^{-8} cm, respectively. The theoretical fracture stress based on these values is approximately 10^{11} dyne/cm^2, or about ten per cent of the value of Young's modulus. Zwicky (2) and Born and Furth (3) have made more detailed calculations on ionic crystals and have reached conclusions

similar to those of Seitz and Read. This theoretical fracture stress, however, is several orders of magnitude greater than the stress required to fracture many types of real crystals. Even the strongest commercial alloys fracture at a stress smaller than predicted by this theory. Furthermore, this simple theory is unable to account for the great dependence of fracture behavior upon the variables of temperature and prior plastic deformation shown by many commercial alloys. Therefore, the actual mechanism of fracture must be much more complicated than indicated by this theory.

The problem of fracture of crystalline solids is similar in some respects to the problem of plastic deformation. The simple theory of a perfect crystalline solid provides an explanation for the experimental fact that plastic deformation in a crystal is not isotropic, but takes place along preferential planes. Frendel (4) produced a simple method for estimating the shear strength of a perfect crystal by assuming that along the preferential slip directions in crystals all the atoms in one plane simultaneously slide over the atoms in an adjacent plane. The magnitude of the critical shear stress for plastic deformation is estimated from this theory to be a few per cent of the shear modulus. However, experimental evidence shows that some metal crystals deform plastically at a stress only 10^{-4} as large. This discrepancy between experiment and theory

was resolved when it was recognized that real crystals contain crystallographic imperfections called dislocations. The concept of dislocations has since received a considerable amount of experimental verification (5). This dislocation theory now can be used to explain some of the simple aspects of plastic deformation.

The success of the dislocation theory suggests that real crystals may contain some other form of imperfection that could satisfactorily explain why these crystals fracture at a stress much lower than the theoretical fracture stress of perfect crystals. The presently accepted models of the atomic structure of dislocations readily explain why dislocations move so easily under an applied shear stress, but they also suggest that individual dislocations should have only a minor effect upon fracture strength.

Griffith (6) postulated that small cracks exist in solids and developed a theory that accounts very well for the fracture strength of glass. This theory considers the surface energy needed to increase the length of a crack and also the reduction of the elastic strain energy in the surrounding material when the crack is lengthened. A spontaneous increase of the length of the crack will occur whenever the change of strain energy is larger than the change of surface energy. A given crack length will increase spontaneously only if the strain energy of the surrounding material initially exceeds a critical magnitude. The stress

required to produce this critical elastic strain energy defines the critical stress necessary to cause fracture. This critical stress will, of course, depend upon the initial size of the crack as well as the elastic properties and the specific surface energy of the material. Griffith's equation for the relationship of these parameters is:

$$\sigma_c^2 = K \frac{E\gamma}{c} \qquad (2)$$

where σ_c is the critical fracture stress, E is Young's modulus, γ is the specific surface energy of the crack, and c is the initial length of the crack. K is a numerical factor that depends upon the shape of the crack but is close to unity for all shapes.

The initial size of a crack that can propagate by this mechanism through a metallic crystal subjected to a particular stress can be estimated by applying Griffith's equation. For example, an initial crack length of about 0.002 in. is predicted for steel (7). This prediction is made by measuring the fracture stress and the elastic properties and by estimating the specific surface energy for steel. A crack of this size should be easily visible when viewed through a metallurgical microscope. However, cracks have not been observed in steel unless the metal has been subjected to a stress that is only slightly less than the stress required to produce complete fracture. Furthermore,

the Griffith theory predicts that single crystals of some metals have cracks large enough to be seen by the unaided eye. Cracks of this size have not been observed in the crystals. Such experimental evidence indicates that the Griffith theory does not explain the initiation of fracture in metals, although this theory may be significant in describing the propagation of cracks after they have been formed by other mechanisms.

The experimental results of several investigators have shown that fracture in metals normally is preceded by plastic deformation (8). Plastic deformation occurs in metals even with the case of so-called brittle fracture, although its magnitude is considerably less than the plastic deformation preceding ductile fracture. This deformation suggests that cracks may be initiated by the strong interaction of several dislocations. Zener (9) and Stroh (10) have proposed that cracks may be nucleated by the large tensile stress produced when several edge dislocations operating on the same slip plane are forced against a strong obstacle such as a grain boundary. Stroh (11) also has suggested that cracks may be nucleated by the large stress associated with a small angle tilt boundary that terminates within a crystal. Cottrell (12) has considered how dislocations on intersecting slip planes can interact to form large sessile dislocations, producing large tensile stress in the vicinity of these dislocations.

Deruyttere and Greenough (13) and Gilman (14) have proposed a theory, based upon energy considerations, that predicts a lowering of cleavage strength along any plane containing a large number of dislocations. Undoubtedly, there could be many other models of crack formation based upon the interaction of dislocations. Therefore, experimental results are necessary to determine if any dislocation interaction model can describe the type of fracture that occurs under a particular set of conditions.

The present research program was undertaken to obtain information on the influence of plastic deformation upon the stress required to fracture crystals. Metallic single crystals were tested mechanically to produce plastic deformation and subsequent fracture. The results of these tests will be compared with the results predicted by each of several different theoretical models of fracture initiation.

An experimental study of the relationship between plastic deformation and fracture initiation in a single crystal requires a close control of the mode of plastic deformation. Zinc, a hexagonal close-packed metal, has several advantages for such studies. First, its plastic behavior is anisotropic. This property is typical of hexagonal close-packed crystals in general; but it is particularly pronounced in zinc, where the distance between atoms along the hexagonal axis of symmetry is 13 per cent greater than this distance would be for ideal spherical packing. Slip

occurs primarily on the basal planes, which contain three crystallographically equivalent slip directions. Measurable slip occurs on other planes only if the resolved shear stress on the basal planes is very small (15).

The second advantage of zinc is its low melting temperature. Thus, large single crystals can be produced with inexpensive equipment. The third advantage is the commercial availability of relatively pure zinc, 99.999 per cent purity zinc costing approximately $1.50/lb. The fourth advantage of zinc is the considerable amount of information already available about its behavior. This information provides a good basis for further work.

Zinc crystals fracture readily along basal planes. This fact has long been known (16), but the mechanism controlling this fracture has not been clear. Fracture was once thought to occur whenever the tensile stress normal to the basal plane exceeded a certain critical value (16). This view has now been seriously questioned (13,14) as a result of an accumulation of experimental evidence. The tensile stress normal to the basal planes at the time of fracture has been found to vary widely, depending upon the conditions of the test.

The primary purpose of this investigation is to determine quantitatively if either the resolved shear stress or the slip along a crystallographic plane is an important factor in producing cleavage along this plane. Mechanical

tests were performed on zinc single crystals. The testing method permitted the tensile stress normal to the basal planes and the shear stress along the basal planes to be varied independently. Cylindrical specimens of zinc were prepared for this purpose with the hexagonal axis of the crystal precisely parallel to the axis of the cylinder. Tensile stress normal to the basal planes was produced by applying a tensile force along the direction of the axis of the cylinder. Shear stress along the basal planes was produced by applying a torque about the axis of the cylinder. Measurements of stress and strain were made for each specimen prior to fracture. These measurements provide a quantitative means of determining if any one of the present theoretical fracture models is an adequate basis for describing the initiation of fracture along an active slip plane.

II. SPECIMEN MATERIAL AND PREPARATION

The specimens for this experimental study of fracture were required to have the following properties:

A. Each specimen must consist of a zinc single crystal.

B. Each specimen must have a cylindrical gage section with the axis of the cylinder parallel to the hexagonal axis (c-axis) of the crystal.

C. The crystals should have a high purity.

D. The crystals should have a low density of dislocations.

E. The crystals should be similar enough so that comparisons among the specimens are possible.

Spherically shaped zinc crystals were grown by the Bridgman (19) method in graphite coated pyrex glass molds of the type shown in Fig. 1 (see Appendix F). The procedure used for growing the crystals is described in Appendix A. The zinc for the crystals was obtained from the New Jersey Zinc Company of Palmerton, Pennsylvania. The supplier stated that the zinc was 99.999 per cent pure, with iron (0.0003 per cent) and lead (0.0002 per cent) as the major impurities. A typical crystal is shown in Fig. 2 (see Appendix F).

The test specimens were machined from the spherical, central portion of the crystals. A special saw and a

special lathe were constructed to facilitate the shaping of the specimens. The cutting mechanism of both of these machines consists of chemically etching the crystals by applying nitric acid to those portions of the crystal that are to be removed. Crystals cut by this method remain free of plastic deformation. The details of the operations of these two pieces of equipment are given in Appendices B and C.

A suitable method of gripping the specimens had to be found before the specimens could be tested mechanically. The plastic anisotrophy of zinc crystals precludes the use of any grip that introduces large stress concentrations. For this reason, the conventional methods of gripping polycrystalline specimens, such as threaded ends, cannot be used for single crystals of zinc. A bonding agent that is strong enough to transmit stress uniformly over a large area is needed to prevent sharp stress gradients. Tin-lead solder was found to be the most suitable of the several bonding agents investigated for this purpose. However, under certain stress conditions, the crystals proved to be stronger than the solder bonds. Thus, the range of stress conditions studied in this program was somewhat limited. This was not a serious limitation, however, because significant information was secured within the obtainable stress range.

A complete specimen assembly is represented in Fig. 3. The center section is a single crystal of 99.999 per cent purity zinc. The hour glass shape of the specimen insures that the maximum nominal stress occurs at the center where this stress will not be complicated unduly by the stress inhomogeneities associated with the solder bonds on either end. The central portion of the test specimen is a sufficiently close approximation to a cylinder to satisfy the geometrical requirements of this testing method. A zinc-copper alloy single crystal containing 0.25 per cent copper is soldered to each end of the specimen crystal. These two alloy crystals have very nearly the same coefficient of thermal expansion as the high purity zinc crystal. Thus, neither stress nor strain is introduced in the specimen by the temperature change associated with the soldering process. A threaded steel cylinder is soldered to each alloy crystal. Since the thermal expansion of steel is approximately the same as the thermal expansion of a zinc crystal in the a-directions, only a small stress is introduced thermally at the solder bonds between the steel cylinders and the alloy crystals. The copper content and the large diameter of the two alloy crystals make them sufficiently strong to withstand the stress to which they are subjected without fracturing. All five pieces of the assembly were held in a fixture during the soldering operation to insure their proper alignment. The hexagonal

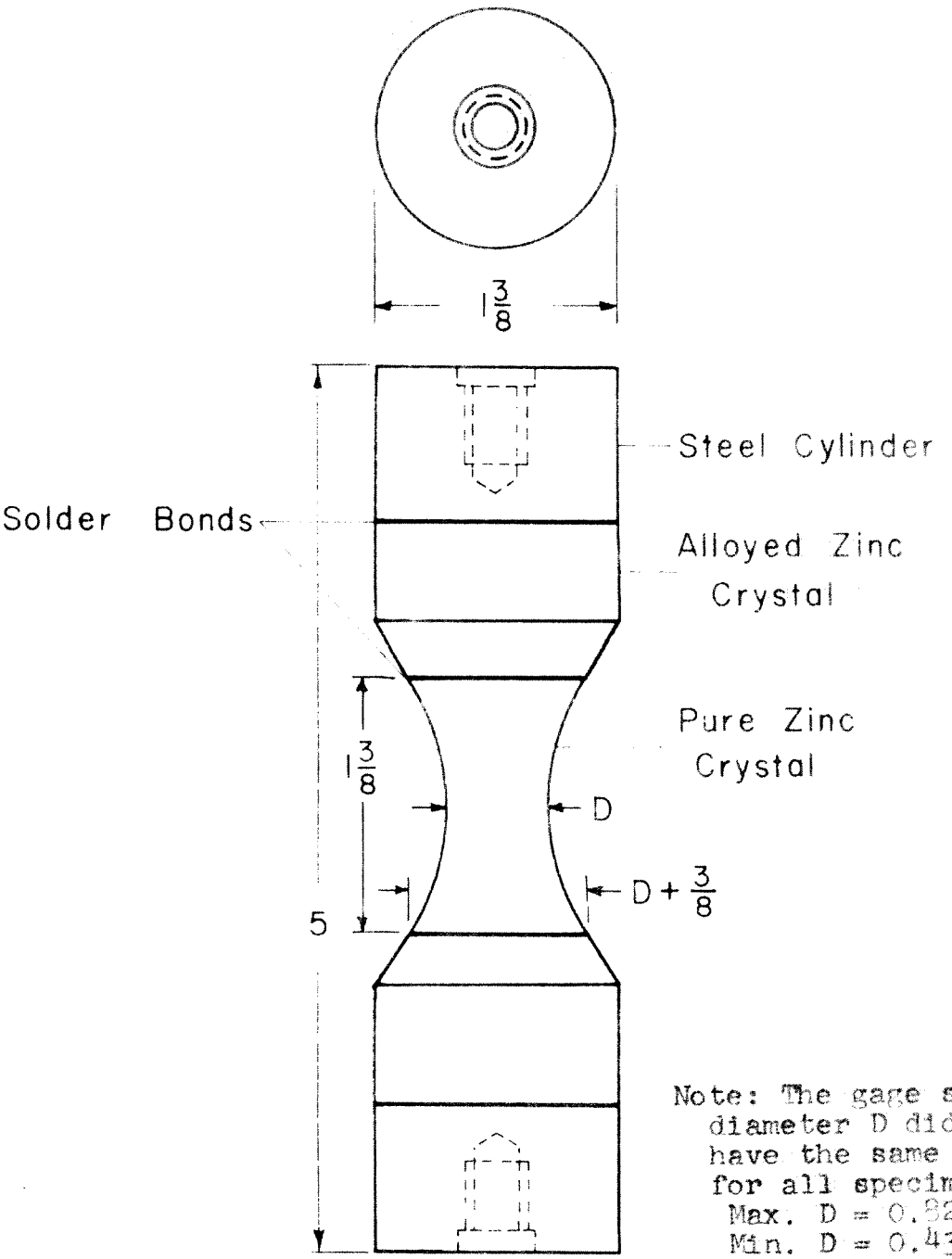

Fig. 3 Complete Specimen Assembly.

axis of each test crystal was parallel to the axis of the specimen assembly to within 1/3 degree. The gage section of each test crystal was concentric with the alignment surfaces on the steel cylinders to within 0.002 in. A detailed description of the method used for preparing the complete specimen assemblies is given in Appendix D.

III. EXPERIMENTAL METHODS

The zinc specimens were tested by applying either tensile or compressive force parallel to the axis of each specimen assembly while independently applying torque about the axis. The tensile strain parallel to the axis of the specimen and the shear strain along the basal planes at the surface of the specimen were measured during the tests.

Description of Equipment

A special testing fixture was manufactured that permits tensile force and torque to be applied independently to a specimen. A schematic drawing of a specimen assembly mounted in the testing fixture is shown in Fig. 4. The upper end of this fixture is attached to the bottom of the moving crosshead of an Instron Tensile Testing Instrument, Model TT-C-L. The lower end of the fixture is fastened to the lower end of the specimen assembly. Tensile stress is produced in the specimen by moving the crosshead and fixture downward while the upper end of the specimen assembly is held in a fixed position. Torque is produced in the specimen assembly by rotating the lower part of the testing fixture about the axis of the assembly. The fixture contains a ball bearing that permits this rotation and a worm and gear drive that controls the amount of rotation.

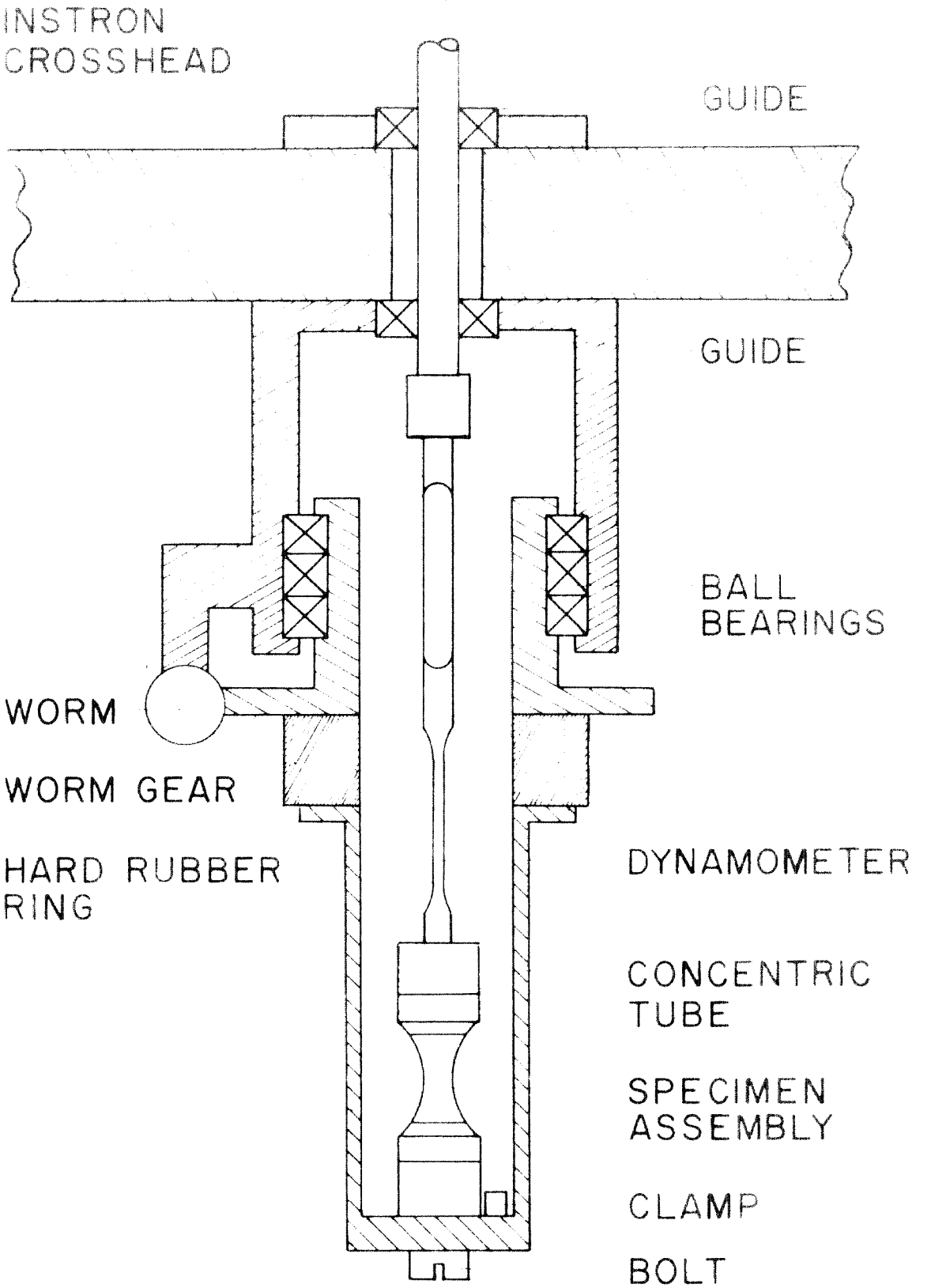

Fig 4 Special Testing Fixture.

A special dynamometer that can measure independently both tensile force and torque is attached to the upper end of the specimen assembly. SR-4 type FA-24-12 foil strain gages are bonded with an epoxy resin to a thin, ribbon-like portion of the dynamometer. These gages are connected electrically to form two Wheatstone bridge circuits that are sensitive to tensile force and torque, respectively. Fig. 5 shows the relative positions of these gages and the circuits of the Wheatstone bridges.

The special dynamometer was calibrated with known tensile forces and known torques. A Baldwin-Lima-Hamilton SR-4 Strain Indicator was connected to each bridge circuit for this calibration. The same indicator was used for measuring torque during the actual tests. The torsional calibration curves for both strain gage bridges are shown in Fig. 6. The tensile calibration curves for both strain gage bridges are shown in Fig. 7. The tensile bridge is relatively insensitive to torque, and the torsional bridge is relatively insensitive to tension. The dynamometer thus provides essentially independent measurements of tension and torsion.

The upper end of the special dynamometer is joined to a standard Instron "F" load cell by a connecting rod. The Instron load cell is bolted rigidly to the frame of the Instron machine. Thus, this load cell, the connecting rod,

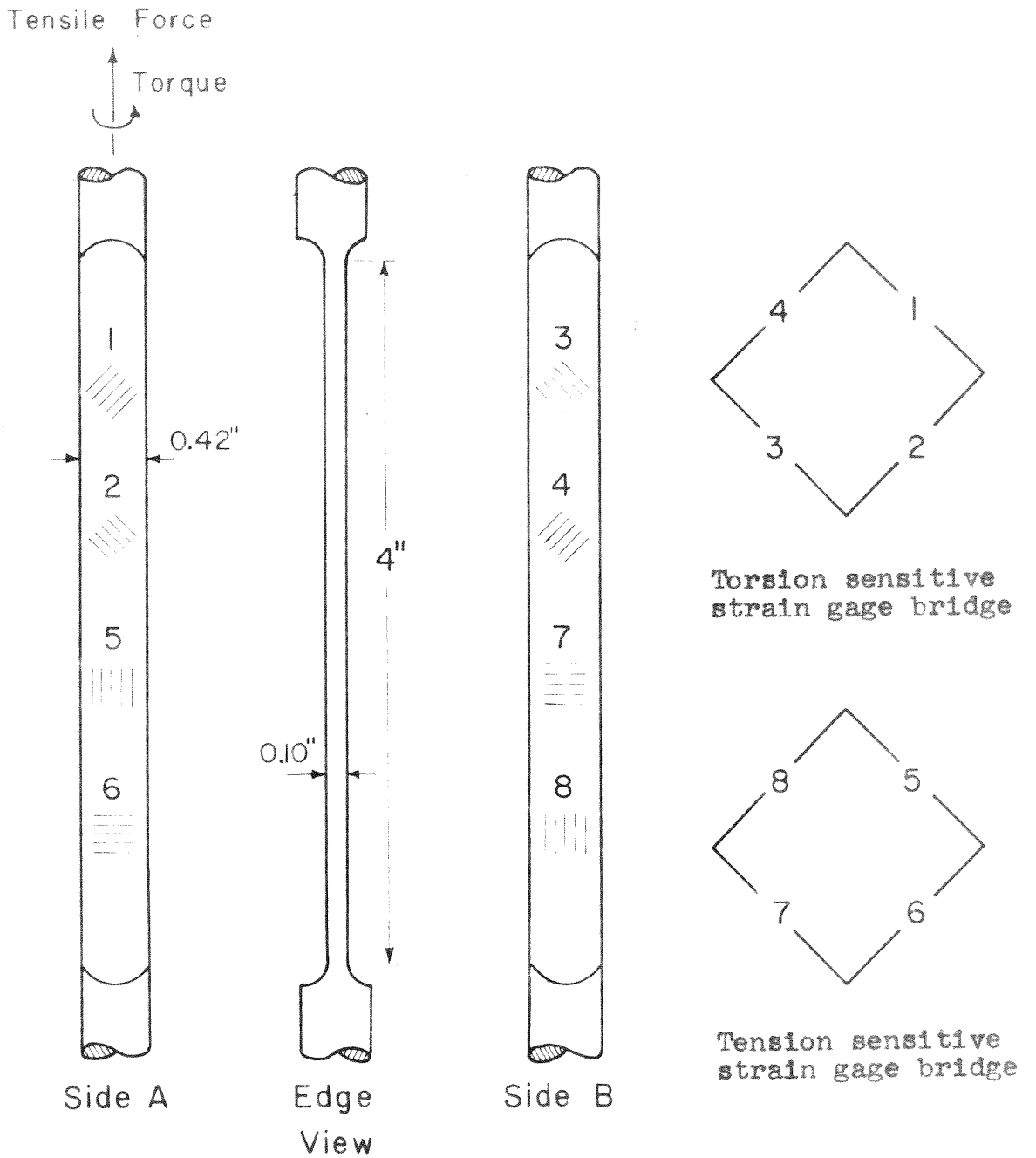

Fig. 5 Arrangement of the SR-4 Strain Gages on the Sensitive Portion of the Tension-Torsion Dynamometer.

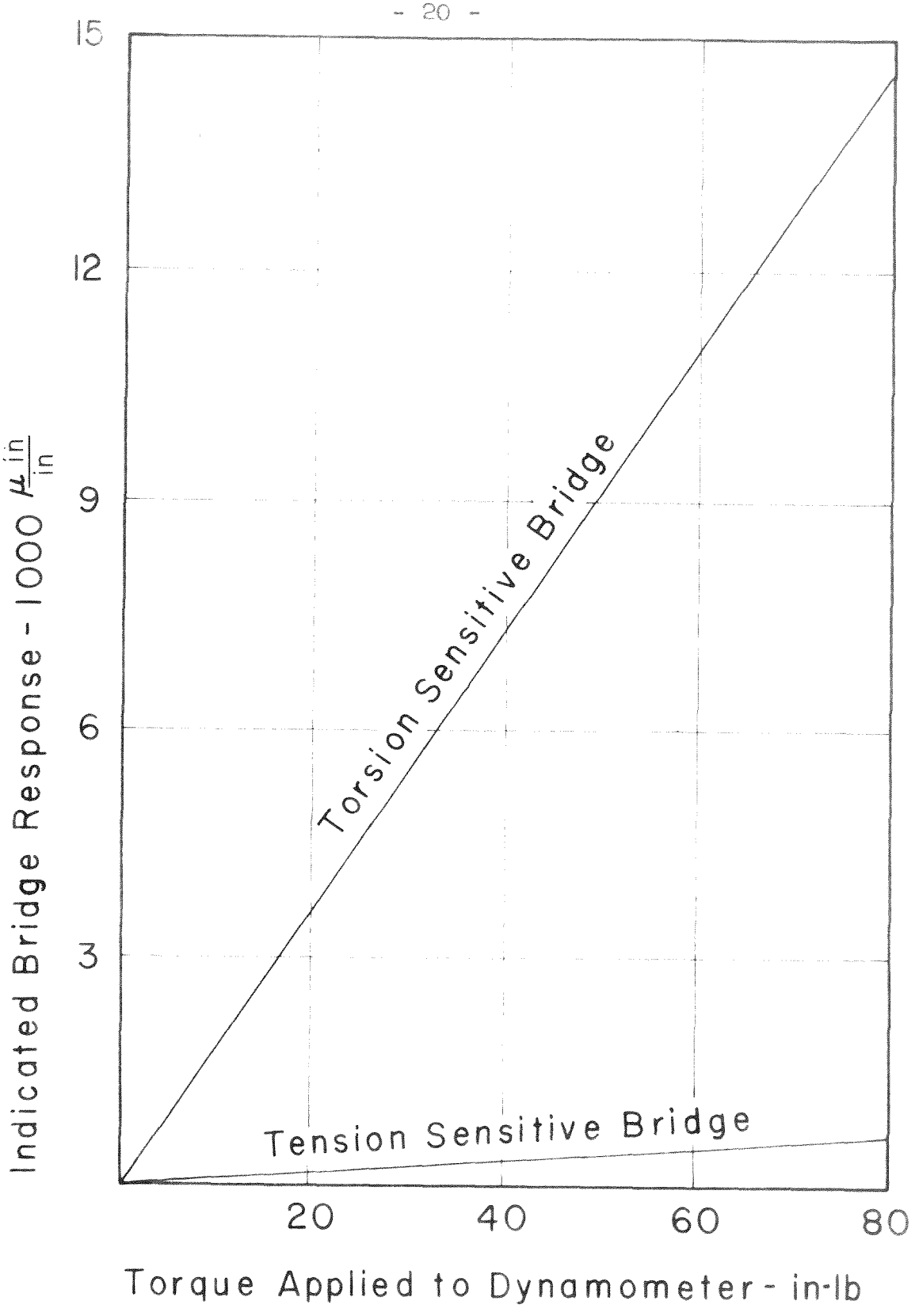

Fig. 6 Torsional Calibration of the Tension-Torsion Dynamometer. The strain gage bridge responses were measured with Baldwin-Lima-Hamilton SR-4 Strain Indicators.

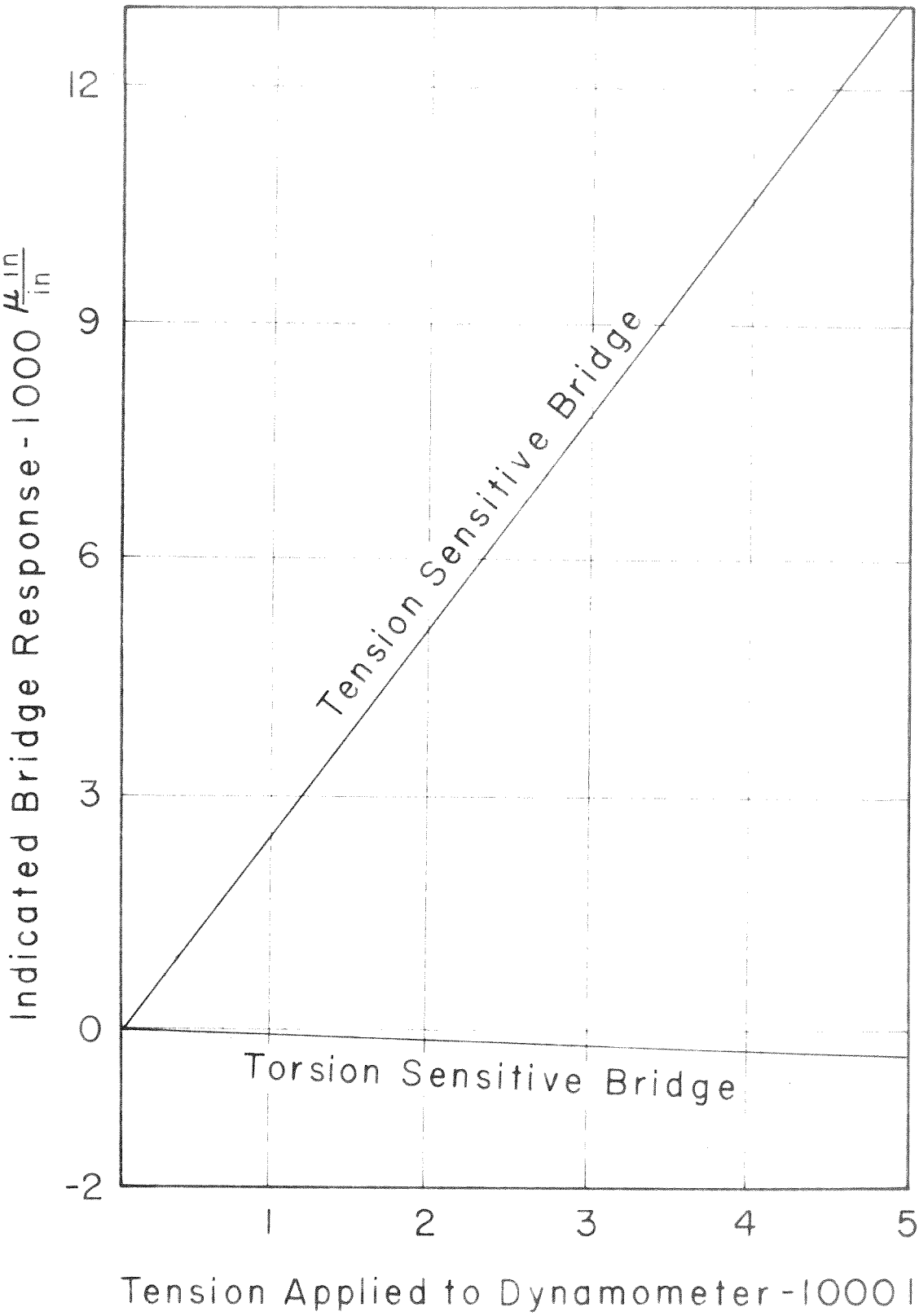

Fig. 7 Tensile Calibration of the Tension-Torsion Dynamometer. The strain gage bridge responses were measured with Baldwin-Lima-Hamilton SR-4 Strain Indicators.

and the special dynamometer do not move during the tests. Two teflon guides accurately determine the lateral position of the connecting rod without interfering with the free vertical movement of the crosshead. These guides introduce only negligible frictional force.

The specimen assembly and testing fixture are aligned to avoid the introduction of bending or lateral forces. The bolt hole in the lower end of the fixture, the two teflon guides, the Instron load cell, and the ball bearing are mutually concentric with the specimen to within 0.003 in., which was the least reading possible with the equipment used for measuring this alignment. The special tension-torsion dynamometer had sufficient flexibility to accomodate any small misalignments of this order without introducing any significant stress in the specimen.

The installation of the specimen assembly into the testing fixture requires that the lower concentric tube of the fixture be removed, thus permitting the upper end of the specimen assembly to be attached to the dynamometer. After the lower end of the fixture is replaced, the specimen and the fixture are fastened together with the bolt and clamp on the lower end of the fixture. The dynamometer and recording instruments are used to measure continuously the force and torque acting upon the specimen while it is being installed in the fixture. These installation operations normally can be done with enough care to prevent damage of the specimen.

Determination of Stress and Strain

Measurements were made during the tests to determine the tensile or compressive stress normal to the basal planes and the shear stress along the basal planes. The tensile or compressive strain normal to the basal planes and the shear strain along the planes also were measured. In addition, the total elongation of the specimen assembly and the relative rotation between the ends about the axis of the specimen assembly were determined. The measurements for determining stress and strain were made throughout the entire test of each specimen to provide a complete history of plastic deformation prior to fracture.

A. Tensile and Compressive Stress and Strain

The tensile or compressive stress normal to the basal planes was computed by dividing the measured axial force by the smallest cross-sectional area of the specimen. The axial force was measured and recorded by the standard Instron "F" load cell and the X-Y Speedomax recorder of the Instron Testing Instrument. The diameter of each specimen was measured with a micrometer before testing. The computed values of the stress normal to the basal planes are estimated to be within 5 per cent of the actual values. This estimate is based on possible errors in the measurements of force and diameter and on possible misalignment of the specimen assembly. The sensitivity of

the force measuring system allowed the detection of a change in stress of 10 lb/in.^{2} in the range from 0 to 1,000 lb/in.^{2}; a change of 25 lb/in.^{2} in the range from 1,000 to 5,000 lb/in.^{2}; and a change in 50 lb/in.^{2} in the range from 5,000 to 10,000 lb/in.^{2}

The tensile or compressive strain parallel to the hexagonal axis of a test crystal was measured by two SR-4 type A-18 wire resistance strain gages bonded to the surface of the crystal. These gages were located on diametrically opposite sides of the narrowest part of the specimen and were oriented with their sensitive directions parallel to the hexagonal axis of the crystal. The change in the resistance of these gages was measured and recorded with the strain recording system incorporated within the Instron testing machine. The measured values of tensile strain are estimated to be within 6 per cent of the actual strain. A change in strain of 10^{-5}in./in. could be detected.

The axial elongation that occurred in a specimen assembly during a test was determined from the movement of the crosshead as indicated by the crosshead position indicating system incorporated within the Instron testing machine. A change of the crosshead position of 0.0005 in. could be detected. The indicated crosshead movement is the sum of the elongation of the specimen assembly and the elastic elongation of the testing equipment.

The elastic elongation of the equipment was determined as a function of the tensile force by separate experiments in which a 1 3/8 in. diameter steel cylinder was substituted for the zinc specimen. The crosshead movement in these calibration experiments was equal to the total elastic elongation of the testing equipment, because the steel cylinder was so rigid that its elongation could be neglected. The elongation of a specimen assembly during its test was determined by subtracting this calibrated value of the elastic deformation of the testing equipment from the total crosshead movement.

Fig. 8 shows the elastic elongation of the testing equipment as a function of the tensile force. The dotted curves indicate the limits of reproducibility. This variation can probably be attributed to the presence of the hard rubber thermal insulating ring. This uncertainty in the elongation of the testing equipment could introduce a maximum error of 30 per cent into the computed value of the elongation of the specimen assembly.

B. Shear Stress and Strain

The shear stress and the shear strain within a plastically deformed cylindrical torsional specimen having a circular cross-section vary along the radius. However, a shear stress versus shear strain curve that is characteristic of the specimen material in pure shear can be derived

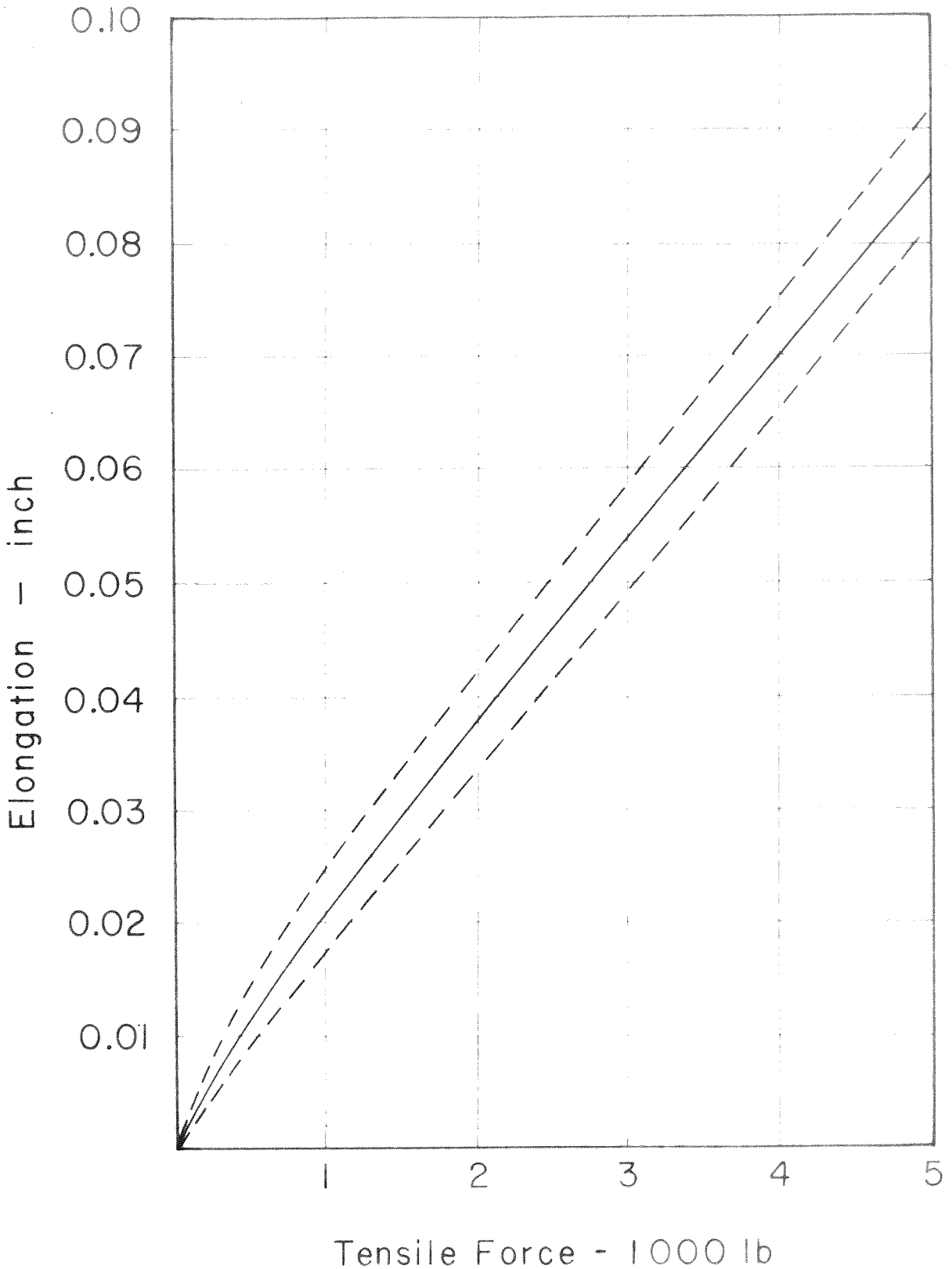

Fig. 8 The Total Elastic Elongation of the Testing Equipment as a Function of the Tensile Force. Dotted curves indicate the limits of reproducibility.

from the experimentally determined relationship of torque versus shear strain at the surface of the specimen. The shear stress, τ , at the maximum radius, r, is computed from the measured applied torque, T, and the shear strain at the surface, γ , by means of the following relationship (20):

$$\tau = \frac{1}{2\pi r^3}\left(\gamma \frac{dT}{d\gamma} + 3\ T\right) \qquad (3)$$

The slope $\frac{dT}{d\gamma}$ of the experimental torque versus shear strain relationship is determined graphically. The shear stress versus shear strain curves for slip along basal planes reported in this thesis were derived by means of equation 3.

The torque was measured by the special tension-torsion dynamometer combined with a Baldin-Lima-Hamilton SR-4 Strain Indicator. These measured values of torque are estimated to be within 3 per cent of the actual values. The accuracy of these measurements was limited primarily by the accuracy of the calibration of the dynamometer. The equipment could detect a change in torque as small as 0.05 in. lb.

The shear strain at the surface of the specimens was measured by a combination of three methods. The first method employed two SR-4 type A-18 wire resistance strain gages bonded to the surface. The active direction of each of these gages was oriented at 45 degrees with respect to the basal planes in such a manner that the shear strain

produced tension in one gage and compression in the other. The change in the resistance of these gages was measured with a Baldwin-Lima-Hamilton Strain Indicator. These gages were a sensitive means for detecting the initiation of plastic deformation. A change of strain of 10^{-5} in./in. could be detected by the gages. The SR-4 strain gages were found to impede slip along the basal planes during the torsional tests. The influence of the strain gages was so large at strains greater than 0.001 in./in. that the strain measured by the gages was not representative of the strain occurring throughout the whole crystal. Because of this influence, SR-4 gages were used only to detect small strain and were not used on every specimen.

The second method of measuring shear strain along the basal planes employed a thin pencil line on the surface of the specimen parallel to the hexagonal axis of the crystal. The shear strain at the surface of a specimen during a torsional test was determined by measuring the angle of rotation of the line. A protractor was fastened near the specimen for measuring this rotation. This method of measuring the shear strain had the advantages of not introducing any surface restraint and of determining how the shear strain was distributed along the length of the specimen. A change of angle of one degree could be measured with this method. This change corresponds to a shear strain of 2 per cent.

The third method for determining shear strain involved measuring the relative rotation between the two ends of the specimen. The measurement was made with a graduated scale incorporated in the worm and gear drive system that was used for twisting the specimen. The relative rotation was measured to within 0.1 degree. The shear strain at the surface of the specimen was calculated from the measured relative rotation by using the effective gage length of the specimen as determined by the change in the position of the pencil line. The precision of the relative rotation measurements made it possible to determine the shape of the torque versus shear strain curve with a greater degree of precision than could be obtained from the measurements of the slope of the pencil line alone. This was especially useful at small strains, where the slope of the torque versus strain curve changes rapidly.

Description of Tests

Four different types of mechanical tests were performed upon the zinc specimens in this investigation. The first type consisted of applying a torque to a crystal without applying any tensile force. The second type of tests was made by applying a tensile or compressive force normal to the basal planes without applying any torque. The tests of the third type were performed by first applying a tensile stress normal to the basal planes and then applying a

torsional shear stress along the basal planes while the tensile stress was still present. The fourth type consisted of tests in which plastic shear strain was introduced along the basal planes by applying a torque, the torque was removed, and then a tensile stress was applied normal to the basal planes.

The first test, in which torque was applied to the specimen without the application of tensile force, was designed to determine if basal cleavage would occur when a zinc crystal is subjected only to a pure torsion about its hexagonal axis. Torque was applied to a specimen (number 29) at a rate of increase of 0.02 in.lb/min. This torque rate produced within the elastic range of deformation, a shear stress rate of 0.4 lb/in.^{2}min on the basal planes at the surface of the specimen. The rate of torque increase was changed to 0.11 in.lb/min after a maximum shear strain of 100 per cent had been obtained. This rate of torque increase was maintained until a maximum shear strain of 350 per cent was obtained.

Another specimen (number 33) was tested in torsion to determine how slip on basal planes could be influenced by the presence of SR-4 wire resistance strain gages on the surface of the crystal. A pencil line parallel to the hexagonal axis was placed on the surface of the crystal. Two SR-4 gages oriented to measure shear strain on the basal planes were cemented to the center of the narrowest

portion of the specimen. Torque was applied about the hexagonal axis of the crystal to produce a maximum shear strain of 32 per cent along the basal planes. This maximum shear strain occurred in a portion of the crystal that was not covered by the strain gages. The torque then was removed. The SR-4 strain gages were removed with acetone, and another pencil line was placed on the surface of the crystal parallel to the axis of the specimen. Torque again was applied about the hexagonal axis of the crystal to produce a maximum shear strain of 32 per cent along the basal planes. The maximum shear strain produced by this second torque application occurred in the narrow portion of the crystal that previously had been covered by strain gages.

The second series of tests was conducted to study the tensile plastic and fracture behaviors of zinc crystals in the absence of shear strain along the basal planes. Tensile stress was applied normal to the basal planes of each of five specimens (numbers 11, 12, 27a, 37, and 49) at a rate of increase of 300 lb/in.^{2} min until either the specimen or a solder bond failed by fracture. None of the specimens except number 27a had been tested previously. Specimen number 27a had previously been subjected (as specimen number 27) to a tensile stress of 2,000 lb/in.^{2} and a shear stress on the basal planes great enough to produce a maximum shear strain of 1 per cent. After its initial test, but before being used in the present series, this crystal

was annealed at 380° C (40° C below its melting point) for four hours.

The tensile strain in the axial direction was measured by SR-4 gages throughout each test of this series. Specimen number 11 had four additional SR-4 gages appropriately oriented to measure two orthogonal components of the shear strain on the basal planes. These shear strains were recorded with the aid of two Baldwin-Lima-Hamilton Strain Indicators.

The tests of this second series were conducted at two different temperatures. Specimens numbers 11, 12, and 37 were tested at room temperature (25°C). Specimens numbers 27a and 49 were tested at the sublimation temperature of dry ice (-77°C).

Each of the low temperature tests was performed with the specimen and the lower end of the testing fixture immersed in a mixture of dry ice and ordinary cleaning solvent. The transient thermally induced stress was minimized by first surrounding the specimen with the liquid at room temperature and then slowly cooling it to testing temperature by periodically placing small pieces of dry ice into the container of liquid.

The third series of tests was conducted to determine if zinc crystals will fracture readily at a small tensile stress if slip occurs on the basal planes while the tensile stress is present. Tensile stress was applied normal to

the basal planes of each of eight specimens (numbers 21, 26, 27, 28, 29, 30, 44, and 46) at a rate of increase of 300 lb/in.^{2} min until the tensile stress reached a predetermined magnitude. The movement of the crosshead of the Instron machine then was stopped so that the tensile stress remained at approximately this magnitude. Next, a torque was applied to the specimen. The magnitude of the torque was increased until either the specimen fractured or the magnitude of the shear strain on the basal planes became large enough to indicate that this strain was not very effective in promoting fracture. Two specimens (numbers 26 and 30) did not fracture when subjected to large shear strain (38 per cent, and 32 per cent, respectively). When this large strain was reached, the rotational movement of the lower part of the testing fixture was stopped so that the torque remained at an approximately constant value. The tensile stress then was increased until the specimen failed at the solder bond.

Two of the specimens (numbers 26 and 44) used in this third test series had been subjected to special treatments prior to their tests. Specimen number 26 had been subjected to a tensile stress of 1,000 lb/in.^{2} and then placed in an oven at 130° C for 16 hours prior to its tensile and torsional test. Specimen number 44 had been subjected to a compressive stress of 2,500 lb/in.^{2} normal to the basal planes prior to its tensile and torsional tests. The other

six specimens used in this test series had not been deformed in any manner prior to their tests.

Four specimens (number 21, 27, 28, and 29) had SR-4 gages for measuring tensile strains normal to the basal planes and other SR-4 gages for measuring shear strain along the basal planes. Three specimens (number 26, 44, and 46) had SR-4 gages for measuring tensile strain only. Specimen number 30 did not have any gages on its surface.

The fourth series of tests was conducted to determine if zinc crystals will fracture readily at a small tensile stress if slip on the basal planes occurs prior to the application of the tensile stress. Different amounts of plastic shear strain along the basal planes were introduced into six specimens (numbers 34, 35, 38, 39, 41, and 45) by applying torque about the axis of the specimens. The torque was removed and tensile stress was applied normal to the basal planes at a rate of 300 $lb/in.^2$ min until the solder bonds failed by fracture.

Two of the specimens (numbers 34 and 35) had SR-4 gages on their surfaces during the introduction of shear strain on the basal planes. These gages remained on the surface during the tensile test. The other four specimens (numbers 38, 39, 41, and 45) did not have any gages on their surfaces during the introduction of shear strain on the basal planes. SR-4 gages for measuring tensile strain normal to the basal planes were placed on these

four specimens after the application of torque but before the application of tensile stress.

Table I summarizes the test procedure employed for each specimen and gives the diameter of the minimum cross-section for each specimen. The number of small angle tilt boundaries within each crystal also is listed.

TABLE I

Summary of Test Procedures

Specimen Number	Gage Diameter (in.)	Basal Tilt Boundary	Test Procedure
Test Series I			
20	0.675	Unknown	Torque increased until a maximum basal shear strain of 350% was obtained.
33	0.610	One of 0.07°	Torque increased until a maximum basal shear strain of 32% occurred in portion of crystal not covered by SR-4 strain gages. Torque removed. Strain gages removed. Torque increased again until a maximum basal shear strain of 32% occurred in portion of crystal previously covered by SR-4 gages.
Test Series II			
11	0.652	Unknown	Tensile stress increased until 1,300 lb/in.^{2} obtained. Tensile strain and two orthogonal components of basal shear strain were measured with SR-4 gages.
12	0.828	Unknown	Tensile stress increased until solder bond failed. Tensile strain measured with SR-4 gages.
37	0.547	None >0.02°	Tensile stress increased until solder bond failed. Tensile strain measured with SR-4 gages.
27a	0.591	One of 0.7°	Tensile stress increased until crystal fractured. Tensile strain measured with SR-4 gages. Test temperature -77°C.
49	0.596	One of 0.08°	Tensile stress increased until crystal fractured. Tensile strain measured with SR-4 gages. Test temperature -77°C.

TABLE I (Continued)

Specimen Number	Gage Diameter (in.)	Basal Tilt Boundary	Test Procedure
Test Series III			
21	0.663	Unknown	Tensile stress of 1,000 lb/in.^{2} applied. Torque increased until crystal fractured. Tensile strain and torsional strain measured with SR-4 gages.
27	0.619	One of 0.7°	Tensile stress of 2,000 lb/in.^{2} applied. Torque increased until a solder bond failed. Tensile strain and torsional strain measured with SR-4 gages.
28	0.631	One each 0.4°,0.3°	Tensile stress of 3,100 lb/in.^{2} applied. Torque increased until crystal fractured. Tensile strain and torsional strain measured with SR-4 gages.
29	0.628	None >0.02°	Tensile stress of 4,200 lb/in.^{2} applied. Torque increased until crystal fractured. Tensile strain and torsional strain measured with SR-4 gages.
30	0.577	Three of 0.02°	Tensile stress of 4,200 lb/in.^{2} applied. Torque increased until a maximum basal shear strain of 32% was reached. Torque left on crystal while tensile stress further increased until solder bond fractured. No SR-4 gages used on this specimen.
44	0.606	None >0.02°	Compressive stress of 2,500 lb/in.^{2} was applied and then removed. Tensile stress of 4,200 lb/in.^{2} applied. Torque increased until specimen fractured. Compressive and tensile strains only measured with SR-4 gages.

TABLE I (Continued)

Specimen Number	Gage Diameter (in.)	Basal Tilt Boundary	Test Procedure
46	0.431	One of 0.12^{o}	Tensile stress of 4,100 lb/in.^{2} applied. Torque increased until specimen fractured. Tensile strain only measured with SR-4 gages.
26	0.615	None $>0.02^{o}$	Tensile stress of 5,100 lb/in.^{2} applied. Torque increased until a maximum basal shear strain of 38% was reached. Torque left on crystal while tensile stress was further increased until solder bond fractured. Tensile strain only measured with SR-4 gages. These SR-4 gages became loose after small shear strain occurred during torque application.
Test Series IV			
34	0.585	None $>0.02^{o}$	Torque increased until a maximum basal shear strain of 8% was obtained. Torque removed. Tension increased until solder bond fractured. SR-4 gages present during torque application. Tensile strain not measured.
35	0.586	None >0.02	Torque increased until a maximum basal shear strain of 45% was obtained. Torque removed. Tension increased until solder bond fractured. SR-4 gages present during torque application. Tensile strain not measured.
38	0.617	One of 0.3^{o}	Torque increased until a maximum basal shear strain of 14% was obtained. Torque removed. Axially oriented SR-4 gages cemented to specimen. Tension increased until solder bond fractured. Tensile strain measured with SR-4 gages.

TABLE I (Continued)

Specimen Number	Gage Diameter (in.)	Basal Tilt Boundary	Test Procedure
39	0.626	One of 0.03°	Torque increased until a maximum basal shear strain of 4% was obtained. Torque removed. Axially oriented SR-4 gages cemented to specimen. Tension increased until solder bond fractured. Tensile strain measured with SR-4 gages.
41	0.437	One each 0.16°, 0.12°	Torque increased until a maximum basal shear strain of 4% was obtained. Torque removed. Axially oriented SR-4 gages cemented to specimen. Tension increased until solder bond fractured. Tensile strain measured with SR-4 gages.
45	0.434	One each 0.18°, 0.12°	Torque increased until a maximum basal shear strain of 50% was obtained. Torque removed. Axially oriented SR-4 gages cemented to specimen. Tension increased until solder bond fractured. Tensile strain measured with SR-4 gages.

IV. EXPERIMENTAL RESULTS

All specimens deformed plastically before fracturing. Thus, quantitative information on both the plastic and the fracture behavior of zinc single crystals was obtained from these tests.

Plastic Deformation

A. Slip on Basal Planes

Slip on the basal planes of zinc crystals was investigated by applying torque about the hexagonal axis of the crystals. A gradual increase in the torque applied to a crystal produced only small shear strain until the shear stress resolved on the basal planes reached a critical value. Large strain occurred with only a very small rate of strain hardening after this critical shear stress was exceeded. This typical behavior is shown in Fig. 9 (specimen number 45). The critical shear stress is defined as the shear stress required to produce the first measurable deviation from a linear stress versus strain relationship.

Several previously undeformed specimens (numbers 34, 35, 38, 39, 41, and 45) were subjected to pure torsion during the first stage of their tests. Fig. 10 shows the stress versus strain curves for shear strain along the basal planes of these specimens. The specimen numbers are shown at the end of their respective curves. None of these specimens fractured during the torsional tests.

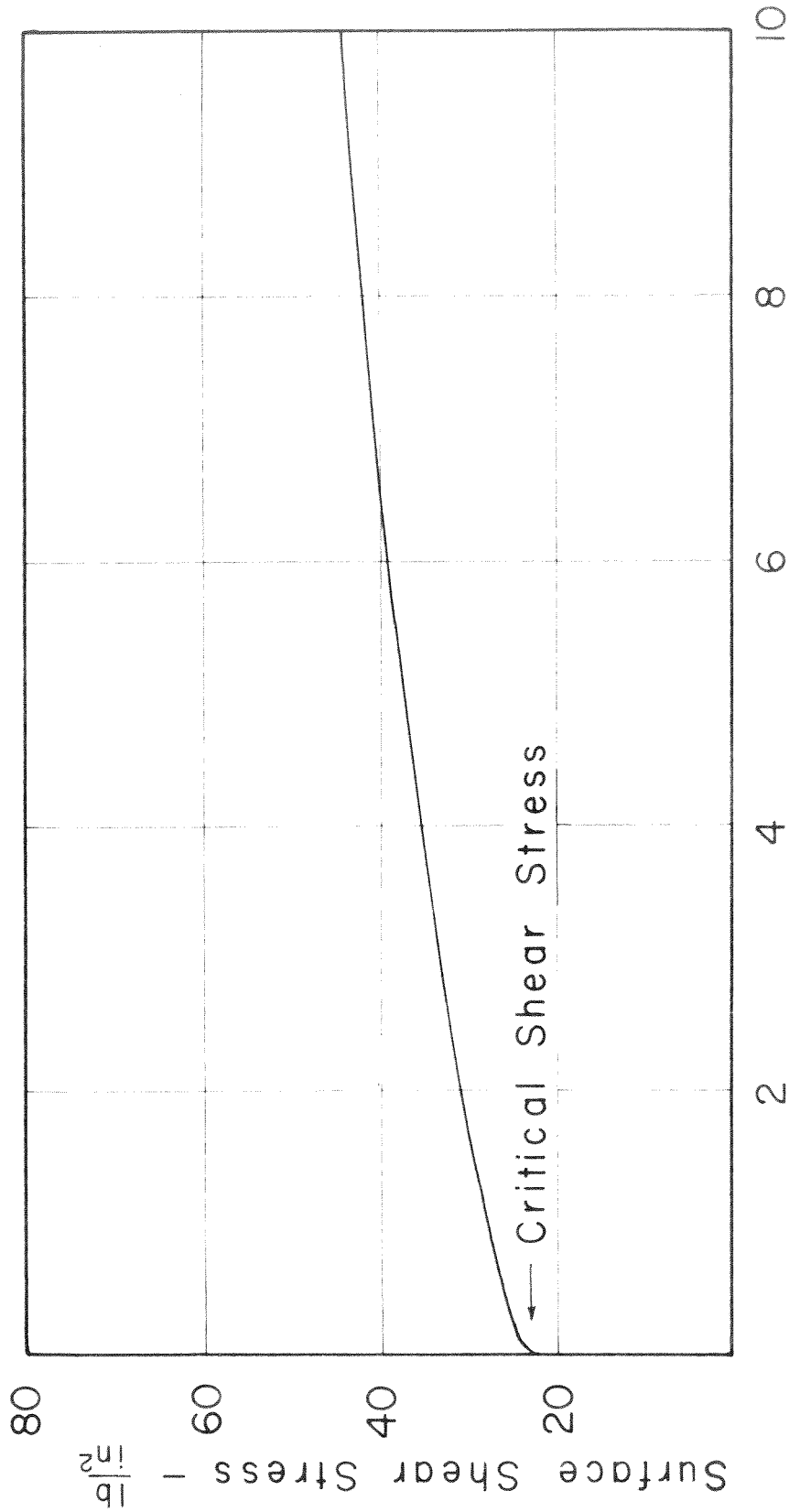

Fig. 9 Typical Curve of Shear Stress vs. Shear Strain for Slip on the Basal Planes of Zinc.

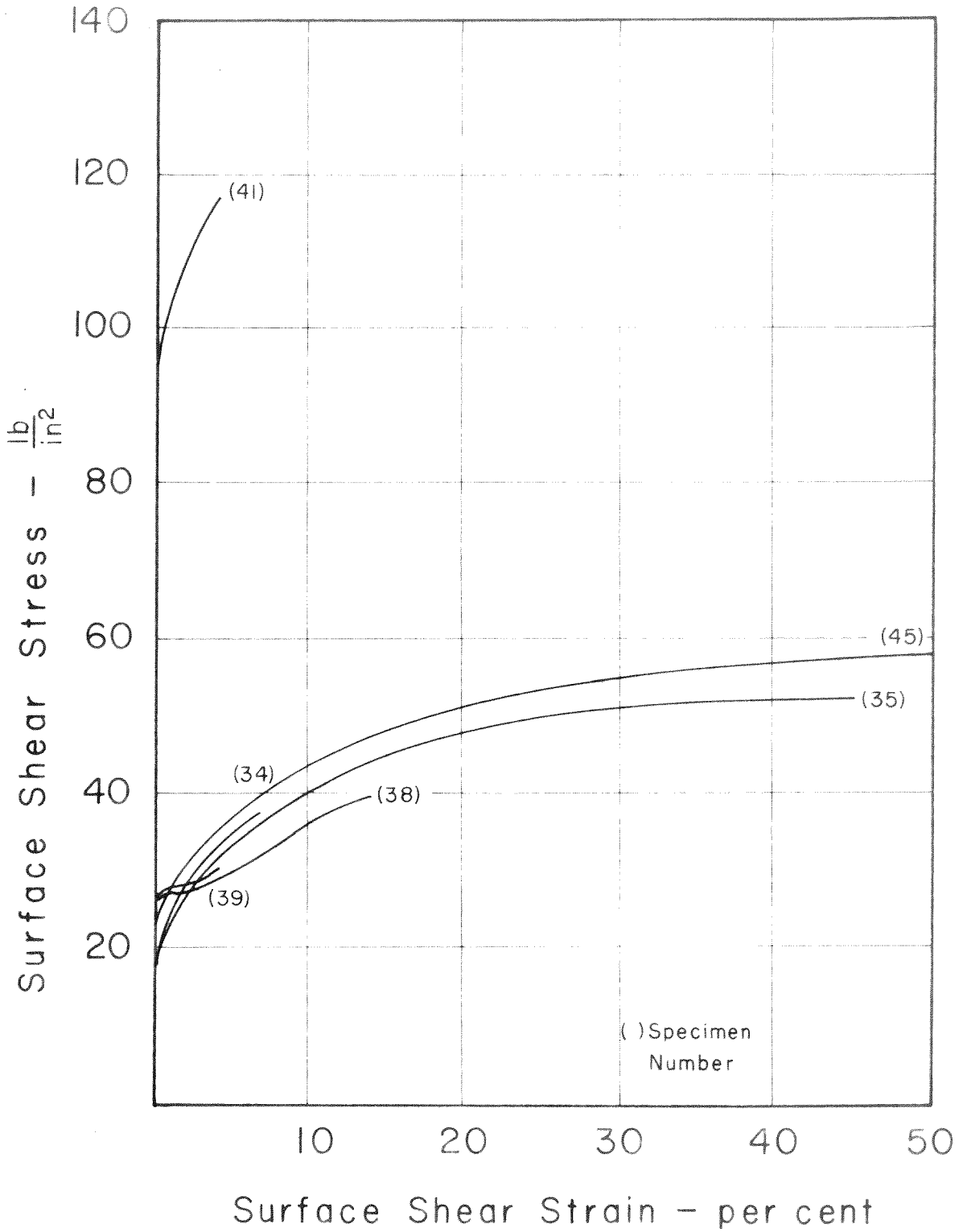

Fig. 10 Curves of Shear Stress vs. Shear Strain for Slip on the Basal Planes of Several Previously Undeformed Zinc Crystals.

Table II contains a summary of information pertaining to these torsional tests. The critical shear stress for all specimens except specimen number 41 is within the range from 17 to 27 lb/in.^{2}. The relatively large magnitude of the critical shear stress for specimen number 41 indicates that this specimen probably was accidentally strained in tension while being placed into the testing fixture. The effect that such tension has upon the critical shear stress for basal slip will be described later in this section.

The rate of strain hardening for slip on the basal planes of zinc increases markedly for shear strains exceeding 150 per cent. This behavior for a torsional test at 25°C is shown in Fig. 11 (specimen number 20). Fracture was not initiated by the large shear stress produced on the basal planes in this manner.

SR-4 wire resistance strain gages bonded to the surface of a zinc crystal were found to impede slip along the basal planes. A specimen (number 33) was twice subjected to torque: first with SR-4 gages on the surface and then without gages on the surface. Fig. 12 summarizes the shear strain behavior produced by each of the two torque applications. The first application of torque produced only a small (1.6 per cent) shear strain under the strain gages. A large (32 per cent) shear strain occurred in that portion of the crystal that was not covered by the gages, even though

TABLE II

A Summary of Information Pertaining to the Basal Shear Strain Behavior of Previously Undeformed Zinc Specimens Subjected to Pure Torsion

Specimen Number	Gage Diam. (in.)	Number of Tilt Boundaries	Stress Rate to Critical Stress ($lb/in.^2$ min)	Critical Basal Shear Stress ($lb/in.^2$)	Maximum Basal Shear Stress ($lb/in.^2$)	Maximum Basal Shear Strain (per cent)
34	0.585	None $>0.02^\circ$	4.5	17	38	8
35	0.586	None $>0.02^\circ$	2.8	17	53	45
38	0.617	One of 0.03°	1.8	27	40	14
39	0.626	One of 0.03°	1.5	27	30	4
41	0.437	One each 0.16°, 0.12°	6.4	94	117	4
45	0.434	One each 0.18°, 0.12°	5.5	23	58	50

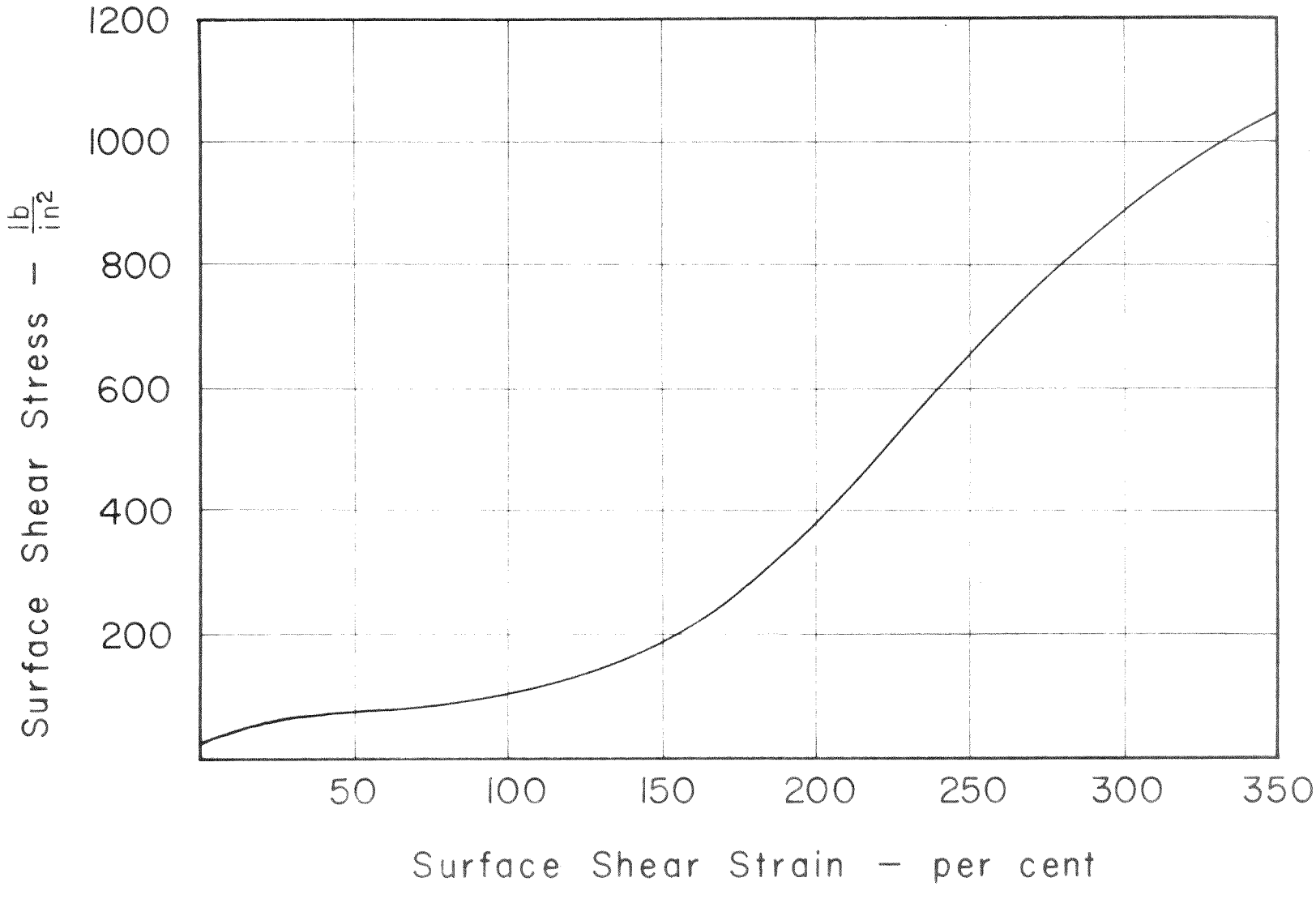

Fig. 11 Curve of Shear Stress vs. Shear Strain for Slip on the Basal Planes of Specimen Number 20.

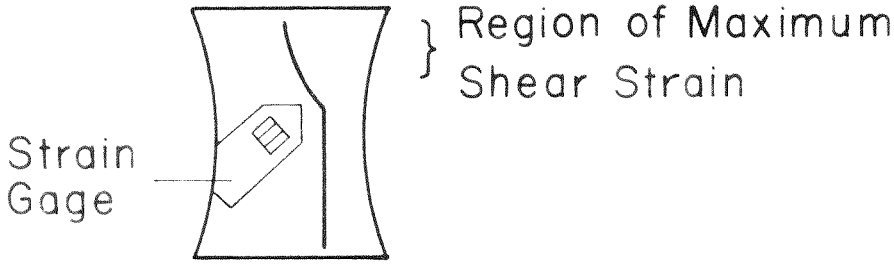

Shear Strain Indicated by Pencil Line on Specimen with SR-4 Strain Gages.

Shear Strain Indicated by Pencil Line on Specimen without SR-4 Strain Gages.

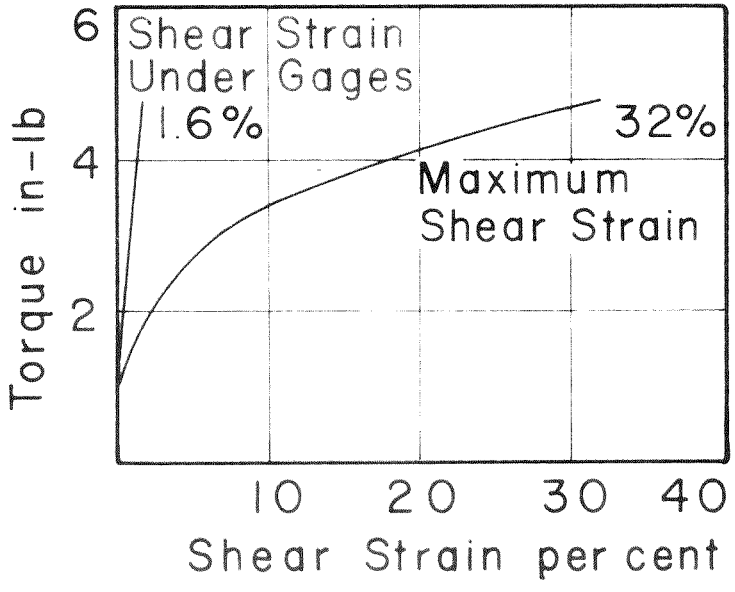

Curves of Torque vs. Shear Strain for Specimen with SR-4 Strain Gages.

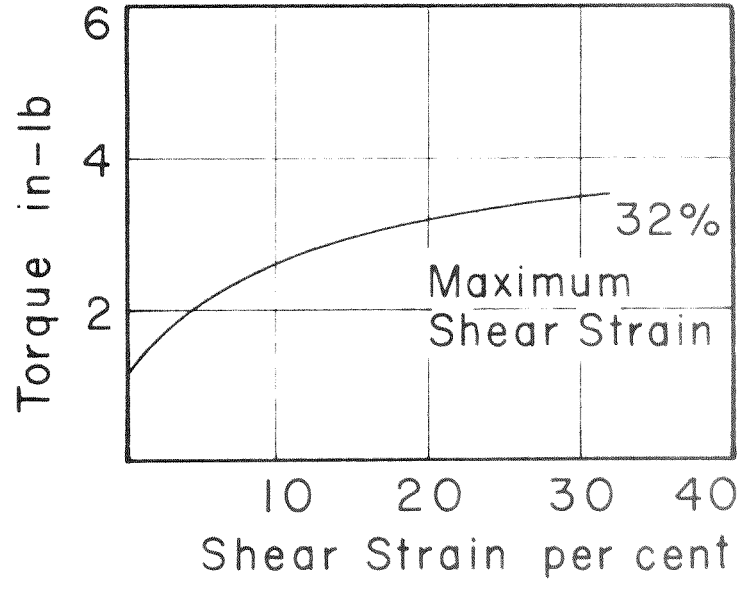

Curve of Torque vs. Shear Strain for Specimen without SR-4 Strain Gages.

Fig. 12 The Effect of SR-4 Strain Gages on the Distribution of Shear Strain on the Basal Planes.

the shear stress was larger in the narrow portion of the crystal under the gages. The second application of torque, when no strain gages were present, produced the maximum shear strain in the narrow, central portion of the crystal that previously had been covered by the strain gages.

B. Plastic Strain Parallel to the Hexagonal Crystal Axis. (25°C)

The tensile tests performed during this investigation also provided information on the plastic behavior of zinc crystals. A small but measurable amount of plastic elongation parallel to the hexagonal axis of a crystal was detected by axially oriented SR-4 strain gages when a tensile stress was applied normal to the basal planes at a temperature of 25°C. This typical behavior is shown in Fig. 13 (specimen number 12).

The axially oriented SR-4 strain gages used to detect the strain were sensitive both to axial elongation and to slip along the basal planes. The change in resistance of these gages was directly proportional to the strain parallel to the hexagonal axis of the crystal and was proportional to the square of the shear strain along the basal planes. Thus, a strain of 10^{-4} in./in. indicated by the gages could be due either to a tensile strain of 10^{-4} in./in. parallel to the hexagonal axis or to a shear strain of 10^{-2} in./in. along the basal planes.

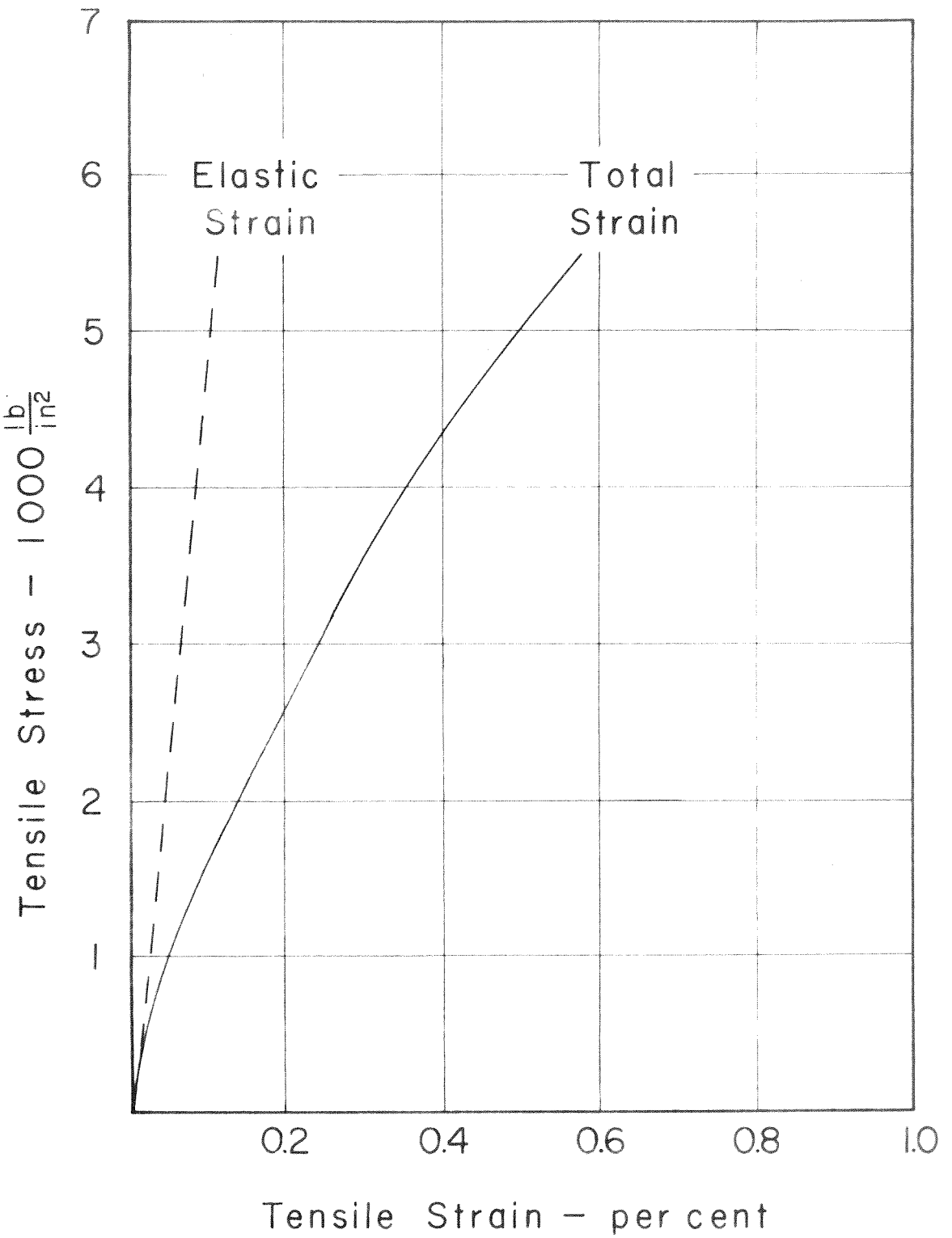

Fig. 13 Typical Curve of Stress vs. Strain for Stress Normal to the Basal Planes of Zinc.

Three independent measurements established that the plastic strain indicated (Fig. 13) by the axially oriented SR-4 strain gages was not due to slip along the basal planes. The first of these measurements was made during the tensile test of specimen number 11. Three pairs of SR-4 strain gages were bonded to the surface of this specimen. The positions of these gages and their three respective Wheatstone bridge circuits are shown in Fig. 14. The active gages of bridge A are parallel to the hexagonal axis of the crystal and thus are sensitive both to axial elongation and to the square of shear strain along the basal planes. The active gages of each of bridges B and C are at 45 degrees to the basal planes. These two bridges are sensitive to two orthogonal components of shear strain along the basal planes but are not sensitive to elongation parallel to the hexagonal axis. A tensile stress was applied parallel to the axis of the specimen, and simultaneous measurements of strain were made with all three bridge circuits. Fig. 15 shows the strain indicated by each bridge circuit (A, B, and C) as a function of the tensile stress applied parallel to the axis of the specimen. The dotted curve in Fig. 15 shows the square root of the plastic strain indicated by bridge circuit A. If basal slip had been

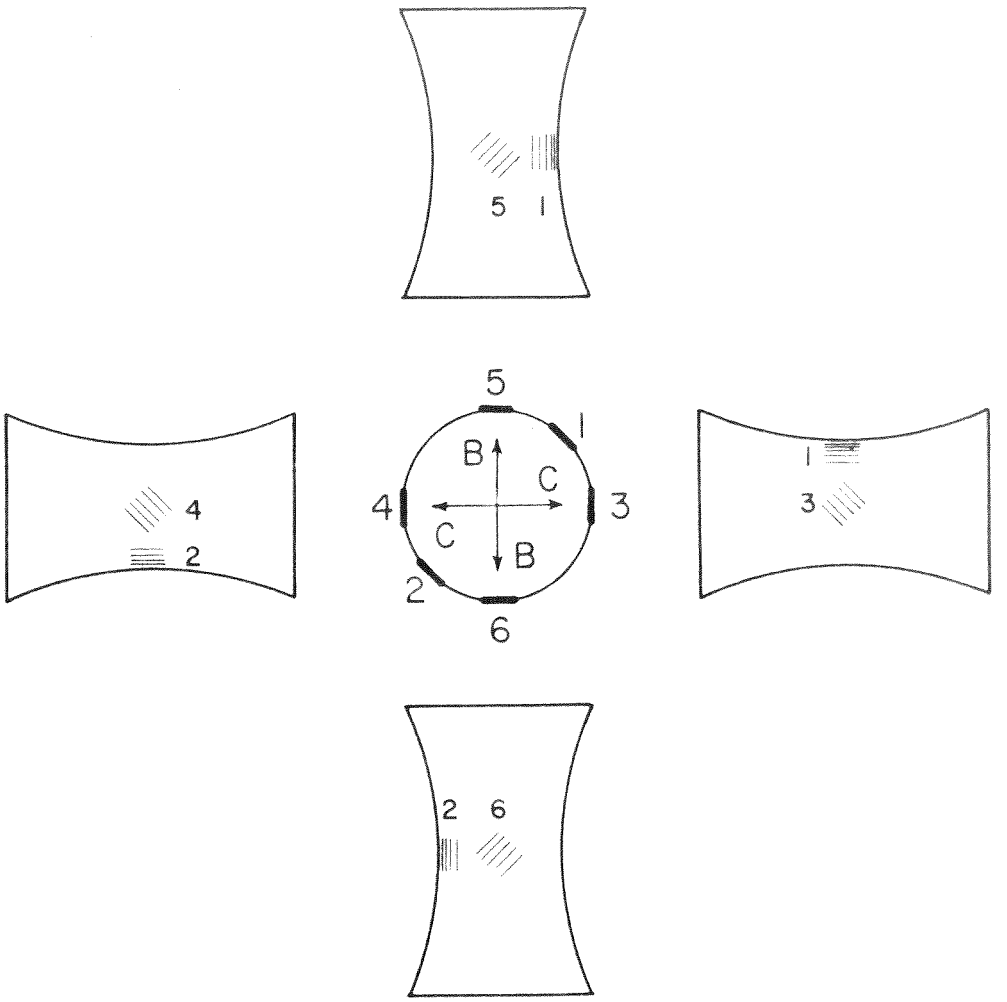

Positions of SR-4 Strain Gages on Specimen Number 11

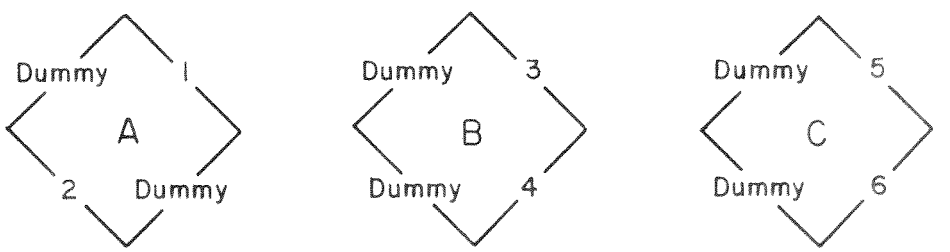

Sensitive to Tensile Strain Parallel to Axis

Sensitive to Shear Strain in B direction

Sensitive to Shear Strain in C direction

Fig. 14 The positions of the SR-4 Strain Gages and their three Wheatstone Bridge Circuits for Specimen Number 11.

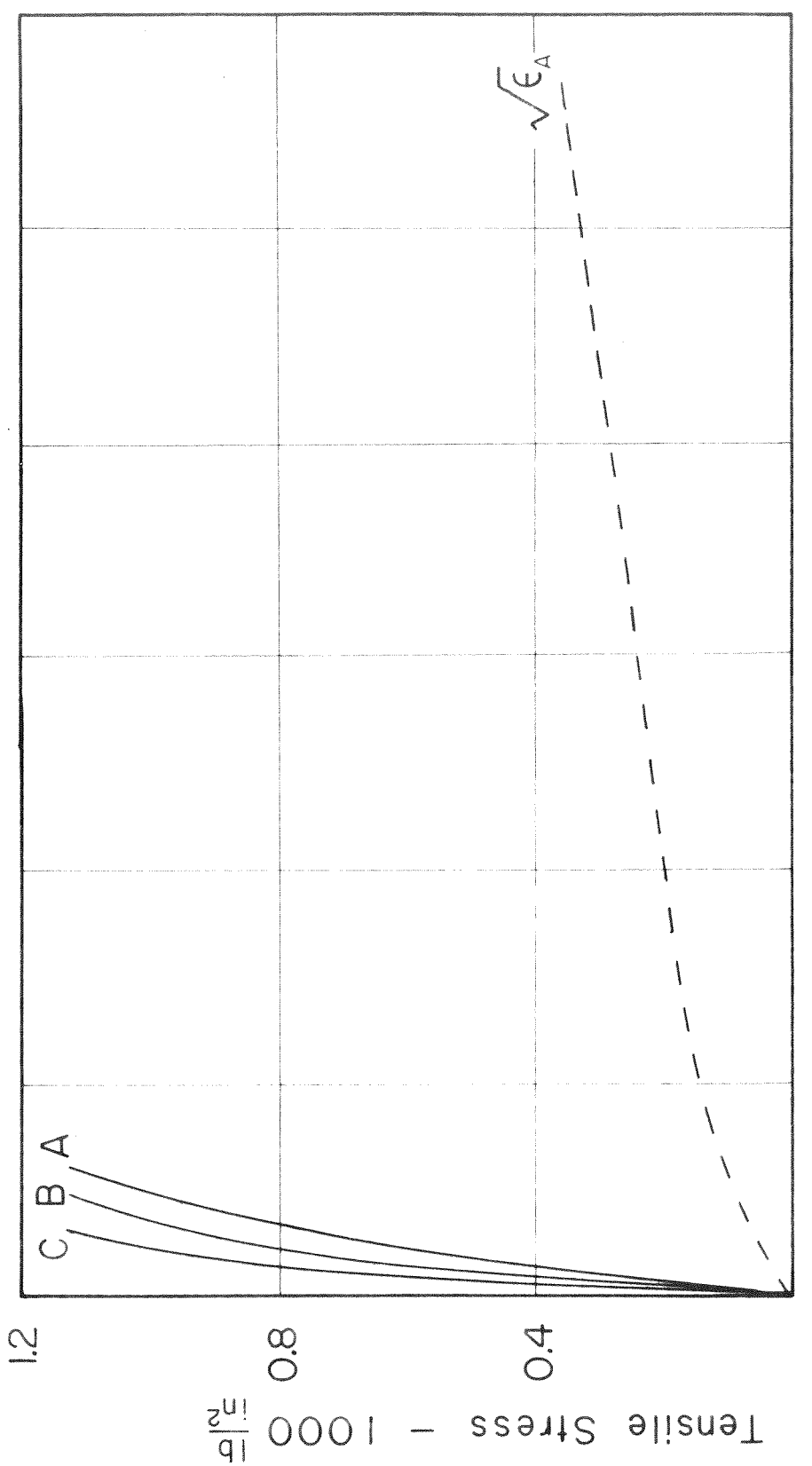

Fig. 15 Strain Indicated by the three SR-4 Strain Gage Bridges on Specimen Number 11. The dotted curve is the square root of the strain indicated by bridge A.

an important factor in producing the plastic strain detected by the gages parallel to the hexagonal axis (bridge circuit A), then the strains indicated by the gages that were at 45 degrees to the basal planes (bridge circuits B and C) would have been approximately equal to the square root (the dotted curve in Fig. 15) of the strain indicated by bridge circuit A. Actually, the strains indicated by bridge circuits B and C for any given stress were slightly less than the strain indicated by bridge circuit A.

The second indication that slip on the basal planes was not an important factor in producing plastic deformation during the purely tensile tests was provided by the test of specimen number 37. The SR-4 strain gages oriented parallel to the axis of this specimen indicated a plastic strain of 0.007 in./in. at the end of the tensile test. If slip along basal planes had been the important factor in producing the plastic strain indicated by the gages, a shear strain of 0.085 in./in. along the basal planes would have been required. A shear strain of this magnitude would have laterally displaced the ends of the specimen assembly by 0.065 in., assuming that the shear strain along the basal planes occurred over a 3/4 in. length of the test crystal. The actual amount of this lateral displacement was measured after the tensile test was completed; and this displacement was found to be less than 0.01 in., which was the limit of the sensitivity of the method used for measuring this displacement.

The third indication that the plastic strain detected by the axially oriented SR-4 strain gages was due to a true axial elongation and not due to slip on basal planes also was provided by the test of specimen number 37. Both the strain indicated by the SR-4 strain gages and the total elongation of the specimen assembly were measured during this test. Fig. 16 shows both the stress versus strain and the stress versus elongation relationships for this tensile test. The specimen assembly elongated approximately 0.012 in. during the tensile test. This elongation in the axial direction could not have been caused by slip on basal planes, for the basal planes were perpendicular to the axis of the specimen.

These three independent measurements of the strain produced during tensile tests show that zinc crystals can elongate plastically in a direction parallel to the hexagonal axis. This plastic elongation implies that slip can occur along non-basal planes with a slip direction that is neither parallel to the basal planes nor parallel to the hexagonal axis.

An investigation was made to determine the slip plane and the slip direction of this newly detected non-basal slip system. Table III lists four possible non-basal slip systems and the important characteristics of each. This information indicates that the most likely non-basal slip system is composed of the $\{\bar{1}\bar{1}22\}$ planes and the $\langle 11\bar{2}3\rangle$ slip

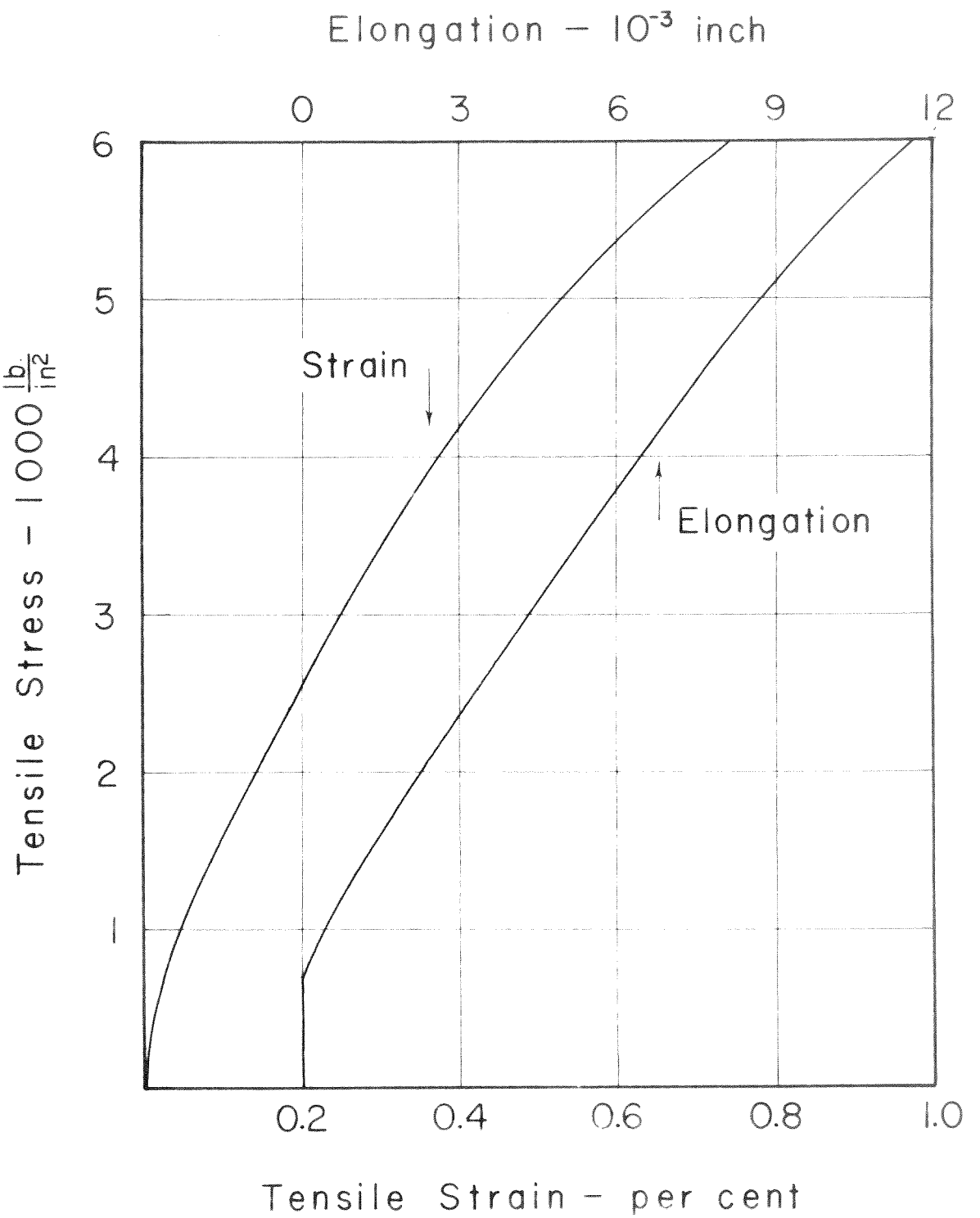

Fig. 16 Curves of Stress vs. Strain and Stress vs. Total Elongation of the Specimen for Stress Normal to the Basal Planes of Zinc.

TABLE III

Possible Non-Basal Slip Systems for Zinc

Slip System	Resolved Shear Stress	Length of Burgers Vector
$[11\bar{2}3]$ $(\bar{1}\bar{1}22)$	0.417 T*	2.11 a+
$[11\bar{2}3]$ $(\bar{1}011)$	0.373 T	2.11 a
$[10\bar{1}1]$ $(\bar{1}012)$	0.499 T	2.54 a
$[10\bar{1}1]$ $(\bar{1}011)$	0.309 T	2.54 a

*T is the tensile stress normal to the basal planes.

+a is the atomic spacing in the close-packed direction.

---

directions. The $\langle 11\bar{2}3\rangle$ directions are relatively close-packed, and the shear stress resolved along the $\{\bar{1}\bar{1}22\}$ planes in the $\langle 11\bar{2}3\rangle$ directions is relatively large. This slip system may be further favored by the possibility of the $1/3[11\bar{2}3]$ dislocations forming extended dislocations by the dislocation reaction of:

$$1/3[11\bar{2}3] \longrightarrow 1/6[20\bar{2}3] + 1/6[02\bar{2}3] \qquad (4)$$

The surfaces of several specimens were examined with the aid of a microscope after the specimens had been deformed plastically by tensile stress, but non-basal slip lines were not detected. The lack of well defined non-basal slip lines is not surprising, however, because slip

would be expected to take place simultaneously on all six of the $\{11\bar{2}2\}$ planes when a tensile stress is applied normal to the basal plane. The strain thus would be expected to form very short, intersecting slip lines that would not be easily visible.

Slip lines indicating slip on non-basal planes were discovered on the exposed basal planes of some zinc crystals that were cleaved at the temperature of liquid nitrogen. These surfaces had been formed as part of the operation of producing specimens from the zinc single crystals (see Appendix D). Cleavage was produced by driving a needle into the zinc crystal. The stresses produced by the needle were not distributed homogeneously. Thus, slip occurred on only a few non-basal planes, and slip lines were plainly visible in the most severely deformed regions. Photomicrographos of two of these regions are shown in Figs. 17 and 18 (see Appendix F). The sides of the small hexagon beside each photomicrograph are parallel to the close-packed $\langle 11\bar{2}0\rangle$ directions. Two edges of a cleavage step are shown in the lower and right hand portions of Fig. 17. These edges are parallel to the close-packed directions. The other heavy lines parallel to the close-packed $\langle 11\bar{2}0\rangle$ directions are probably traces of the intersection of twin planes with the exposed basal planes. Fine lines, parallel to the $\langle 10\bar{1}0\rangle$ directions, also are present. These lines are most easily explained as slip lines resulting from the intersection of

$\langle 11\bar{2}3 \rangle \{\bar{1}\bar{1}22\}$ type slip systems with the basal planes. The small dots randomly distributed throughout both photomicrographs are merely water stains caused by the frost that formed on the basal surfaces after the crystals were cleaved at liquid nitrogen temperature and are not related to the microstructure of the crystal.

Chemical etching techniques recently developed at the California Institute of Technology (21) can produce small pits on the surface of 99.999 per cent purity zinc. Fig. 19 (see Appendix F) shows a few of these pits on a basal surface. The hexagonal shape of the pits is the result of the six-fold symmetry of the zinc crystal. The bright lines in the pits are perpendicular to the close-packed directions. This etching technique was used to investigate the character of the non-basal slip that occurred in a zinc specimen (number 29) subjected to a tensile stress of 4,200 lb/in.^{2} normal to the basal planes. After the tensile test was completed, the specimen was cooled to a temperature of -196°C; and a surface parallel to the basal planes was produced by cleaving the crystal with a needle. This surface then was etched to produce pits. Fig. 20 (see Appendix F) shows a portion of this etched surface. The dark, straight lines parallel to the close-packed directions probably are the traces of the intersection of twin planes with the exposed basal plane. The wavy line in the lower portion of the

photomicrograph is a scratch made by the needle. Several linear arrays of pits parallel to the $\langle 10\bar{1}0 \rangle$ directions are visible, suggesting that the pits represent dislocations lying on $\{\bar{1}\bar{1}22\}$ type planes. The linear arrays probably were produced by the non-homogeneously distributed stress associated with the cleaving of the crystal. Another surface parallel to the basal planes was produced from the same specimen by cutting the crystal with the special acid saw (see Appendix B). This method of producing a surface did not introduce any plastic deformation. Consequently, the zinc at the surface is representative of the zinc crystal plastically deformed by a tensile stress of 4,200 lb/in.^{2} normal to the basal planes. This surface also was etched to produce pits. Fig. 21 (see Appendix F) shows a portion of this etched surface. The pits are distributed randomly, suggesting that the tensile stress applied normal to the basal planes produced slip on all six possible $\{\bar{1}\bar{1}22\}$ planes without favoring any particular one.

The detection of a plastic elongation in a direction parallel to the hexagonal axis of zinc and the observation of slip lines and linear arrays of etch pits on the basal surface of zinc suggest that slip can occur on a non-basal slip system, probably along the $\{\bar{1}\bar{1}22\}$ planes in the $\langle 11\bar{2}3 \rangle$ directions. Several characteristics of this non-basal slip system were determined during this investigation. The initial portion of the tests of several specimens (numbers 12,

21, 27, 28, 29, 37, and 46) consisted of applying a tensile stress normal to the basal planes of zinc crystals that had not previously been strained in any way. The tensile stress versus strain curves for these specimens are so similar that they all lie within a narrow band. The limits of this band are shown in Fig. 22. The individual stress versus strain curves overlap each other, making it impractical to include each curve in Fig. 22. The characteristics of the individual tensile tests are listed in Table IV. None of these purely tensile tests at 25°C produced fracture in the narrow gage section of the specimens.

A compressive stress normal to the basal planes of zinc also produces slip on non-basal planes. A specimen (number 44) was subjected to a compressive stress of 2,500 lb/in.^{2}. The stress then was removed. The compressive stress versus strain curve for this specimen is shown in Fig. 23. A typical tensile stress versus strain curve (specimen number 37) also is shown in Fig. 23 for comparison purposes. Both curves are shown as having positive values, thus facilitating comparison. The strain behavior in compression is quite similar to the strain behavior in tension. The surface of specimen number 44 was examined with a low power binocular microscope after the completion of the compressive test. Evidence of twinning was not observed. The lack of abrupt changes in the compressive stress versus strain curve also indicates that twinning did not occur.

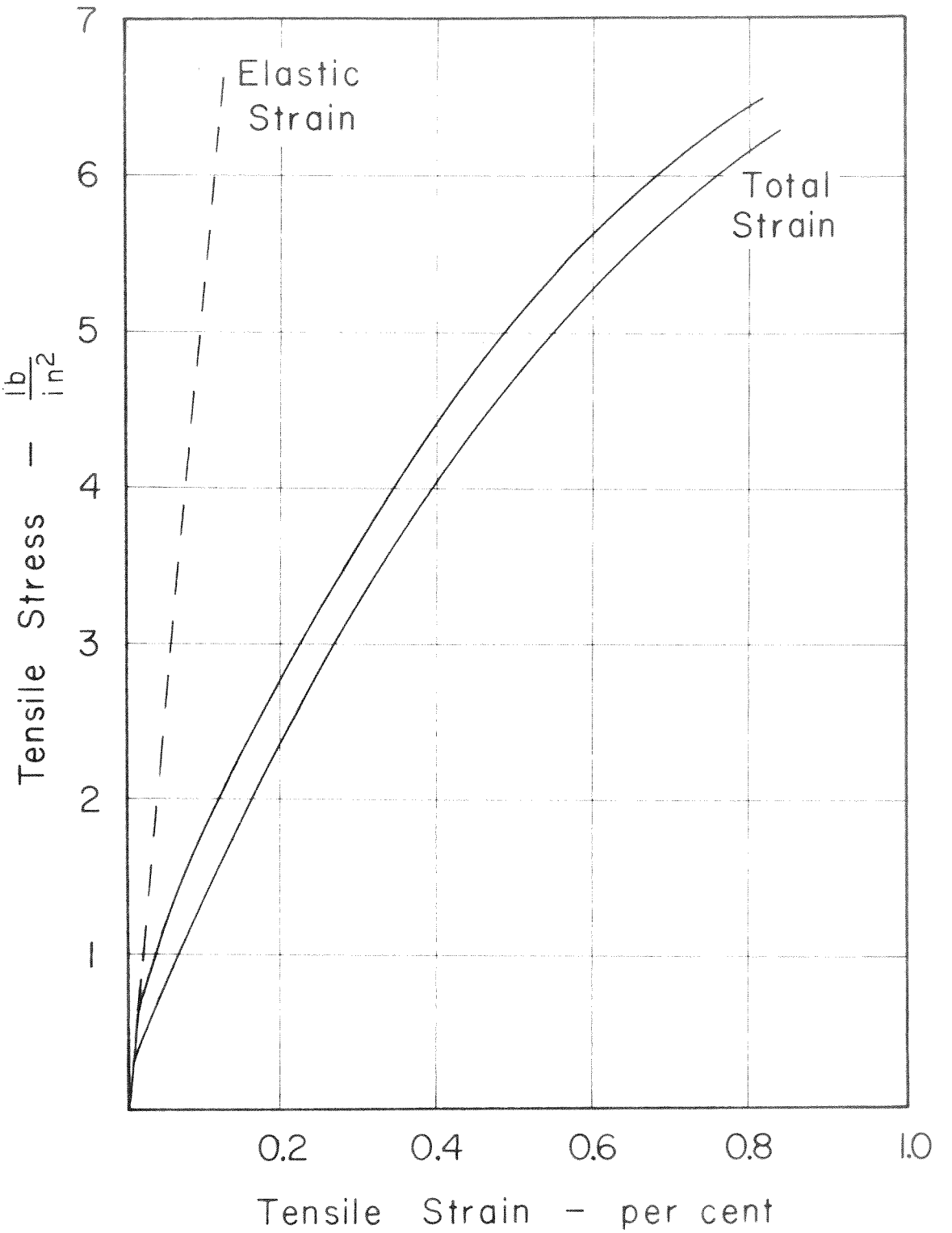

Fig. 22 Reproducibility Limits for Curves of Stress vs. Strain for Stress Normal to the Basal Planes of Zinc.

TABLE IV

A Summary of Information Pertaining to the Room Temperature Tensile Tests of Previously Undeformed Zinc Specimens

Specimen Number	Gage Diam. (in.)	Number of Tilt Boundaries	Critical Tensile Stress for Slip ($lb/in.^2$)	Final Tensile Stress ($lb/in.^2$)	Total Tensile Strain (per cent)
12	0.828	Unknown	600	5500	0.58
21	0.663	Unknown	250	1000	0.07
27	0.619	One of 0.7^o	600	2020	0.14
28	0.631	One each 0.4^o, 0.3^o	500	3100	0.25
29	0.628	None $>0.02^o$	300	4190	0.40
37	0.547	None $>0.02^o$	650	6200	0.81
46	0.431	One of 0.12^o	500	4060	0.35

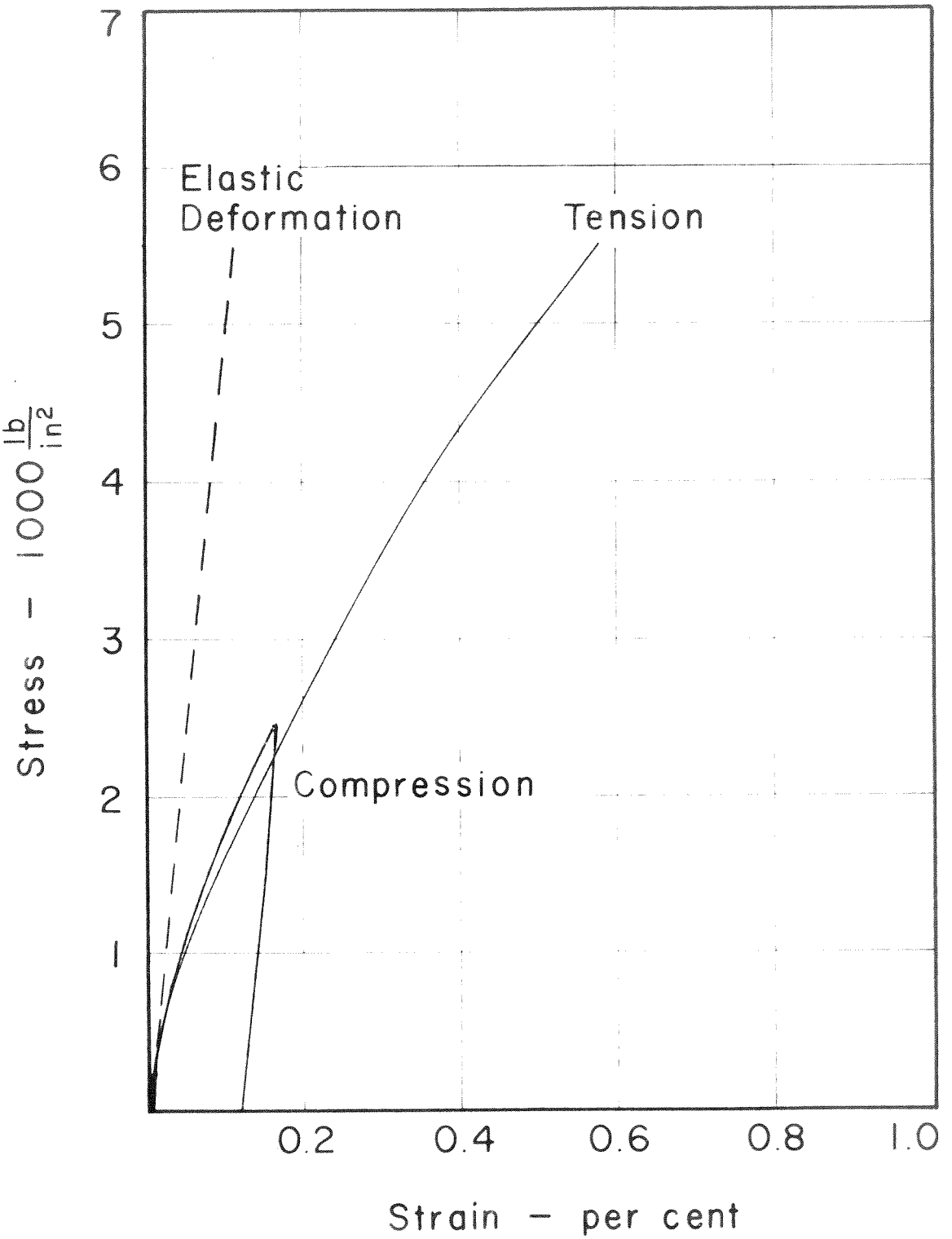

Fig. 23 A Comparison of a Compressive and a Tensile Test for Stress Applied Normal to the Basal Planes.

A tensile stress was applied normal to the basal planes of specimen number 44 after the completion of its compressive test. Both the compressive and tensile stress versus strain curves for this specimen are shown in Fig. 24. Both curves are shown as having positive values in order to facilitate comparison, and the tensile curve has been offset so as not to interfere with the compressive curve. The strain hardening induced during the compressive test was effective in raising the tensile stress required to produce plastic deformation during the tensile test. However, the magnitude of the critical tensile stress for yielding was less than the maximum magnitude of the compressive stress applied during the compressive test.

C. Plastic Strain Parallel to the Hexagonal Crystal Axis. (-77°C)

A plastic elongation parallel to the hexagonal axis of a zinc crystal also is produced by a tensile stress normal to the basal planes at a temperature of -77°C. The tensile stress versus strain curve for a specimen (number 27a) tested at -77°C is shown in Fig. 25. A typical stress versus strain curve of a tensile test (specimen number 37) at 25°C also is included in Fig. 25 for comparison purposes. The rate of strain hardening at -77°C is approximately 4×10^5 lb/in.^{2} per in./in., which is less than half of the rate of strain hardening at 25°C.

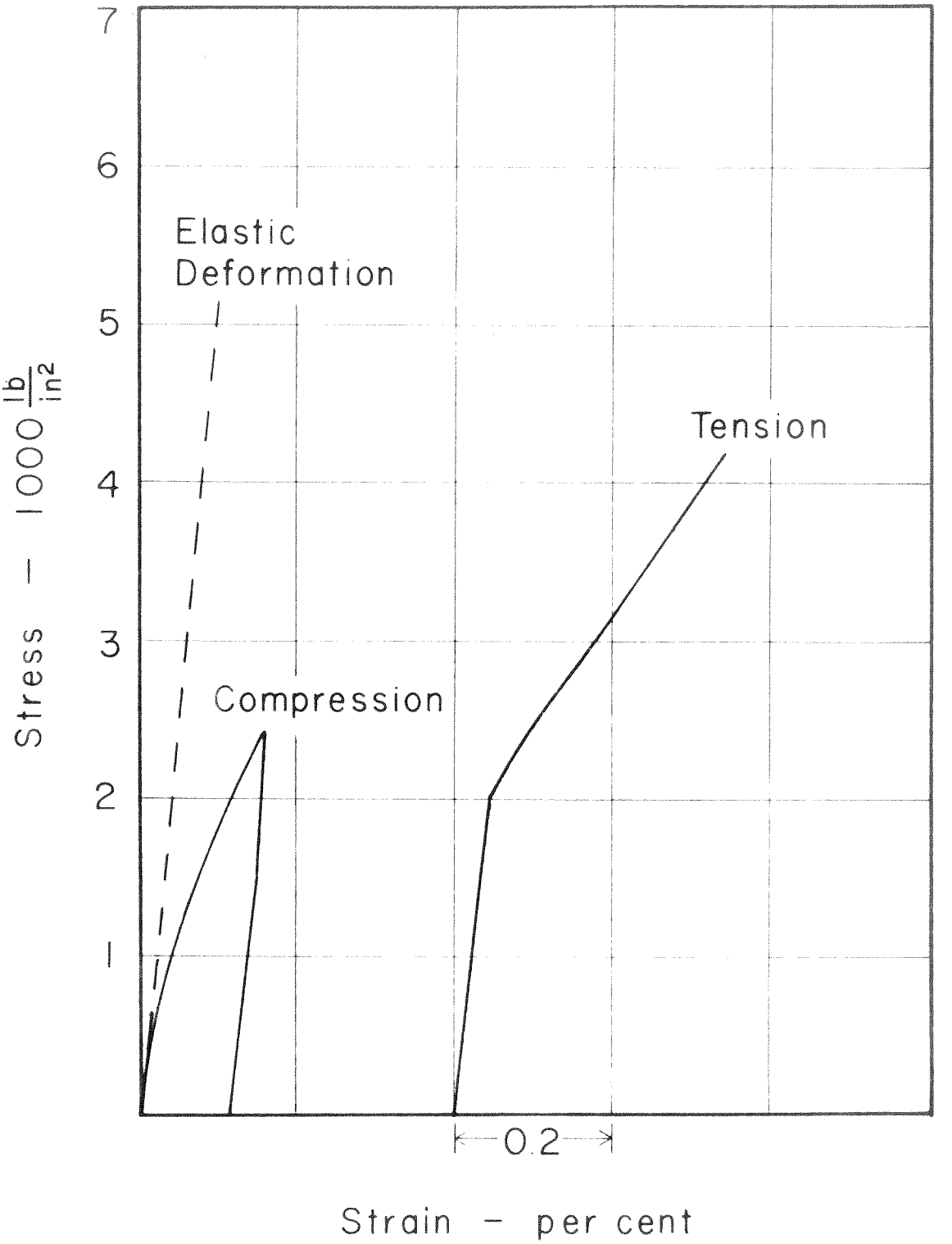

Fig. 24 Curves of Stress vs. Strain for Compressive Stress and Subsequent Tensile Stress Normal to the Basal Planes of Zinc.

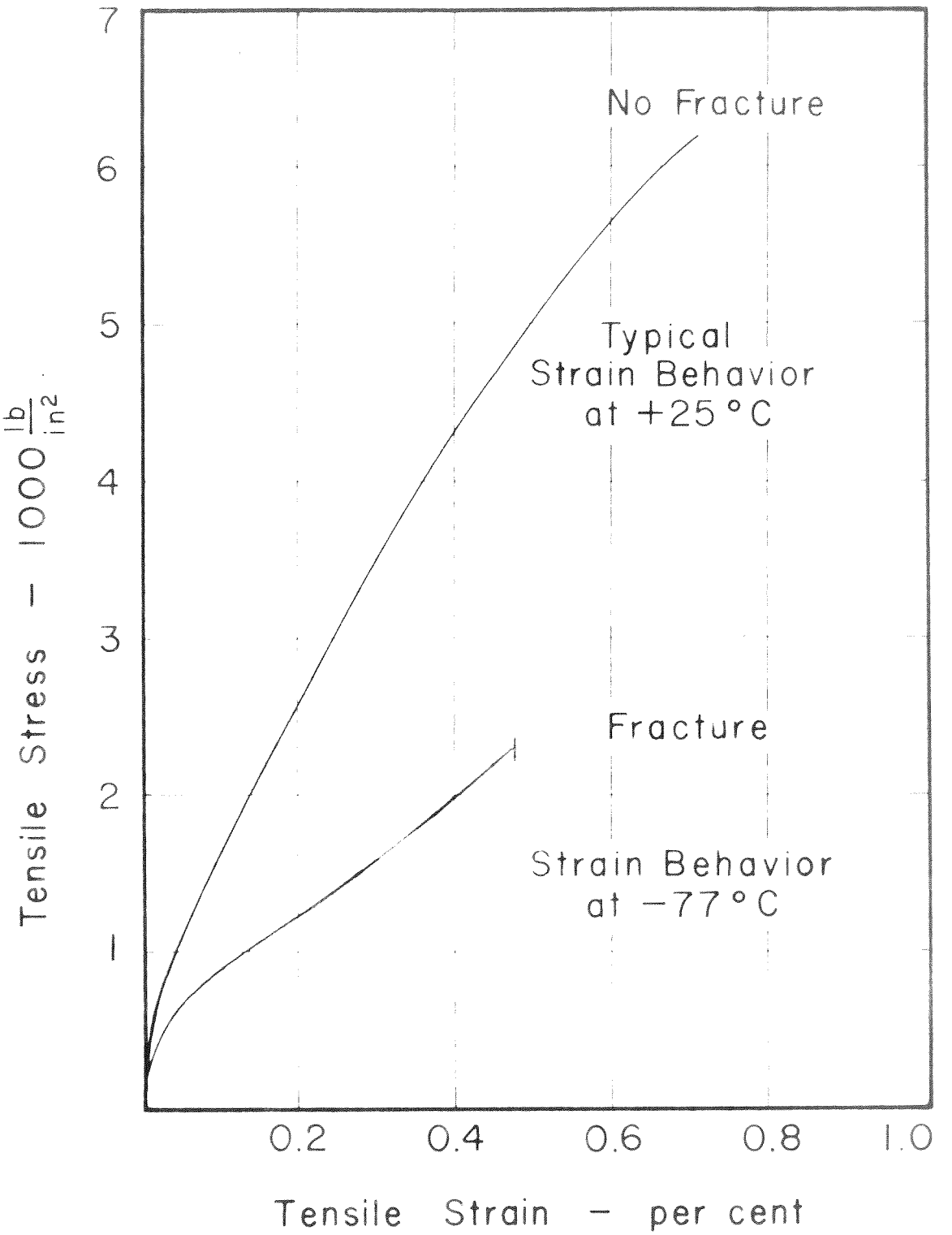

Fig. 25 Temperature Dependence of Strain Produced by Tensile Stress Normal to the Basal Planes of Zinc.

The tensile tests at -77°C were terminated when basal cleavage occurred in the narrow gage section of the crystals.

D. Interactions Between Basal and Non-Basal Slip

The basal slip system and the newly detected non-basal slip system are not independent of each other; slip on either one of these two systems can affect appreciably the subsequent stress versus strain behavior for slip on the other system. The tests showing this interaction between the two slip systems can be divided into two categories: those tests in which the non-basal slip system was activated first, and those tests in which the basal slip system was activated first.

The slip on non-basal planes produced by applying a tensile stress normal to the basal planes is very effective in raising the magnitude of the critical shear stress required to produce slip on the basal planes. Slip along non-basal planes was produced in each of several specimens (numbers 21, 26, 27, 28, 29, 30, 44, and 46) by applying a tensile stress normal to the basal planes. The tensile stress remained on each specimen while a shear stress along the basal planes was applied. The stress versus strain behavior produced by the tensile stress normal to the basal planes has already been described in previous paragraphs (Fig. 22, Table IV). The stress versus strain curves produced by the shear stress along the basal planes are shown in Fig. 26. The two numbers listed to the right of

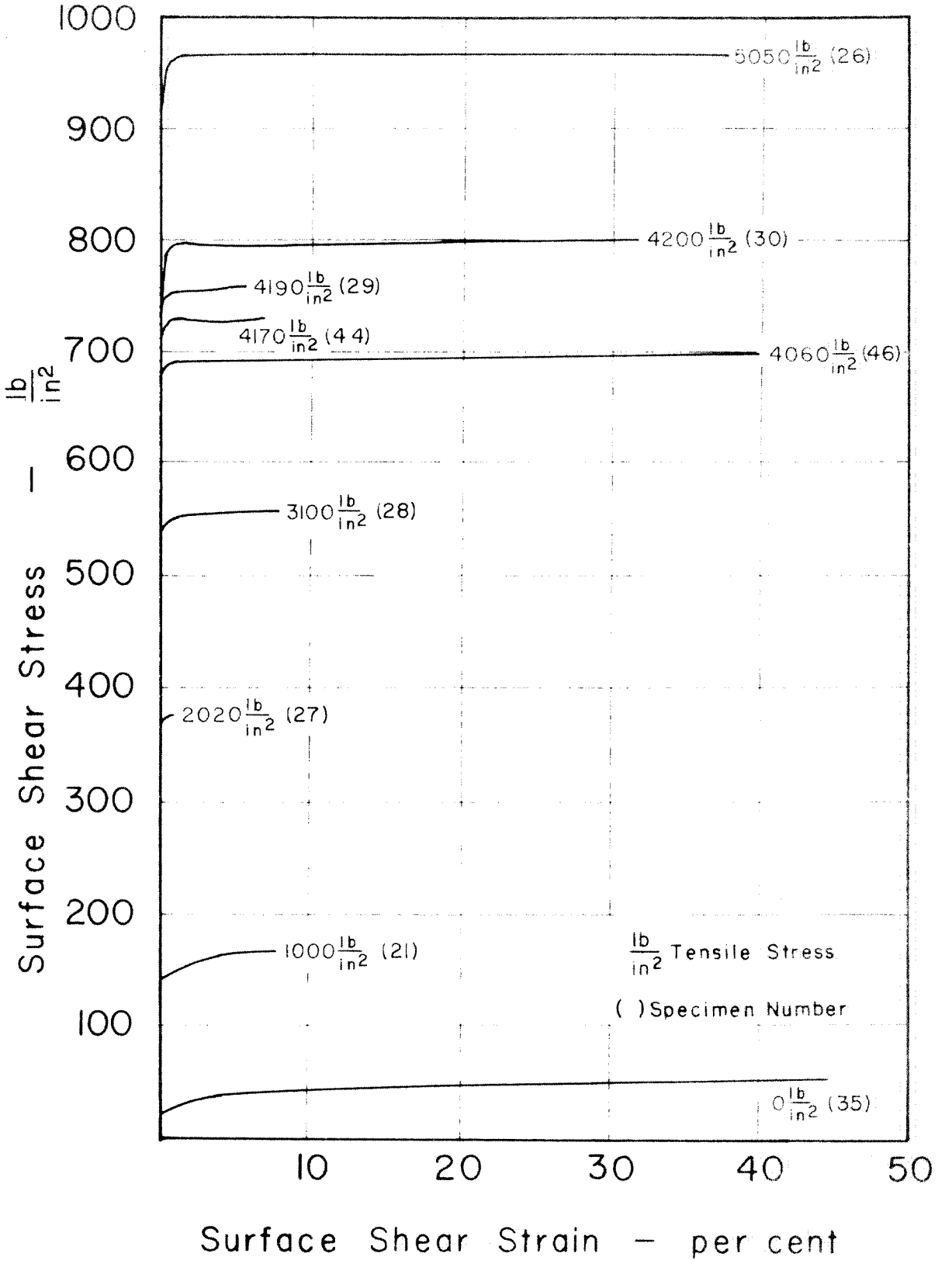

Fig. 26 Curves of Shear Stress vs. Shear Strain for Basal Slip of Several Crystals Previously Deformed by Tensile Stress Normal to the Basal Planes.

each curve represent the tensile stress normal to the basal planes and the specimen number, respectively.

The quantitative information provided by these tests shows that the critical resolved shear stress required to cause slip on basal planes may be increased by a factor of at least 40 as the result of strain hardening caused by slip on non-basal planes. The information pertaining to these tests is summarized in Table V. Fig. 27 shows the linear relationship between the critical shear stress required to produce slip on basal planes and the value of the tensile stress normal to the basal planes. Fig. 28 shows the relationship between the critical shear stress required to produce slip on basal planes and the amount of plastic tensile strain produced prior to the application of shear stress along the basal plane.

These tests also provided information about the formation of slip bands in zinc. Slip bands were formed parallel to the basal planes during the torsional portion of each test. The character of these bands, however, was not the same for all specimens. The slip bands were very fine and closely spaced on the specimens that did not previously have a tensile stress applied normal to the basal planes. These fine bands could be seen only with the aid of a low power microscope and were not distinct with even the best viewing conditions. Slip bands that were coarse and easily seen

TABLE V.--A summary of information pertaining to the critical shear stress required to produce slip on basal planes for specimens simultaneously subjected to a tensile stress normal to the basal planes

Tensile Stress ($lb/in.^2$)	Tensile Plastic Strain (per cent)	Shear Stress Rate to Critical Stress ($lb/in.^2$ min)	Critical Shear Stress ($lb/in.^2$)	Gage Diam. (in.)	Specimen Number
0	0.0	2.8	17	0.585	35
1000	0.050	2.5	135	0.663	21
2020	0.110	5.8	365	0.619	27
3100	0.195	5.6	545	0.631	28
4060	0.275	7.1	690	0.431	46
4170	0.265	38.4	730	0.606	44
4190	0.335	5.6	750	0.628	29
4200	0.335	8.5	795	0.577	30
5050	0.325	9.6	960	0.615	26

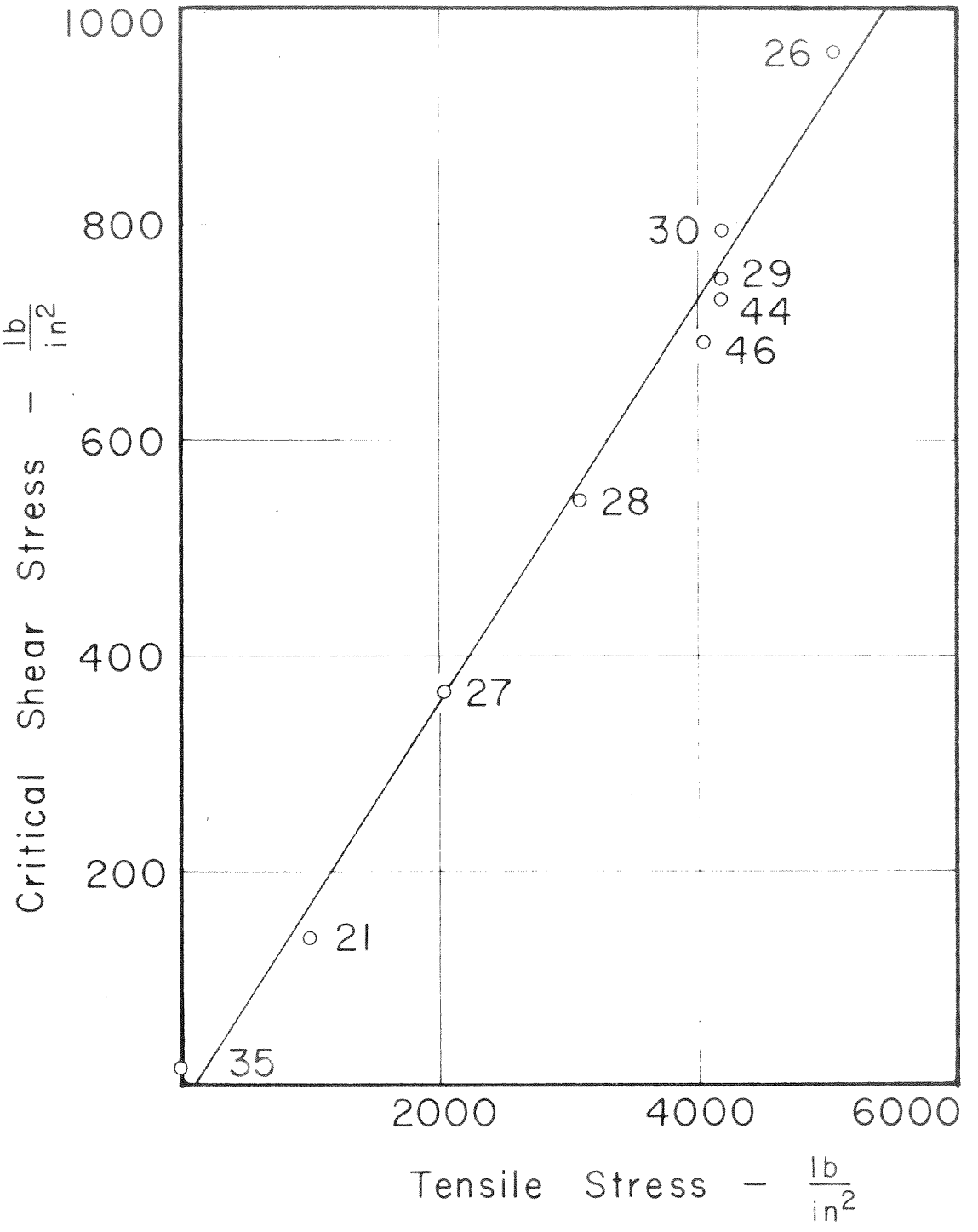

Fig. 27 Critical Shear Stress for Basal Slip vs. Tensile Stress Previously Applied Normal to the Basal Planes.

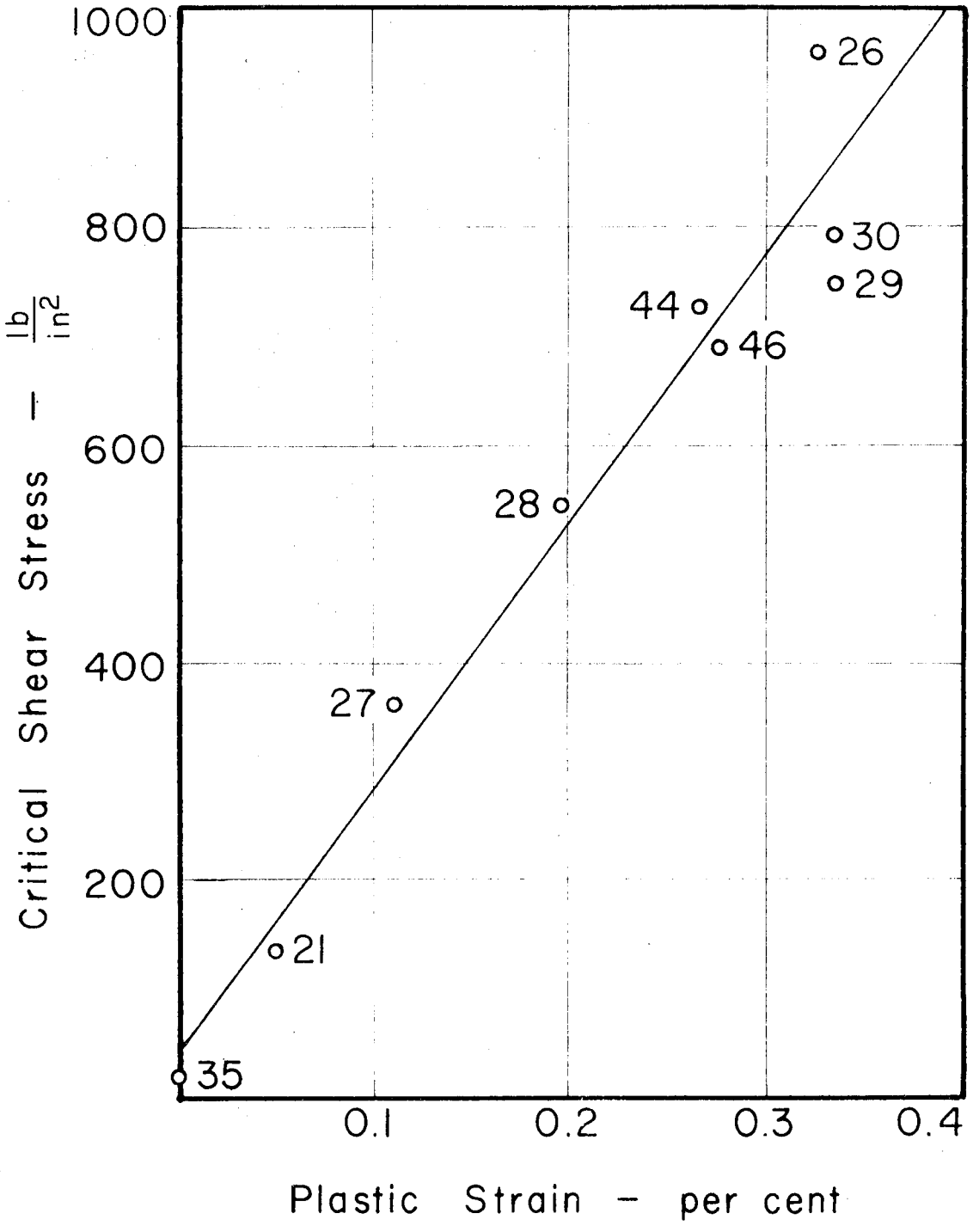

Fig. 28 Critical Shear Stress for Basal Slip vs. Tensile Strain Previously Produced Normal to the Basal Planes.

with the unaided eye were formed when an applied torque produced slip along basal planes after a large tensile stress had been applied normal to the basal planes. Fig. 29 (see Appendix F) shows coarse slip bands along basal planes in a specimen (number 30) that had been subjected to torque after a tensile stress of 4,200 lb/in.^{2} had been applied normal to the basal planes. The curved line running along the length of the specimen is a pencil line that was straight before the torsion test. The displacement of this pencil line is discontinuous at the slip bands, indiciating that most of the plastic deformation was caused by slip occurring within these visible slip bands.

Tests conducted during this investigation also show that slip produced along basal planes can be effective in raising the tensile stress versus strain curve for subsequent slip along non-basal planes that is produced by applying tensile stress normal to the basal planes. Slip on basal planes was produced in several specimens (numbers 38, 39, 41, and 45) by applying torque about the hexagonal axis of the crystal. A tensile force then was applied normal to the basal planes. The stress versus strain behavior of slip on basal planes has already been described in previous paragraphs (Fig. 10, Table II). The stress versus strain curves for subsequent tensile stress applied normal to the basal planes are shown in Fig. 30. The two numbers at the termination of each curve represent the maximum amount of previously introduced

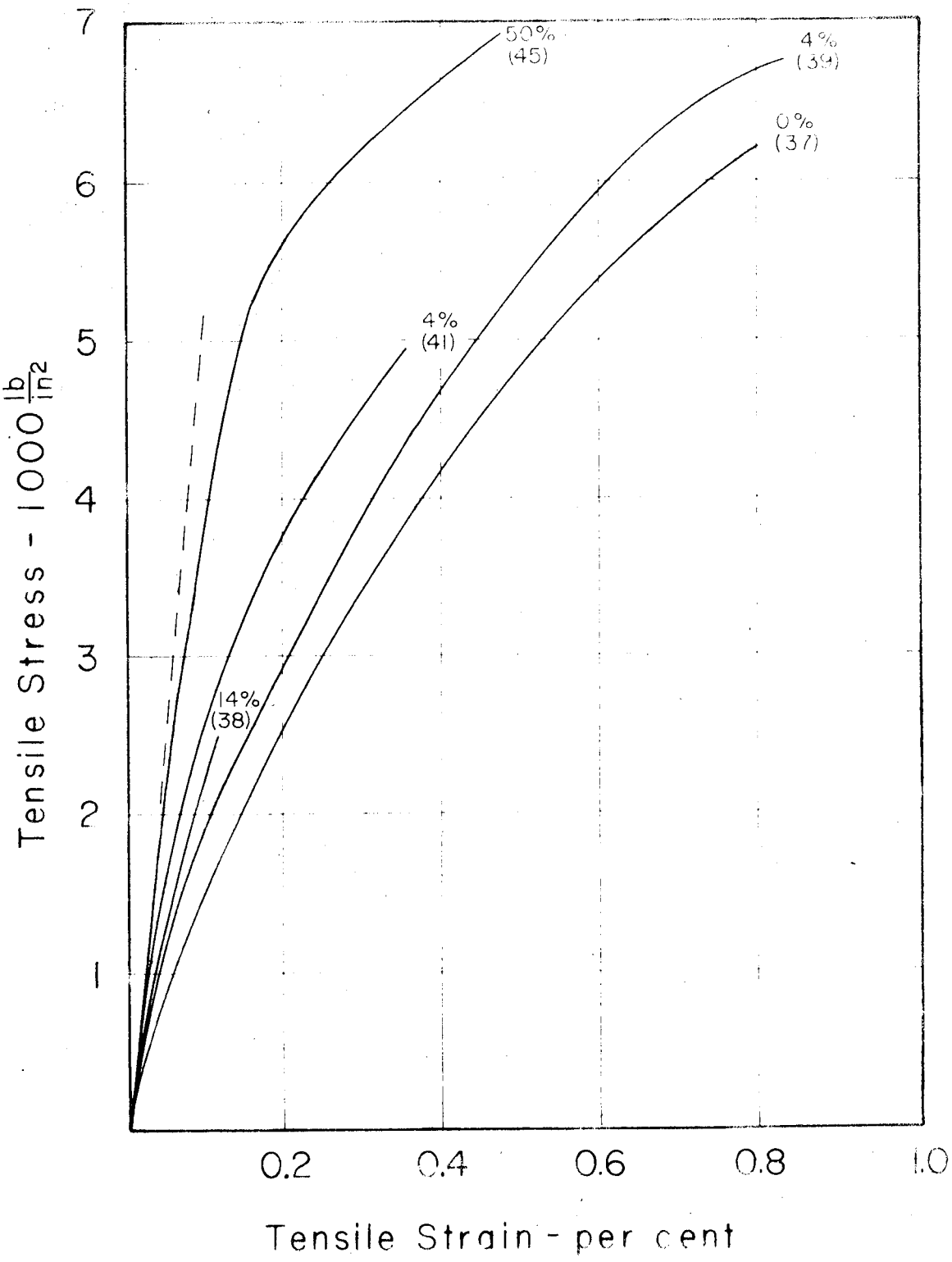

Fig. 30 **Curves of** Stress vs. Strain **for Tens**ile Stress Normal **to the Basa**l Planes for **Specimens Pre**viously Deformed in Torsion. Percentage at end of each curve indicates maximum plastic shear strain on basal planes prior to application of tensile stress. Number in parentheses at end of each curve indicates specimen number.

shear strain along the basal planes and the number of the specimen, respectively. The tensile stress versus strain curve of a specimen (number 37) that did not have slip on the basal planes prior to the tensile test also is included in Fig. 30 for comparison purposes. Each of these tensile tests was ended by the fracture of a solder bond, not a fracture in the narrow gage section of the crystal.

Fracture

Fracture of the zinc single crystal specimens occurred by cleavage along basal planes. Many specimens fractured near a solder bond. The other specimens fractured within the narrow, central portion of the test crystal when either of two test conditions existed: 1) a pure tensile stress normal to the basal planes at a temperature of -77°C, or 2) a combination of tensile stress normal to the basal planes and shear stress along the basal planes at a temperature of 25°C while SR-4 strain gages were bonded firmly to the surface of the crystal.

A. Fracture Near a Solder Bond

Several specimen assemblies failed by fracturing near a solder bond rather than in the narrow central portion of the test crystal. An inspection of each of these fracture surfaces consistently revealed two things. First, the fracture did not go through the solder, but occurred in the zinc crystal at a very small distance (less than a few

thousandths of an inch) from the solder. Second, the solder bonds were very inhomogeneous, containing gas bubbles and particles of entrapped flux. A photograph of one of these fracture surfaces is shown in Fig. 31 (see Appendix F). The dark, irregular areas are voids that did not contain sufficient solder to provide an effective bond in these regions. The light surrounding area is a cleaved basal plane of the zinc crystal. Although a considerable amount of time was spent in trying to find a better method of bonding the specimen assemblies, the soldering method described in Appendix D and typified by the type of bond shown in Fig. 31 (see Appendix F) produced the best bonds that could be obtained. The inhomogeneities of the solder bonds produced large stress concentrations in the zinc near the bonds. Large shear stress and large tensile stress certainly must have existed near the voids at the time of fracture, but the difficulty of estimating the magnitude of this stress makes it impossible to obtain any significant quantitative information about fracture of zinc crystals from the failure of the bonds themselves.

The tests of the specimen assemblies that fractured at a solder bond do provide some quantitative information on the fracture behavior of zinc crystals, however, because they show that zinc crystals are able to withstand relatively large nominal stress without fracturing at the gage section. A pure shear stress of 1,000 lb/in.^{2}

resolved along the basal planes with a resulting shear strain of 350 per cent did not produce fracture (specimen number 20). A pure tensile stress of 6,200 lb/in.^{2} normal to the basal planes did not fracture a specimen (number 37) that had not been deformed prior to the application of tensile stress. A pure tensile stress of 6,900 lb/in.^{2} normal to the basal planes did not fracture a specimen (number 45) that had a maximum shear strain of 50 per cent along the basal planes prior to the application of tensile stress. A tensile stress of 5,000 lb/in.^{2} normal to the basal planes, followed by the application of a shear stress of 970 lb/in.^{2} resolved along the basal planes while the tensile stress was still present did not produce fracture (specimen 26). A test sequence (specimen number 30) of a tensile stress of 4,200 lb/in.^{2}, followed by the application of a shear stress of 800 lb/in.^{2} while the tensile stress was still present, followed by the increase of the tensile stress to 7,200 lb/in.^{2} while the shear stress was still present did not produce fracture. A maximum shear strain of 200 per cent along the basal planes was produced within some of the slip bands of this crystal during the application of shear stress (Fig. 29, Appendix F). All of these various tests indicate that neither shear stress along the basal planes nor slip along the basal planes is a sufficient condition for significantly lowering the magnitude of tensile stress normal to the basal planes required to produce basal cleavage.

B. Effect of Surface Restraint on Fracture

The combination of tensile stress normal to the basal planes and shear stress along the basal planes was effective in producing fracture at a temperature of 25°C when SR-4 strain gages were firmly bonded to the surface of the crystal. Table VI lists information about the tests of the specimens that fractured under these conditions. The effectiveness of the SR-4 strain gages in aiding fracture may have been due to their ability to impede slip along the basal planes. Three of the specimens (numbers 21, 28, and 29) listed in Table VI had SR-4 strain gages that were oriented for measuring shear strain along the basal planes. The shear strains indicated by these gages are smaller than the maximum shear strains measured by means of the pencil lines, even though the nominal value of the shear stress under the SR-4 gages was at least as large as the shear stress in the region of maximum shear strain. The test of specimen number 33 (Fig. 12) also indicates that SR-4 gages bonded to the surface of a zinc crystal are effective in impeding slip on basal planes.

Fracture was initiated at the edge of a strain gage in at least one of the specimens (number 44). The fracture surface of this specimen is shown in Fig. 32 (see Appendix F). This surface contains a distinct river pattern of cleavage steps that may be used to locate the origin of the

TABLE VI

A Summary of Information Pertaining to the Tests of the Specimens that Fractured with SR-4 Strain Gages on their Surfaces

Specimen Number	Tensile Stress$_2$ (lb/in.^{2})	Maximum Basal Shear Stress$_2$ (lb/in.^{2})	Maximum Basal Shear Strain (per cent)	Type of Strain Gages Present	Maximum Shear Strain Under Gages (per cent)	Tilt Boundaries
21	1,000	170	8	tension, shear	0.55	Unknown
28	3,100	560	8	tension, shear	2.92	One each 0.4^o, 0.3^o
29	4,190	760	6	tension, shear	2.53	None $>0.02^o$
44	4,170	740	7	tension only	-	None $>0.02^o$
46	4,060	700	40	tension only	-	One of 0.12^o

fracture. The cleavage step patterns on the fracture surfaces of the other specimens that fractured with SR-4 strain gages on their surfaces were not as distinct as the pattern on specimen number 44, but these cleavage step patterns suggest that these fractures also may have started near the strain gages.

C. Effect of Temperature on Fracture

Two specimens were subjected to a pure tensile stress normal to the basal planes at a temperature of -77°C. One of these specimens (number 27a) fractured at a tensile stress of 2,250 lb/in.^{2}; the other specimen (number 49) fractured at a tensile stress of 2,500 lb/in.^{2} (Fig. 25). A similar specimen (number 37) subjected to a pure tensile stress of 6,200 lb/in.^{2} normal to the basal planes at a temperature of 25°C did not fracture.

V. DISCUSSION

The plastic deformation occurring in zinc crystals prior to fracture initiation has a complex character. Slip can occur both on basal planes and on non-basal planes, and strong interactions will occur between dislocations moving on intersecting slip planes. The distribution of stress in the vicinity of interacting dislocations should have an important influence on fracture initiation. Thus, a thorough understanding of plastic deformation is required before the process of fracture initiation can be understood.

Plastic Deformation

A. Slip on Basal Planes

Slip in zinc crystals occurs most readily along the basal (0001) planes. This slip may take place in any of the three crystallographically equivalent $11\bar{2}0$ directions. The characteristics of this slip system have been studied by several investigators (17,18,22,23). The shear stress required to produce slip on the basal planes generally is quite small, but it depends somewhat upon the crystallographic perfection (22) and the purity (18) of the crystal. A shear stress of from 20 to 40 lb/in.^{2} resolved along the basal planes is required to produce slip along the basal planes in 99.999 per cent purity zinc. The rate of strain hardening at a temperature of 25°C is small for small shear

strains but increases for shear strains exceeding 150 per cent (23). The characteristics of the slip produced along the basal planes of previously undeformed crystals during this investigation agree quite well with those of the previous investigators. This agreement is evidence that the mechanism of slip along the basal planes produced by applying a torque about the hexagonal axis is similar to the mechanism of slip produced by applying a shear stress uniformly over the basal planes.

B. Slip on Non-Basal Planes

Plastic deformation of zinc will occur when either a purely tensile or a purely compressive stress is applied normal to the basal planes. This deformation implies that slip can occur along non-basal planes with a slip direction that is neither parallel to the basal planes nor parallel to the hexagonal axis. The results of the experiments conducted during this investigation show that the most likely non-basal slip system consists of slip along the $\{\bar{1}\bar{1}22\}$ planes in the $\langle 11\bar{2}3\rangle$ slip directions.

Three other investigators, Bell and Cahn (24), Gilman (25), and Price (26), also have recently found evidence of slip on non-basal planes in zinc. Bell and Cahn (24) prepared several cylindrically shaped zinc crystals 0.05 in. in diameter, with the basal planes approximately parallel to the axis of the cylinder. Tensile stress was applied parallel to the basal planes, and a small plastic deformation occurred. Non-basal slip lines were noticed on some

of these specimens. Bell and Cahn tested at least thirty-two specimens, but only four of these specimens had non-basal slip lines that were "sufficiently bold and continuous to permit their crystallographic identification." Bell and Cahn concluded that slip probably occurred on the $\{\bar{1}\bar{1}22\}$ planes in the $\langle 11\bar{2}3\rangle$ directions. However, they believed they detected a slight departure from the $\{\bar{1}\bar{1}22\}$ planes and suggested that the slip may possibly occur along a slip plane that is crystallographically irrational.

Gilman (25) prepared several cylindrically shaped zinc crystals 0.15 in. in diameter, with the basal planes approximately parallel to the axis of the cylinder. Tensile stress was applied parallel to the basal planes of some of these crystals, and compressive stress was applied to others. Gilman did not detect plastic deformation in the tensile tests, but he did detect plastic deformation in the compressive tests. He first concluded that the plastic deformation was a form of "micro-kinking," but he later (27) decided that the plastic deformation may have been caused by slip on $\{\bar{1}\bar{1}22\}$ planes.

Price (26) has deformed thin ($< \frac{1}{2}\mu$) zinc whiskers and platelets within an electron microscope and has studied the resulting motions of individual dislocations by the electron transmission technique. He found dislocations with Burgers vectors of the 1/3 $\langle 11\bar{2}3\rangle$ type. Most of these dislocations moved along $\{\bar{1}\bar{1}22\}$ planes; but a few were found to move along $\{\bar{1}011\}$ planes, which also contain the $\langle 11\bar{2}3\rangle$ directions.

The possibility of slip along $\{\bar{1}\bar{1}22\}$ planes in zinc thus has been established in this investigation and in three other recent investigations. The information provided by these investigators indicates that slip along $\{\bar{1}\bar{1}22\}$ planes in zinc generally is complex. Some of the information provided by these investigations appears to be contradictory. Additional experimental study of this slip system in zinc will be required before this slip can be fully understood. However, the presently available information does provide some understanding of this mode of deformation.

Slip will occur along the non-basal $\{\bar{1}\bar{1}22\}$ planes only if the shear stress resolved along these planes exceeds a critical magnitude. This critical shear stress is not the same for all zinc crystals. Slip occurred along non-basal planes in specimens of this investigation when the tensile stress normal to the basal planes exceeded 250 to 650 lb/in.^{2}. This range of tensile stress corresponds to a range of shear stress resolved along the $\{\bar{1}\bar{1}22\}$ planes of 100 to 270 lb/in.^{2}. A compressive stress of the same magnitude applied normal to the basal planes also produced slip along non-basal planes. This investigation thus indicates that the critical stress required to produce slip along the non-basal planes in zinc is independent of the direction of the applied stress.

Gilman (25), on the other hand, concluded from his experiments that the critical stress required to produce deformation along non-basal planes may depend upon the

direction of the applied stress. A compressive stress applied parallel to the basal planes produced slip on non-basal planes when the shear stress resolved along the non-basal planes reached a stress of 200 lb/in.^{2}. A tensile stress applied parallel to the basal planes did not produce any detectable slip on the non-basal planes for a resolved shear stress as high as 2,200 lb/in.^{2}, the upper limit to the tensile stress in this type of test being limited by the initiation of twinning.

Bell and Cahn (24) also applied tensile stress parallel to the basal planes of several zinc crystals. Slip on non-basal planes was not detected until the shear stress resolved along the non-basal planes exceeded a critical stress of from 1,400 to 2,000 lb/in.^{2}, with the twinning stress being about twice this magnitude. Bell and Cahn compared these results with the experimental results obtained by Gilman and also suggested that this newly detected non-basal slip system in zinc may be anomalous in that it exhibits plastic properties that are different in tension and in compression. However, the results of the present investigation indicate that the differences in the critical stress detected by Gilman and Bell and Cahn probably were the result of their method of testing the zinc crystals and do not indicate a basic property of the $\langle 11\bar{2}3\rangle$ $\{\bar{1}\bar{1}22\}$ slip system.

The rate of strain hardening for slip along the non-basal planes is very large. Stress applied normal to the

basal planes at a temperature of 25°C produces a rate of strain hardening of approximately 7.5×10^5 lb/in.^{2} per in./in., which is 15 per cent of Young's modulus in the direction parallel to the hexagonal axis of the crystal. A rate of strain hardening this large is unusual for slip in metallic single crystals. Stress applied normal to the basal planes of zinc produces slip simultaneously on all six intersecting $\{\bar{1}\bar{1}22\}$ planes. Thus, the large rate of strain hardening may be explained partially by the large number of interactions that will occur between dislocations moving on intersecting slip planes.

A quantitative comparison of the results of this investigation with the results of Gilman's investigation (25), however, suggests that the number of intersecting active slip planes may not be the only factor leading to the large rate of strain hardening for non-basal slip in zinc. Gilman applied compressive stress parallel to the basal planes of several zinc specimens. This stress was applied parallel to a close-packed $[11\bar{2}0]$ direction for some specimens, producing slip simultaneously along two equally stressed $\{\bar{1}\bar{1}22\}$ planes. These specimens had a rate of strain hardening of 1.1×10^6 lb/in.^{2} per in./in. Other zinc specimens were tested by applying compressive stress parallel to the basal planes along a $[1\bar{1}00]$ direction, thus producing slip simultaneously along four equally stressed $\{\bar{1}\bar{1}22\}$ planes. The latter specimens had a rate of strain hardening of

3.8×10^6 lb/in.^{2} per in./in. Slip was produced simultaneously along six equally stressed $\{\bar{1}\bar{1}22\}$ planes during the tests of the present investigation. These specimens had a rate of strain hardening of only 0.75×10^6 lb/in.^{2} per in./in. A detailed analysis of the total number of secondary slip systems that could be expected to operate under each of these three different stress orientations also shows that the greatest amount of cross-slip would be expected when the stress is applied normal to the basal planes. Thus, the number of active slip planes does not appear to be the only factor in determining the rate of strain hardening for slip along non-basal planes. The other factors involved in producing a high rate of strain hardening are not known. The nominal purity of the specimens was the same for all cases. The testing temperature and the strain rates also were similar. The diameters of the specimens were not all the same, but this investigation shows that the specimen's diameter is not an important factor in determining the rate of strain hardening for slip on non-basal planes.

The temperature dependence of the rate of strain hardening for slip along $\{\bar{1}\bar{1}22\}$ planes in zinc is anomalous. In most metals the rate of strain hardening increases with decreasing temperature, and this behavior certainly is true for slip on the basal planes of zinc (17). However, the rate of strain hardening for slip along the $\{\bar{1}\bar{1}22\}$ planes of zinc decreases with decreasing temperature. Thus, the

total plastic strain produced by a given stress was found to be less at 25°C than at -77°C. Gilman (25) also found that the rate of strain hardening for slip along non-basal planes decreases with decreasing temperature, his tests covering the temperature range from -150°C to +150°C.

C. Interactions Between Basal and Non-Basal Slip

The basal slip system and the newly detected non-basal slip system are not independent of each other. Slip along the $\{\bar{1}\bar{1}22\}$ planes can be very effective in producing obstacles to the movement of dislocations on the basal planes. These obstacles may raise by a factor of at least 40 the critical resolved shear stress required to produce slip on the basal planes. The rate of strain hardening for slip on basal planes after the critical shear stress is exceeded is not appreciably affected by prior slip on non-basal planes.

This type of behavior is in agreement with Mott's suggestion (28) that hexagonal crystals may contain a high density of relatively immobile dislocations parallel to the hexagonal axis. This prediction was deduced from the known characteristics of slip along the basal planes of zinc and was made prior to the discovery of slip along non-basal planes in zinc. The discovery of slip on $\{\bar{1}\bar{1}22\}$ planes suggests that the relatively immobile dislocations probably are 1/3 $\langle 11\bar{2}3\rangle$ screw dislocations. Mott based his prediction on a suggestion by Cottrell (29) that an array or

"forest" of dislocations intersecting a slip plane can provide an effective barrier to the movement of dislocations along the slip plane. This resistance to movement is dependent upon the energy required to produce jogs in the dislocations. Seeger (30) has pointed out that the details of this type of interaction can be very complicated. The number of jogs formed may be zero, one, or two, depending upon the type of dislocations involved. The energy required to form these jogs will depend strongly on the magnitude of the Burgers vector of the dislocations and on whether or not the dislocations are extended.

The quantitative analysis made by Cottrell and by Mott has been restricted to the simplest case. For this reason, the analysis can be used only for estimating the order of magnitude of the critical shear stress required to produce slip on a crystallographic plane. Cottrell and Mott estimated that the critical shear stress should be approximately equal to:

$$\tau_c = \frac{\alpha G b}{d} \qquad (5)$$

where τ_c is the critical shear stress, G is the shear modulus, b is the magnitude of the Burgers vector, d is the average spacing between the dislocations that intersect the slip plane, and α is a numerical constant approximately equal to two.

This theoretical expression relating the critical shear stress to the dislocation content may be used for estimating the average spacing between the non-basal dislocations in the zinc specimens deformed in this investigation. For example, a specimen (number 29) that was subjected to a tensile stress of 4,200 lb/in.^{2} normal to the basal planes subsequently required a shear stress of 750 lb/in.^{2} to produce slip along the basal planes. The average spacing between the non-basal dislocations produced by the applied tensile stress thus should be of the order of magnitude of $\alpha Gb/\tau_c$, or 10^{-4} in. Fig. 21 (see Appendix F) is a photomicrograph of an etched basal plane of this zinc specimen. The pits may represent the intersection of non-basal dislocations with the basal plane. The predicted spacing of 10^{-4} in. corresponds to approximately 1/16 in. in Fig. 21. The minimum spacing of the pits shown in this photomicrograph certainly is of this order of magnitude, but the average spacing is considerably larger. However, two things must be kept in mind when comparing the photomicrograph with the theoretical prediction. First, the technique for producing pits on the basal surface of zinc was not developed until several days after the specimen shown in Fig. 21 (see Appendix F) had been tested, and the dislocation density may have decreased during this time. Second, the etching technique is not yet fully developed, and etch pits may not have been produced at every dislocation.

Seeger's theoretical approach to the problem of the critical shear stress required to produce slip included a consideration of the effect of thermal fluctuations. He concluded that the expression proposed by Cottrell and by Mott is valid only at very low temperatures. The critical shear stress required to cause slip should decrease slightly as a linear function of increasing temperature. The temperature dependence predicted by Seeger was not observed in the present investigation because the torsional tests were conducted at only one temperature. However, the testing methods developed for this investigation could be used for checking Seeger's prediction. This would be accomplished by introducing a known density of non-basal dislocations into several specimens and then testing these specimens in torsion at different temperatures. These tests could be made as part of the second program suggested in Appendix E.

Fracture

Fracture of zinc single crystals occurs by cleavage along basal planes. The nominal magnitude of the tensile stress normal to the basal planes at the time of fracture is not the same for all test conditions. Thus, this tensile stress is not the only important factor in producing fracture of zinc. Temperature, plastic deformation, and the shear stress along the basal planes are all additional factors that affect the initiation of fracture. The relationship between all of the factors affecting fracture

is complex, and the exact atomic mechanisms leading to fracture cannot be determined from the presently available experimental evidence. Nevertheless, the quantitative results of this investigation, combined with the results of other investigations, may be used to evaluate the theoretical models that have been proposed previously to explain the initiation of fracture in zinc.

The earliest criterion for predicting the basal fracture of zinc is Sohncke's Normal Stress Law (16). This law predicts that cleavage will occur whenever the stress normal to the cleavage plane reaches a particular critical magnitude. An early investigation (16) indicates that the critical cleavage stress for zinc has a magnitude of 300 $lb/in.^2$ and is nearly independent of temperature and plastic deformation. The present investigation, however, shows that Sohncke's Law is not a valid criterion for predicting fracture of zinc. A tensile stress of 7,000 $lb/in.^2$ normal to the basal planes was not sufficient to produce fracture in at least one specimen. Furthermore, the stress normal to the basal planes at the time of fracture has been found to vary greatly with both temperature and plastic deformation. The results of recent investigations by Deruyttere and Greenough (13) and by Gilman (14) also conflict with Sohncke's Law. The information now available shows that Sohncke's Law was based upon a much too limited range of

experimental variables and thus cannot serve as a general criterion for predicting the cleavage of zinc crystals.

Two theoretical models of fracture initiation based upon dislocation interactions previously have been suggested for zinc single crystals (11,13). Both of these models are restricted to interactions between dislocations on basal planes. This limitation was due to the belief that slip on basal planes is the only important form of plastic deformation in zinc crystals. The quantitative results of this investigation do not agree with predictions based on these models. Furthermore, the discovery of slip on non-basal planes suggests that other dislocation interactions may occur. The previously proposed models of fracture initiation in zinc thus need to be re-examined.

The presence of basal tilt boundaries in zinc crystals has been considered an important factor in producing cracks along the basal planes. Orowan (31) has pointed out that there is a large tensile stress normal to the slip plane at the termination of a tilt boundary within a crystal. The magnitude of this stress depends upon the angle of the tilt boundary. Friedel (32) has shown how such a terminating wall may be formed by slip along a slip plane and has estimated that cleavage will be initiated if the angle of the tilt boundary exceeds 5 degrees. This mechanism of crack formation is illustrated in Fig. 33. Stroh (11) has expanded the quantitative approach; and by making certain

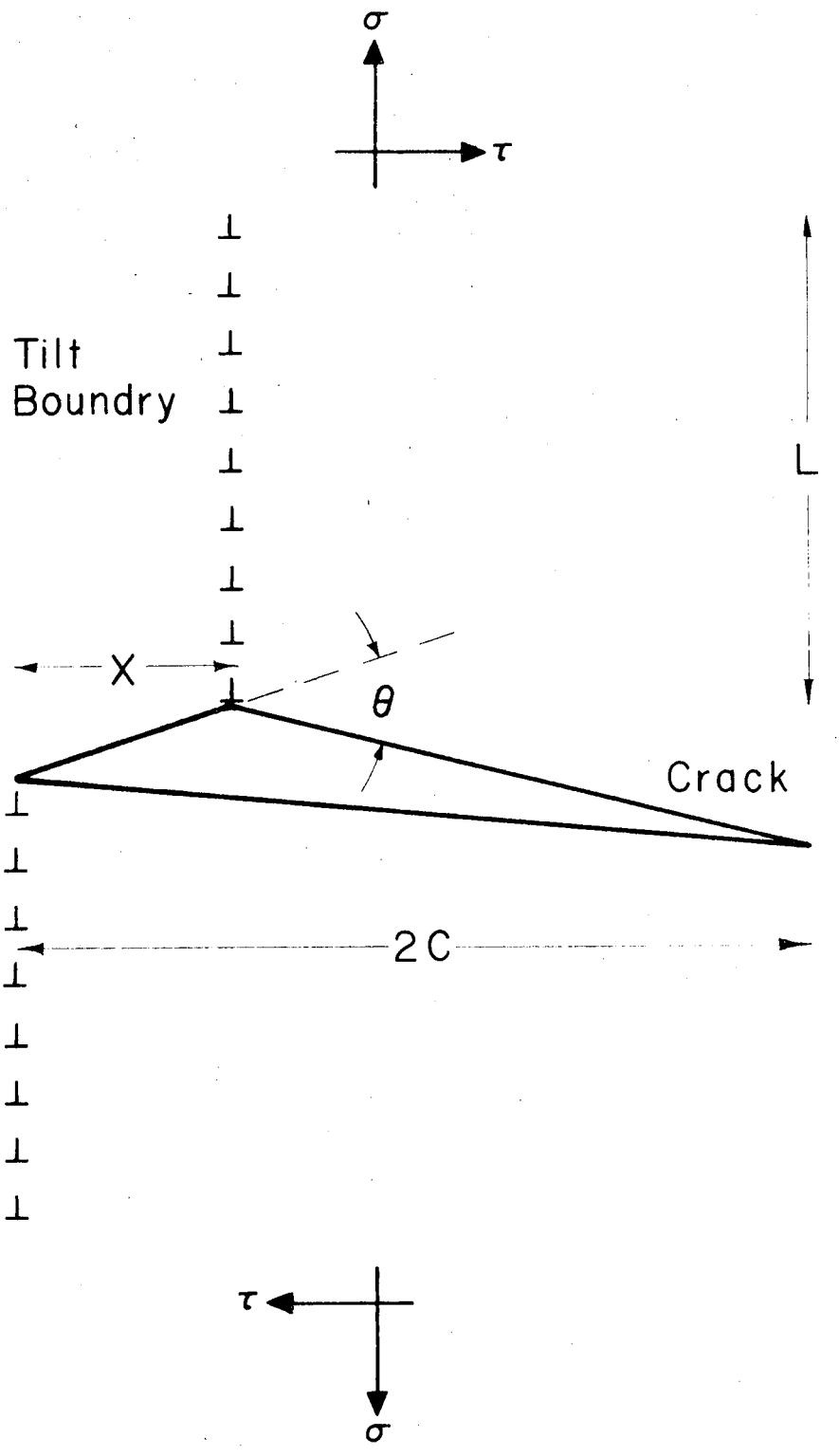

Fig. 33 Fracture Initiation at a Separated Tilt Boundary.

assumptions, he transformed the theory into a form that compares favorably with the zinc fracture results obtained by Deruyttere and Greenough (13).

Stroh treated the problem by considering the balance between various energy terms and did not calculate explicitly the stress associated with the initiation and propagation of a crack.

Stroh based his theory on the following assumptions:

1) A wall of edge dislocations can be separated into two segments by a shear stress on the basal planes. A small crack along the active slip plane will be initiated by the large stress at the newly formed ends of these segments.
2) The distance between the two wall segments (x in Fig. 33) is determined by the balance between the forces of attraction of the dislocations in the wall segments and the force of separation caused by the externally applied shear stress. Thus, the length of the crack is a function of the shear stress on the basal planes.
3) The crack will spread catastrophically by the Griffith mechanism if it exceeds a certain critical size. This critical size is determined by the magnitude of the stress normal to the basal planes.
4) The stress concentration at the end of a dislocation wall or at the tip of a crack on the basal planes will not be reduced by plastic flow.

These assumptions enabled Stroh to derive for the condition of fracture:

$$(\tau - \tau_c)\,\sigma L > K \qquad (6)$$

where τ is the shear stress on the basal planes, τ_c is the critical shear stress required to cause slip on the basal planes, σ is the tensile stress normal to the basal planes, and L is the height of the dislocation wall. The right hand portion, K, of this expression is a constant that depends only upon the physical properties of zinc crystals. Stroh's calculations show K to have a theoretical value of 4,000 $lb^2/in.^3$. Stroh applied his theory to the test results of Deruyttere and Greenough (13) and obtained an experimentally determined value of K of 3,000 $lb^2/in.^3$.

The test results of the present investigation show that Stroh's simple theoretical model cannot provide a general explanation of the fracture of zinc single crystals for all conditions. Large tensile stress normal to the basal planes and large shear stress on the basal planes can exist simultaneously without producing basal fracture. The application of Stroh's theory to the test result of a specimen (number 30) that contained a tilt boundary of 0.20 degree indicates the experimentally determined value of K can exceed 5×10^6 $lb^2/in.^3$. This is three orders of magnitude larger than Stroh's theoretical value of K. The fact that fracture did not occur in this specimen agrees with Friedel's

prediction that fracture cannot be initiated by a tilt boundary unless the angle exceeds a critical magnitude. The magnitude of the critical angle predicted by Friedel (5 degrees) is larger than the tilt boundary angles normally found in carefully grown zinc crystals. Thus, Stroh's version of this theory may be applicable only if large angle tilt boundaries are produced during plastic deformation.

The discovery of slip on non-basal planes in zinc also is important in evaluating the general applicability of Stroh's assumptions. Stroh apparently was unaware of the possible existence of slip on non-basal planes and of the large effect this slip can have upon the critical shear stress required to cause slip on basal planes. He assumed that the critical shear stress, τ_c, required to cause slip on the basal planes has a constant value of about 75 lb/in.^{2}, independent of the magnitude of the tensile stress normal to the basal planes. This investigation shows that the critical shear stress can have a marked dependence upon the tensile stress normal to the basal planes. The discovery of slip on non-basal planes also shows that the large stress concentration at the end of a wall of dislocations or at the tip of a crack can be reduced by slip along non-basal planes.

Fracture occurred in some of the specimens of this investigation under conditions not predicted by Stroh's model. Many specimens with SR-4 strain gages on their surfaces fractured even though they contained only relatively

small basal tilt boundaries. The specimens tested at -77°C fractured without shear stress on the basal planes. Furthermore, the tensile stress required to produce fracture is smaller at -77°C than at 25°C. The simple dislocation model considered by Stroh does not provide a ready explanation for this temperature dependence.

Another dislocation model to describe the initiation of fracture in zinc was suggested by Bullough and expanded by Deruyttere and Greenough (13) and by Gilman (14) in an effort to provide an interpretation of their respective test results. This model is based upon a modified form of Griffith's theory that states that part of the energy needed to form a crack can be provided by the strain energy associated with dislocations. The density of dislocations would have to be extremely large in the region of the incipient crack for this mechanism to be successful. Such a large density of dislocations might occur in zinc whenever shear stress on the basal planes forces a long queue of basal dislocations against a strong barrier. If the shear stress is large enough, the dislocations may become so densely packed that their strain energy alone is sufficient to start a basal crack. However, the density of dislocations would not have to be this large if an externally applied tensile stress normal to the basal planes is present. The macroscopically distributed strain energy associated with this externally

applied stress could provide part of the energy needed to form the crack. The operation of this crack forming mechanism is represented in Fig. 34.

This theoretical model requires barriers to slip that are strong enough to permit the formation of long queues of dislocations. The SR-4 strain gages may have been instrumental in forming dislocation queues during the room temperature tests of this investigation. This model is thus qualitatively consistent with the observed results. Gilman believed that the necessary obstacles in his specimens were provided by the brass grips that were soldered to each end of his specimens. Deruyttere and Greenough could not identify any obstacles that could satisfactorily explain the fracture of their zinc specimens.

A quantitative analysis of the stress that would be required to produce fracture in zinc by this mechanism raises doubt about the usefulness of the model. Deruyttere and Greenough were not satisfied with the quantitative comparison between the predictions of this theory and their experimental results. Gilman, on the other hand, believed that this theory was quantitatively self-consistent with at least part of his experimental results. He developed an expression for the fracture condition:

$$\tau \sigma D > N \qquad (7)$$

where τ is the shear stress on the basal planes, σ is the

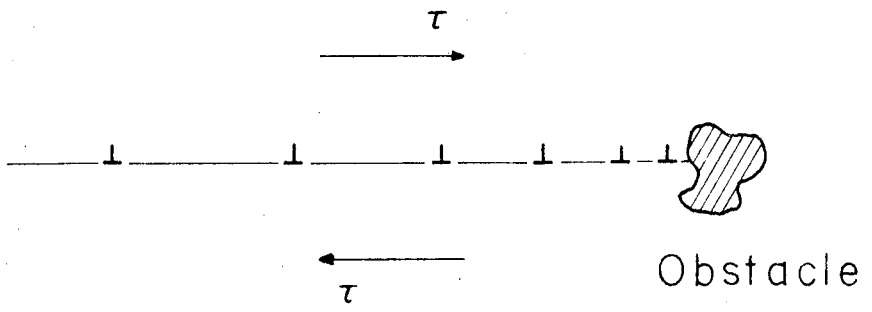

a. Initial condition

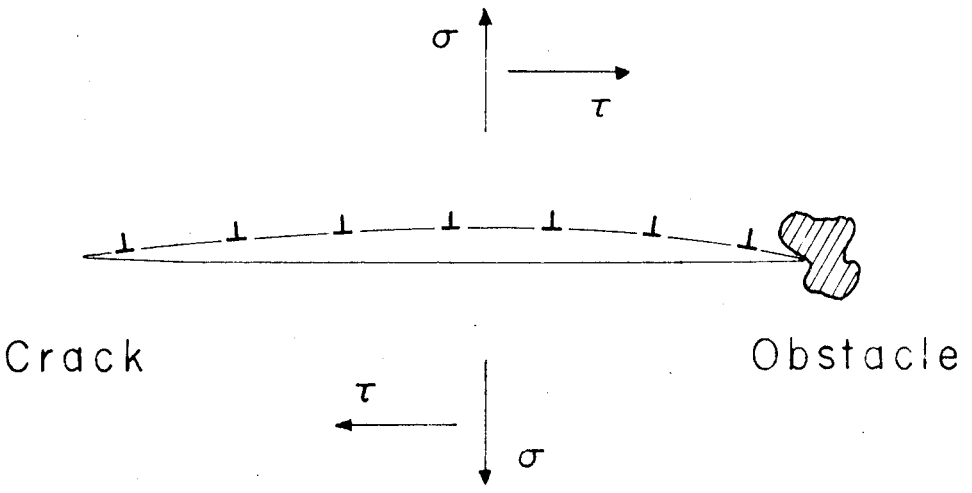

b. Final condition

Fig. 34 Fracture Initiation by a Queue of Dislocations on the Plane of Fracture.

tensile stress normal to the basal planes, D is the length of the glide plane, and N is a constant that depends upon physical properties of zinc crystals. Gilman estimated the value of N to be about 3×10^4 $lb^2/in.^3$.

The application of Gilman's fracture condition to the results of the present investigation requires a knowledge of the effective length of the glide planes in the torsional specimens. The non-uniform distribution of shear stress within a torsional specimen with SR-4 gages on the surface makes it difficult to estimate this length. Furthermore, slip on non-basal planes produces obstacles to basal dislocations and these obstacles may influence the formation of dislocation queues. Consequently, the deformation produced in the specimens of this investigation is too complex to be analyzed quantitatively by the simple method used by Gilman.

The tests at $-77^{\circ}C$ show that pile-ups of dislocations on basal planes cannot provide a general explanation for fracture initiation in zinc single crystals. Fracture occurred in these tests even though the shear stress on the basal planes was negligible and strong obstacles to slip were not present in the region of the fracture. The mechanism represented in Fig. 34 could not have been important in these low temperature tests.

The results of this investigation show that neither of these two previously suggested models provides an adequate

description of fracture initiation in zinc. Fracture was found to occur under conditions that are not predicted by either of these two models. Other mechanisms, therefore, must be important in producing fracture.

The discovery of slip along non-basal planes in zinc now makes it possible to consider interactions between dislocations moving on intersecting slip planes. This investigation shows that slip on non-basal planes can occur readily for a tensile stress normal to the basal planes that is much smaller than the stress required to produce fracture. This experimental evidence suggests that slip on non-basal planes generally precedes the initiation of fracture and may be an important factor in initiating fracture.

Several dislocation models involving the interaction of dislocations on intersecting slip planes already have been proposed to explain fracture initiation in cubic crystals. The discovery of slip on non-basal planes in zinc suggests that a modified form of some of these models may be used to describe fracture in hexagonal close-packed metals.

Zener (9) has pointed out that cracks may be initiated by the large tensile stress present at the head of a long queue of edge dislocations forced against a strong obstacle. Stroh (10) has calculated that the tensile stress has its maximum value along the plane that makes an angle of 70 degrees with the slip plane. A pile-up of edge dislocations on a $(11\bar{2}2)$ plane in zinc thus must produce a large tensile

stress normal to the basal planes. This stress might be large enough to initiate a crack. A pile-up of edge dislocations and the resulting crack formation is shown in Fig. 35. A similar pile-up of screw dislocations would not produce the tensile stress necessary to form a crack.

Stroh (10) estimated that a crack will be initiated by a pile-up of edge dislocations whenever

$$n\tau > 0.7\ G \qquad (8)$$

where n is the number of dislocations within the pile-up, τ is the nominal shear stress applied along the slip plane, and G is the shear modulus. Once a crack is initiated in this manner, all the dislocations will run into it; and it will propagate catastrophically under the influence of the applied stress. The application of Stroh's calculations to zinc crystals shows that a large pile-up of dislocations is required to produce fracture. For example, a tensile stress of 4,000 lb/in.^{2} applied normal to the basal planes produces a resolved shear stress of 1,700 lb/in.^{2} along the $\{\bar{1}\bar{1}22\}$ slip planes. A pile-up of 2,000 edge dislocations on a $(\bar{1}\bar{1}22)$ plane would be required to produce fracture on a basal plane. This pile-up would be about 1/16 in. long.

The obstacles necessary for the operation of this fracture mechanism must be strong enough to resist break-down in order to allow the stress at the head of the pile-up to become large enough to initiate fracture. Furthermore, the

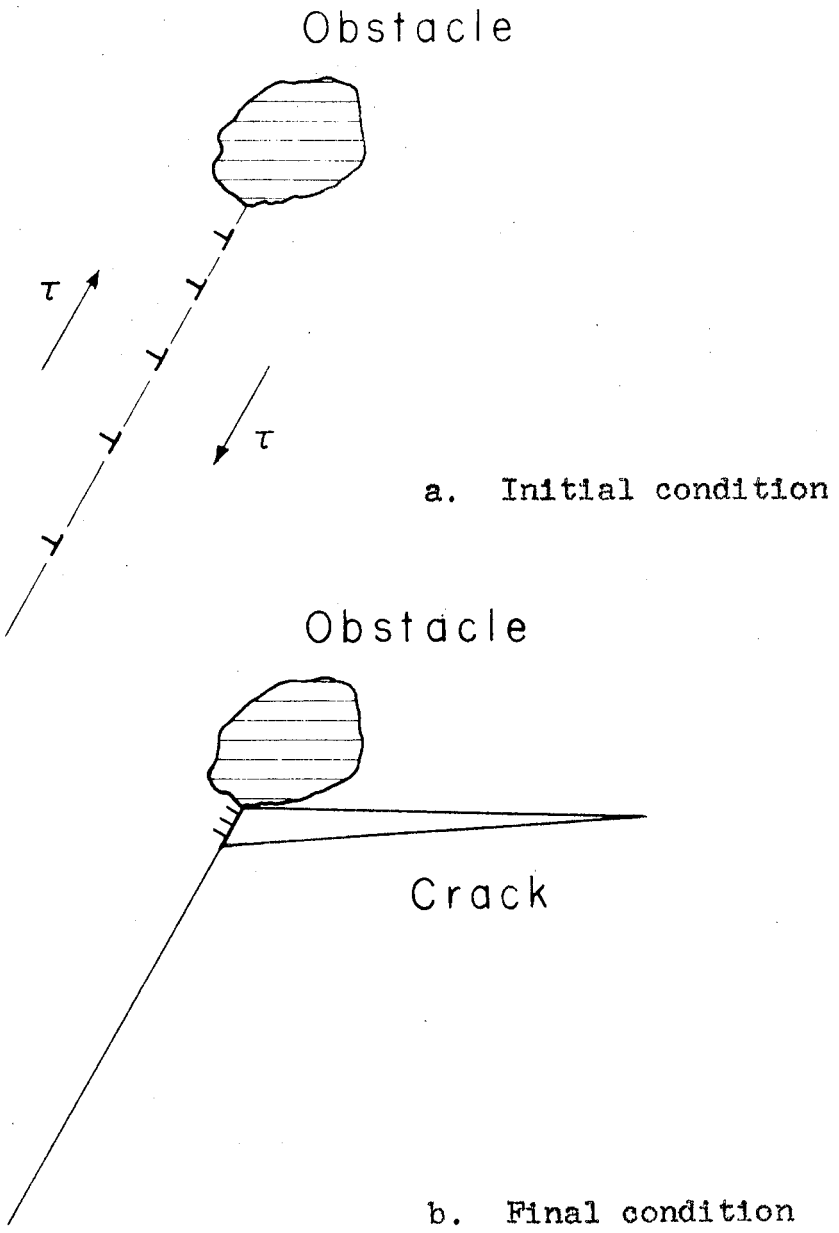

Fig. 35 Fracture Initiation by a Pile-up of Edge Dislocations on a Non-Basal Plane.

obstacles must be spaced far enough apart to permit the formation of long queues of edge dislocations. Such obstacles generally are not present within zinc crystals. Thus, this mechanism cannot be important in initiating cracks within a crystal. Although this mechanism may have been important in this investigation in initiating fracture at the solder bonds, the inhomogeneity of the bonds makes it impossible to analyze these fractures.

Cottrell (12) has proposed a mechanism wherein edge dislocations moving on intersecting slip planes may initiate a crack. The operation of this mechanism is indicated in Fig. 36. The discovery of non-basal slip planes in zinc suggests that symmetrical pile-ups of edge dislocations on intersecting $\{\bar{1}\bar{1}22\}$ planes may be able to initiate a crack along the common basal plane. However, there are three reasons for believing that this is not the usual mechanism of fracture initiation in zinc. First, this mechanism does not account for the fact that the tensile stress required to produce fracture can be lowered if slip along basal planes is impeded. Second, long queues of dislocations on non-basal planes would be needed to explain the low fracture stress required for zinc crystals. The lack of well defined non-basal slip lines on the surface of zinc crystals suggests that long queues of dislocations generally are not formed on non-basal planes. Third, this simple mechanism does not explain why the tensile stress required to produce fracture can have a large dependence upon temperature.

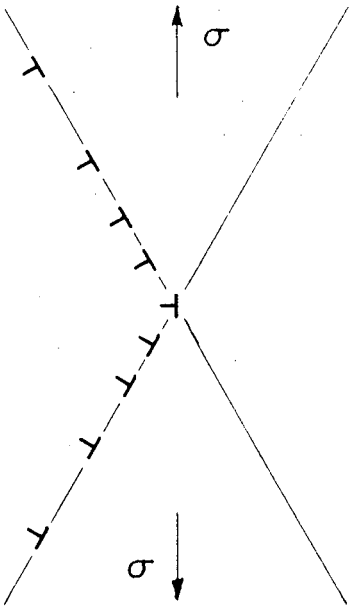

a. Initial condition

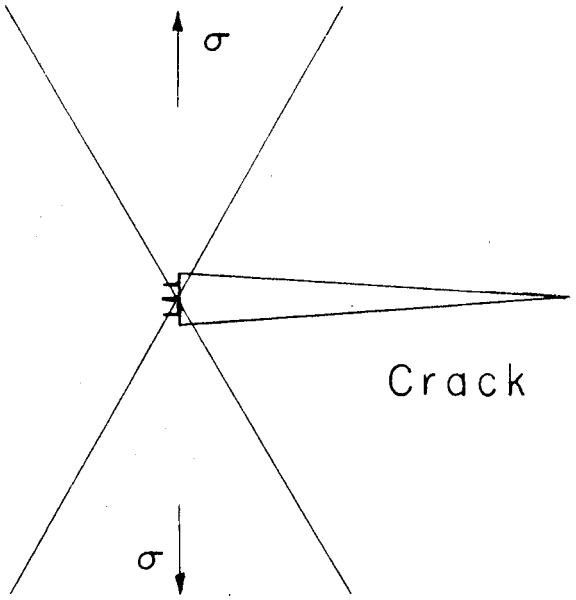

b. Final condition

Fig. 36 Fracture Initiation by Parallel Edge Dislocations Moving on Intersecting Slip Planes.

Fracture might be initiated in zinc by the combination of basal edge dislocations with non-basal edge dislocations in a manner somewhat similar to Cottrell's proposal. The operation of this mechanism is indicated in Fig. 37. The leading dislocation of each queue can combine readily to form an edge dislocation with a Burgers vector, c[0001], that is parallel to the hexagonal axis of the crystal, because this combination would result in a decrease of strain energy. The tensile side of this edge dislocation may be considered as a very small crack. This small crack would be enlarged if the other dislocations in the queues could combine with the initially formed c[0001] dislocation. A large stress would be required to force these dislocations to combine. Such a large shear stress on the basal planes would be accompanied by a similar large shear stress on the $(11\bar{2}0)$ plane, which is the slip plane for the c[0001] dislocation. Thus, the c[0001] dislocation probably would glide out of the way before the stress became large enough to force the other dislocations to combine. However, if the c[0001] dislocation were held in position by some obstacle, then the other dislocations on the basal plane and on the non-basal plane could be forced to combine with the c[0001] dislocation and form a crack large enough to spread by the Griffith mechanism. This model of fracture initiation qualitatively agrees with the fact that the tensile stress required to

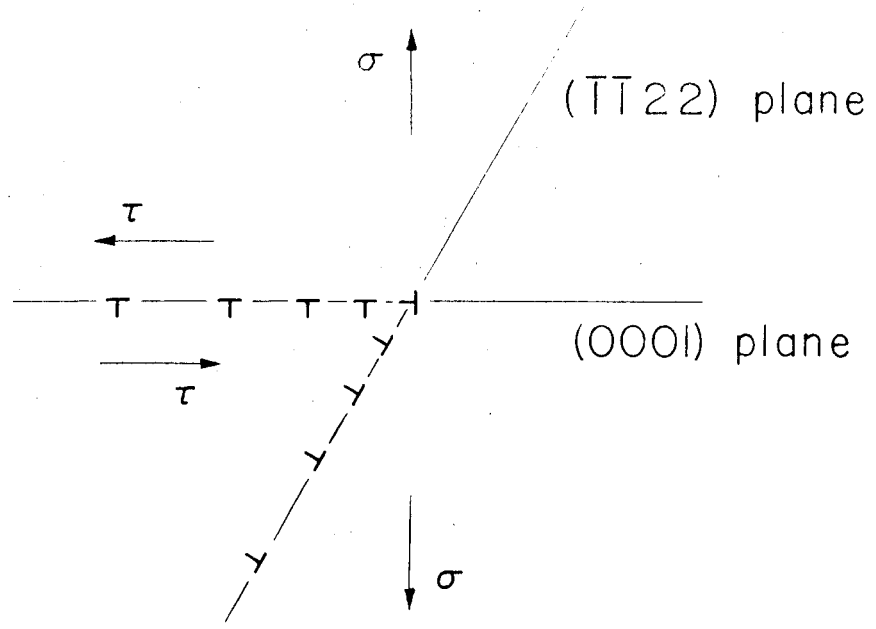

a. Initial condition

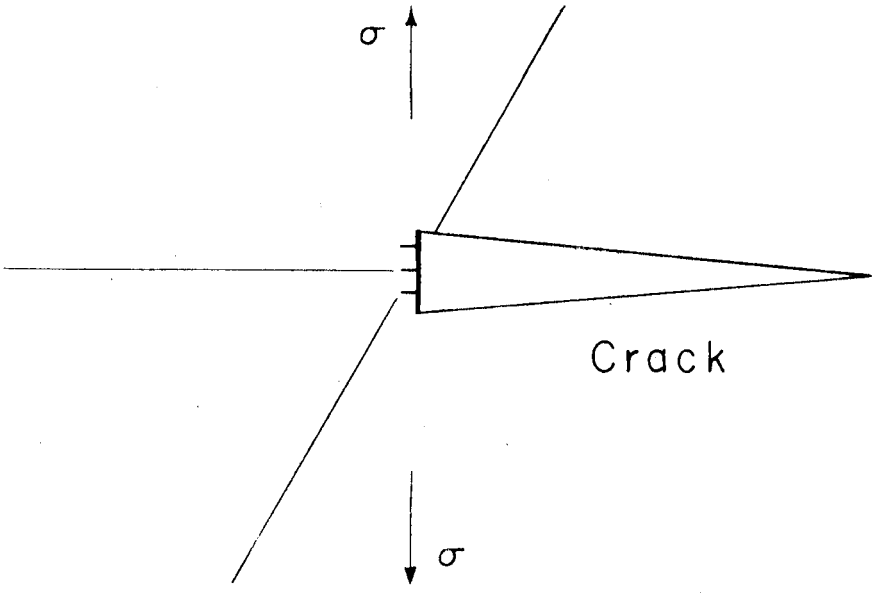

b. Final condition

Fig. 37 Fracture Initiation by Parallel Edge Dislocations Moving on a Basal Plane and a Non-Basal Plane.

produce fracture can be lowered if slip along the basal planes is impeded. However, it does not suggest a reason for the marked temperature dependence of fracture initiation.

The crossing of screw dislocations also might lead to fracture. A tensile stress normal to the basal planes produces slip on intersecting $\{\bar{1}\bar{1}22\}$ planes. The crossing of screw dislocations on these non-basal planes would produce rows of interstitial atoms. Deformation at low temperatures could produce a high density of interstitial atoms within a very small volume, and these atoms could act as a wedge to initiate a crack on a basal plane. Interstitial atoms resulting from deformation at high temperatures might diffuse fast enough to prevent the accumulation of a high density in a small volume and therefore would be less effective in producing fracture. This mechanism qualitatively explains why the stress required for fracture can depend upon temperature, but it does not explain why fracture can be influenced by an impediment to slip on basal planes.

More complex interactions involving non-basal dislocations could be imagined, but the limited amount of quantitative experimental data on fracture of zinc does not justify the consideration of such detailed models at this time. The available information on slip along non-basal planes and the resulting types of dislocation interactions also is very limited and in some cases contradictory. The unusual temperature dependence of the rate of strain hardening for slip

along the non-basal planes suggests that the dislocation interactions may be complex. A better understanding of the interactions associated with non-basal slip will be required before a satisfactory theory of fracture can be established.

VI. SUMMARY AND CONCLUSIONS

Mechanical tests were performed on zinc single crystals to determine the effect of plastic deformation upon the stress state required to produce cleavage fracture along a basal plane. The important results of the tests are:

1) Cleavage fracture produced by a tensile stress normal to the basal planes is preceded by plastic elongation of the crystal in the direction of the hexagonal crystallographic axis. This plastic deformation probably occurs by slip on $\{\bar{1}\bar{1}22\}$ planes in $\langle 11\bar{2}3\rangle$ directions.

2) The rate of strain hardening for slip along non-basal planes is large relative to the rate of strain hardening for slip along basal planes. The non-basal slip system differs from most other slip systems in that the rate of strain hardening increases with increasing temperature in the range from $-77^{\circ}C$ to $25^{\circ}C$.

3) Prior slip along non-basal planes produces a marked increase in the resolved shear stress required for slip on the basal planes.

4) The macroscopic tensile stress normal to the basal planes at the time of fracture is not the same for all test conditions.

5) The tensile stress normal to the basal planes at the time of fracture is not a unique function of

the shear stress on the basal planes, the shear strain on the basal planes, nor any simple combination of these two parameters.

6) A non-uniform distribution of slip on the basal planes can be an important factor in initiating fracture. In particular, slip on basal planes impeded locally by SR-4 strain gages on the surface of the crystal facilitated fracture when both tensile stress normal to the basal planes and shear stress along the basal planes were present.

7) Fracture can occur along a basal plane when neither shear stress nor shear strain exists on this plane. In this case, the tensile stress required to produce fracture is smaller at -77°C than at 25°C.

These test results are not consistent with the dislocation models of fracture initiation that are based solely upon the interaction of dislocations on the basal planes. The true mechanism of basal fracture must generally be more complex than is indicated by these simple models.

Slip on non-basal planes can be an important factor in causing basal cleavage in hexagonal close-packed metals and may be a necessary condition for cleavage. This slip was apparently the only mode of plastic deformation prior to fracture in the zinc specimens tested at -77°C. The importance of slip on non-basal planes in zinc has not previously been recognized.

Dislocation interactions produced by slip on non-basal planes depend upon temperature. Obstacles to slip form more readily at 25°C than at -77°C, while interactions leading to fracture form more readily at -77°C than at 25°C. A better understanding of the processes involved in slip on non-basal planes is required before a complete understanding of fracture initiation in hexagonal metals can be obtained.

APPENDIX A

Procedure for Growing Zinc Crystals

The zinc crystals were grown in pyrex glass molds of the type shown in Fig. 1 (see Appendix F). The internal surface of the lower portion of each mold was coated with a thin layer of graphite to prevent the zinc from adhering to the glass. The proper amount of zinc was placed in the upper reservoir portion of each mold. The air was evacuated from the molds, and the molds were sealed.

The graphite coating required careful preparation. The surface of each mold was cleaned first with a solution of trisodium phosphate in water, then with a solution of potassium dichromate in sulfuric acid, and finally was rinsed with water several times. A collodial suspension of graphite in alcohol was placed into the mold, the mold was shaken vigorously to insure complete coverage of the surface, and the excess fluid was poured out. The remaining thin coating was allowed to dry for several days at room temperature.

The graphite coating could not have significantly changed the purity of the zinc crystals. The mass of this coating is estimated to be only 10^{-4} as large as the mass of the crystal. The manufacturer of the graphite dispersion stated, on the basis of a spectrographic analysis, that the combined concentration of all metallic elements in the graphite was less than one per cent.

An electric furnace was used for growing the crystals. This furnace has two independently controlled electrical heating elements, one above the other. A sealed glass mold was placed in this furnace and the mold was heated uniformly until the zinc melted and ran down into the lower, graphite coated portion of the mold. Next, the power input to each of the heating elements was adjusted to provide a thermal gradient of 90°F/in. outside of the glass mold. Solidification of the zinc occurred when the temperature was lowered by slowly reducing the power input to the heating elements. The average temperature of the zinc sphere changed from 1110°F to 660°F over a period of 20 hours. The crystal and mold then were annealed at 700°F for 4 hours, followed by slow furnace cooling.

The production of a single crystal requires that nucleation take place at only one point within the mold. The long, conical portion of the glass mold at the bottom of the sphere provided a high ratio of surface area to volume near the apex of the cone. Thus, heat could be removed easily from the zinc in this region. One end of a copper rod was in contact with the apex of this cone; the other end of the rod extended to the outside of the furnace. This rod provided an effective heat sink and insured that nucleation occurred only at the apex of the cone. This method of growing crystals was quite satisfactory for this investigation.

Care was taken to avoid plastic deformation of the crystals while they were being removed from the molds. The glass molds were opened without applying external mechanical force. This was accomplished by placing a scratch on the outer surface of the spherical portion of each mold and touching this scratch with a hot glass rod. The rapid heating of the outer surface of the mold wall induced stress in the glass, and a crack was formed at the scratch. This crack was propagated by repeatedly placing the hot glass rod near the advancing end of the crack. The glass mold wall was thick enough to insulate the crystal from the thermal shock of the hot glass rod. Once a circumferential crack had been produced around the spherical portion of the mold, the two halves of the glass mold could be removed without causing any plastic strain in the crystal. A typical crystal is shown in Fig. 2 (see Appendix F).

APPENDIX B

Acid Saw

A special saw was constructed for cutting zinc single crystals. The low (20 to 30 lb/in.^{2}) stress required to produce plastic deformation of these crystals precludes the use of a conventional, toothed saw. The specially constructed saw cuts zinc crystals in a strain free manner by the controlled application of a solution of nitric acid.

A schematic drawing of the acid saw is shown in Fig. 38. A Nichrome wire (0.010 in. diameter) is held tautly on a frame that oscillates linearly along a direction that is precisely parallel to the axis of the wire. Acid is applied to the wire by means of a pair of glass capillary plates, one on each side of the wire. The lower ends of these plates extend down into a reservoir of acid. The distance between the two plates (0.025 in.) is large enough to permit easy movement of the wire but small enough to allow acid to rise between the plates by capillary action to a height sufficient to wet the wire. The acid on the wire is carried to the crystal during one half of each oscillation; a mixture of acid and zinc ions is returned to the plates during the other half. The wire moving through the acid between the plates produces a pumping action that causes a continual transfer of acid between the reservoir and the capillary plates at a much faster rate than would be possible by diffusion alone. The

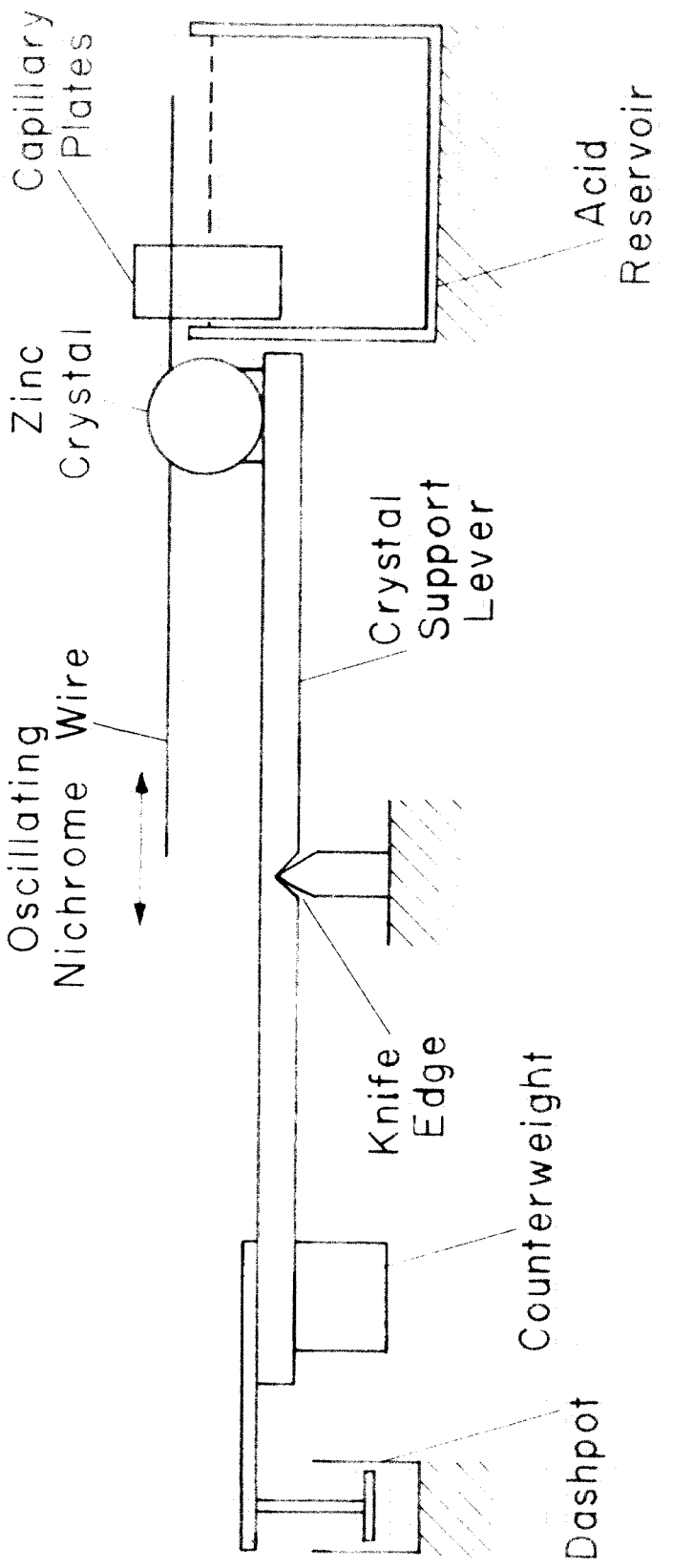

Fig. 38 Schematic Drawing of the Acid Saw.

concentration of zinc ions between the capillary plates therefore never becomes large enough to adversely affect the cutting action of the acid.

The crystal is held against the lower side of the oscillating wire by a counterweighted lever resting on a knife edge. The counterweight is adjusted to provide a force of a few grams between the crystal and the wire. The movement of the lever is damped with an oil filled dash pot to prevent the occurrence of small oscillations that would otherwise be present due to the cyclic action of the wire.

The crystal to be cut must be held firmly. This is accomplished by cementing the crystal to a fixture on the end of the counterweighted lever. The orientation between the plane of the saw cut and any crystallographic plane can be established to within 0.1 degree when this fixture is in the proper position.

The saw produces satisfactory cuts with the following operating conditions:

A Nichrome wire of 0.010 in. diameter

A stroke length of 3 1/2 in.

A stroke rate of 30 cycles/min

A cutting force of 4 gm

A 70 per cent solution of nitric acid in water

A zinc cylinder 1 in. in diameter can be cut in about 12 hours with these conditions. The specified conditions can be changed to increase the cutting rate, but the surfaces produced by the cut will not be flat and parallel.

APPENDIX C

Acid Lathe

A special lathe was constructed for shaping the zinc specimens. This lathe removes zinc in a stress free manner by the controlled application of a solution of nitric acid.

A schematic drawing of this acid lathe is shown in Fig. 39. The zinc crystal is rotated continuously about the intended axis of symmetry of the specimen while it is held against the periphery of a continuously rotating wheel that is covered with a thin film of acid. The shape of the peripheral surface of this wheel determines the final shape of the specimen.

The rotating crystal is supported on the end of a counterweighted lever. The counterweight is adjusted to maintain a force of a few grams between the crystal and the shaping wheel. The removal of material from the crystal would soon alter the relative balance of the lever unless there were a means of compensating for this loss of weight. This compensation is provided by a weight added to the lever directly above the knife edge. A decrease of the radius of the crystal produces a change of the angular position of the lever, and the center of the compensating weight shifts toward the crystal. The size and position of this weight were chosen so that this shift compensates closely for the weight of the material removed from the crystal.

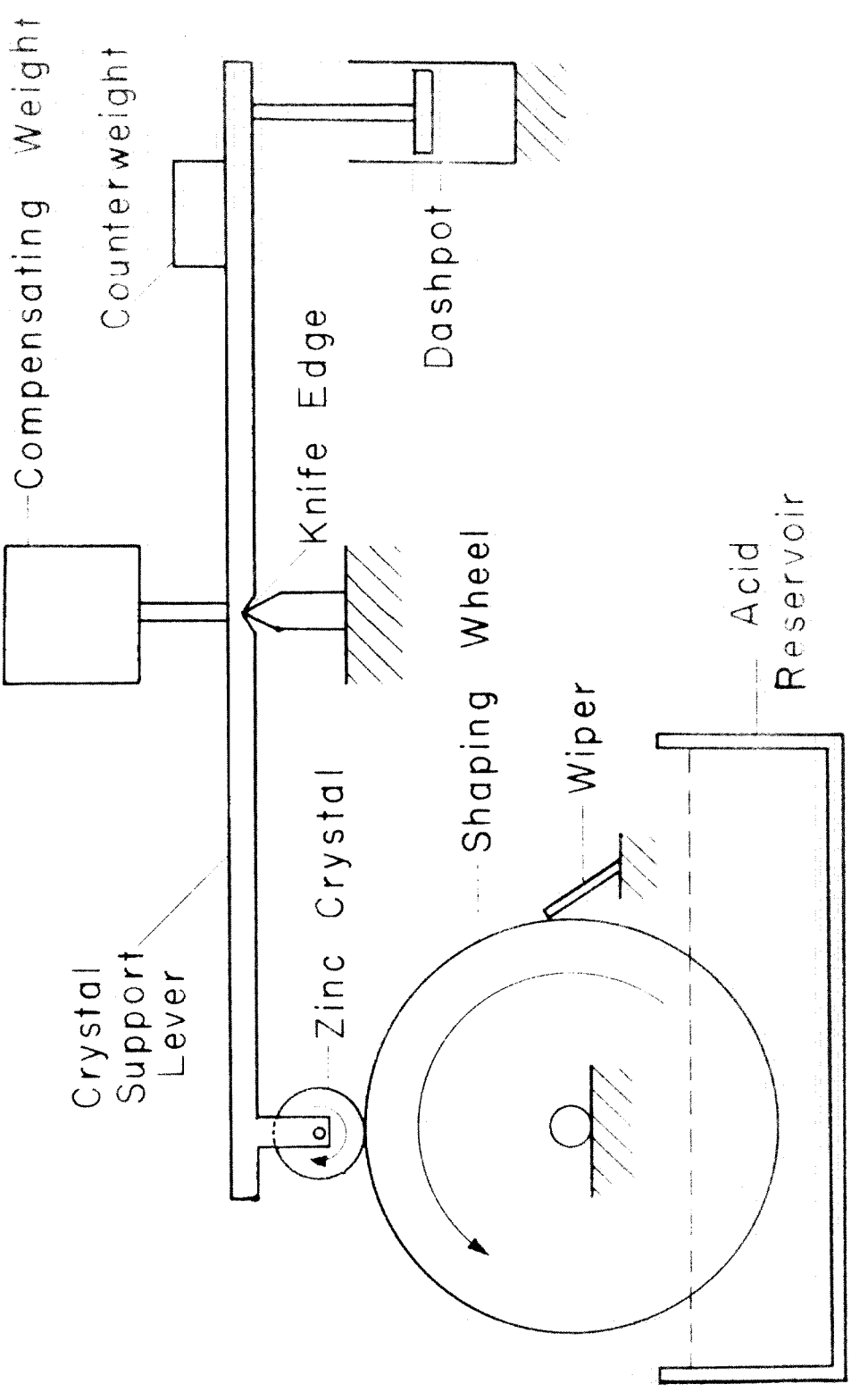

Fig. 39 Schematic Drawing of the Acid Lathe.

The shaping wheel is made of Lucite. This plastic is not attacked chemically by nitric acid, but it does absorb sufficient acid to form a soft, spongy surface that is an excellent base for transporting a thin film of acid to the crystal. The lower portion of the shaping wheel is immersed in nitric acid contained in a large reservoir. The wheel is rotated continuously so that a fresh film of acid always is maintained on its periphery. The thickness of the film is controlled by a movable wiper. A thick film is used for the rapid removal of material; a thin film is better for producing a contour on the specimen that accurately matches the contour of the periphery of the wheel.

The following operating conditions were found to be satisfactory for shaping the zinc specimens of this investigation.

Crystal rotated at 1 rpm

Shaping Wheel rotated at 4 1/2 rpm

Dimensions of Shaping Wheel:

7 in. in diameter

2 in. thick

A contact force of about 3 gm

A 40 per cent solution of nitric acid in water

These conditions can remove 1/4 in. from the radius of a zinc crystal in about 24 hours.

APPENDIX D

Preparation of Zinc Specimens

Several operations were required to produce a specimen from a spherical zinc crystal. First, the crystallographic orientation was determined. Second, the crystal was formed into a properly shaped specimen. Finally, mechanical grips were bonded to each end of the specimen so that force could be applied.

The approximate orientation of the crystallographic directions was determined by chemically etching the surface of the sphere with a 30 per cent solution of hydrochloric acid in water. This etch produced a narrow, lustrous line along the center of each of the six prismatic faces.

The precise orientation of the basal planes was established by cleaving a small portion of zinc from each end of the hexagonal axis and thereby exposing two basal planes. This operation was carried out at a temperature of $-320^{\circ}F$ in order to minimize plastic deformation of the crystal. The maximum rate of temperature change was limited to $5^{\circ}F/min$ to prevent transient thermal stress.

The exposed basal planes served two functions. First, they provided an accurate crystallographic reference surface. Second, they provided a means for estimating the number and magnitudes of the basal tilt boundaries within the crystal. The magnitudes of the boundaries were meas-

ured by reflecting a focused light beam off the planes. Tilt boundaries as small as 0.02 degree could be detected by this method.

Each test specimen was produced from a spherical crystal by using the special acid machining equipment. The acid lathe was used to form the crystal into a specimen of the proper shape and orientation. The acid saw was used to remove approximately 1/16 in. of zinc from each end of the specimen, thus eliminating any metal that might have been deformed plastically by the cleaving operation. The exposed basal planes were used as references during the shaping and sawing operations to insure that the cylindrical axis of the completed specimen would be parallel to the hexagonal axis of the crystal. After the completion of all the shaping operations, each crystal was annealed at 700°F for 3 hours.

Mechanical grips were bonded to both ends of each specimen so that force could be applied during the tests. Each of these grips was composed of two sections: a copper-zinc alloy single crystal and a threaded steel cylinder. A complete specimen assembly is represented in Fig. 3 (page 14).

The procedure for bonding the pieces of the specimen assembly required several operations. The individual pieces of the assembly first were heated, and the surfaces to be bonded were "tinned" with tin-lead (60-40) solder. After cooling, the pieces were placed in their proper sequence on a large V-block. A liberal amount of paste flux was

placed between each piece. The concentricity of all parts was maintained by supporting the crystals on shims of the proper size. A thin (0.004 in.) piece of teflon was placed between each shim and the surface of the crystal as a precaution against damaging the surface.

The solder bonds were formed by heating the specimen assembly in an atmosphere of dry nitrogen. When the solder melted, a vacuum was produced around the specimen assembly and maintained until most of the flux had vaporized. The assembly then was allowed to cool slowly to room temperature. Nitric acid was used to remove approximately 0.010 in. from the surface of the specimen, leaving a clean, pure zinc surface. The specimen assembly then was ready for testing.

This method of bonding the components did not produce ideal bonds, because some flux always remained entrapped within the bonds. However, bonds produced by this method were stronger than those produced with less flux or those produced with other bonding agents. The other bonding agents tried were epoxy resins, cadmium base solder, and Wood's metal.

APPENDIX E

Suggested Research Programs

The present investigation shows that the mechanical behavior of zinc can be quite complex. The non-basal slip system was found to have unusual properties not predicted by current theories. Furthermore, there are not any adequate theories for describing the fracture behavior of zinc.

The results of this investigation suggest areas where further work on zinc might be particularly fruitful. The following proposed programs would not only provide a better understanding of the mechanical properties of zinc but might also be useful in broadening the experimental basis of the general theoretical interpretations of strain hardening and fracture.

Program I - A Study of the Temperature Dependence of Slip on Non-Basal Planes.

The testing methods developed for the present investigation are well suited for the study of non-basal slip in zinc. The results show that both the plastic and the fracture behaviors of zinc vary with temperature. A series of tensile tests performed at different temperatures would provide a more complete determination of the temperature dependence of the critical stress for plastic flow, the

rate of strain hardening, and the fracture strength. A similar series of compressive tests could provide information on the relationship of non-basal slip and twinning. This proposed program could be expanded by making tests at several strain rates and also by testing crystals of more than one purity.

The plastic deformation produced during these tests could be studied in several ways. Wire resistance strain gages could be used to measure the strain produced in the specimens; but capacitance type gages might prove to be better, because they would introduce smaller surface restraints. A highly polished surface on the specimens would help reveal any non-basal slip lines that might form at low temperatures. The etch pit techniques being developed at The California Institute of Technology under the direction of Dr. Vreeland would be particularly useful in correlating dislocation density with the plastic, fracture, and twinning behaviors of zinc.

Program II - A Study of the Interaction Between Basal and Non-Basal Slip Systems

The present investigation shows that strong interactions occur between the basal and the non-basal slip systems. Further studies of this type may provide detailed information on the mechanism of the interaction. Such a testing program would be particularly meaningful if it were

conducted after the completion of the first proposed program. Then the basal slip behavior could possibly be correlated with the density and distribution of the non-basal dislocations. This relationship would make it possible to test the hypothesis that a forest of dislocations intersecting a slip plane provides a strong obstacle to the motion of dislocations along that plane.

Wire resistance strain gages would not be suitable for these tests, so other means of measuring strain must be found. The other testing techniques used in the present investigation, however, would be satisfactory for a study of the interaction of the two slip systems.

APPENDIX F

Photographs

Fig. 1 Pyrex Glass Mold for Growing Zinc Crystals.

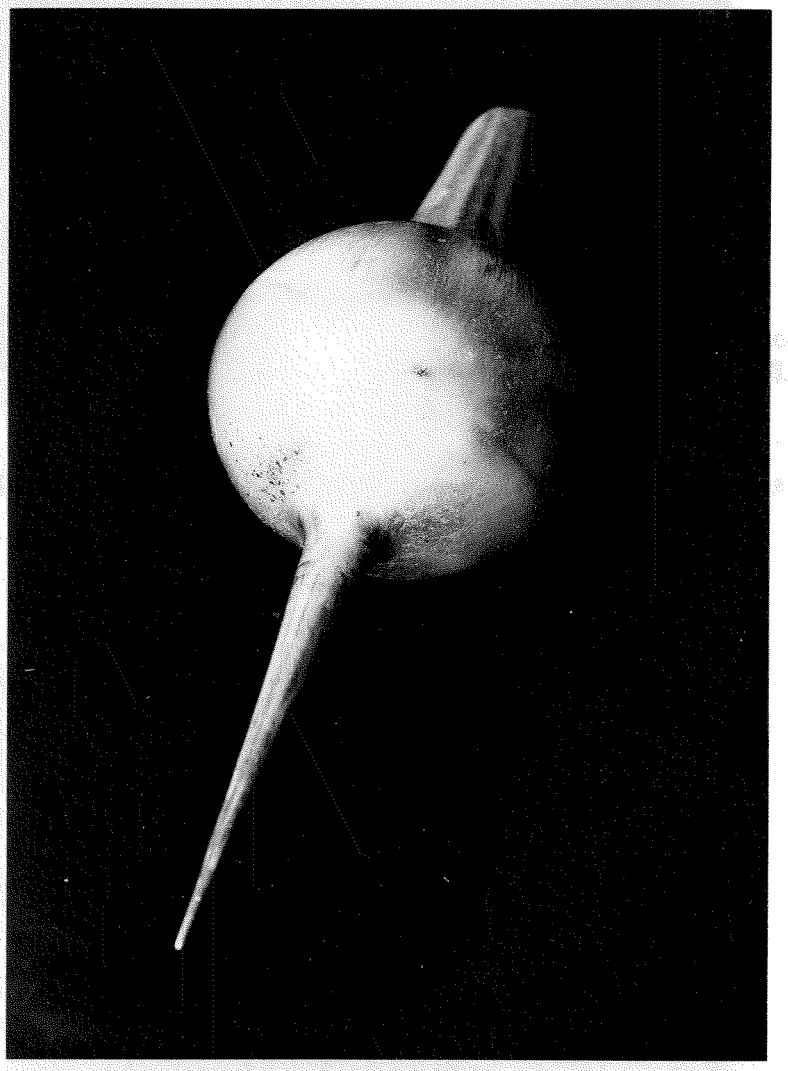

Fig. 2 Zinc Crystal.

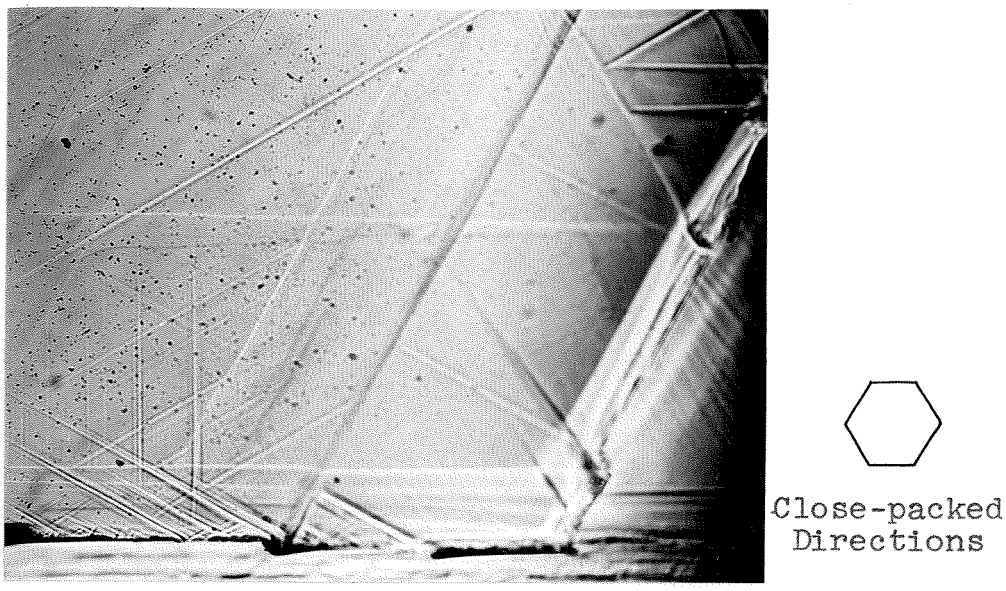

Fig. 17 Slip Lines and a Cleavage Step on a Basal Surface of Zinc. 150 X

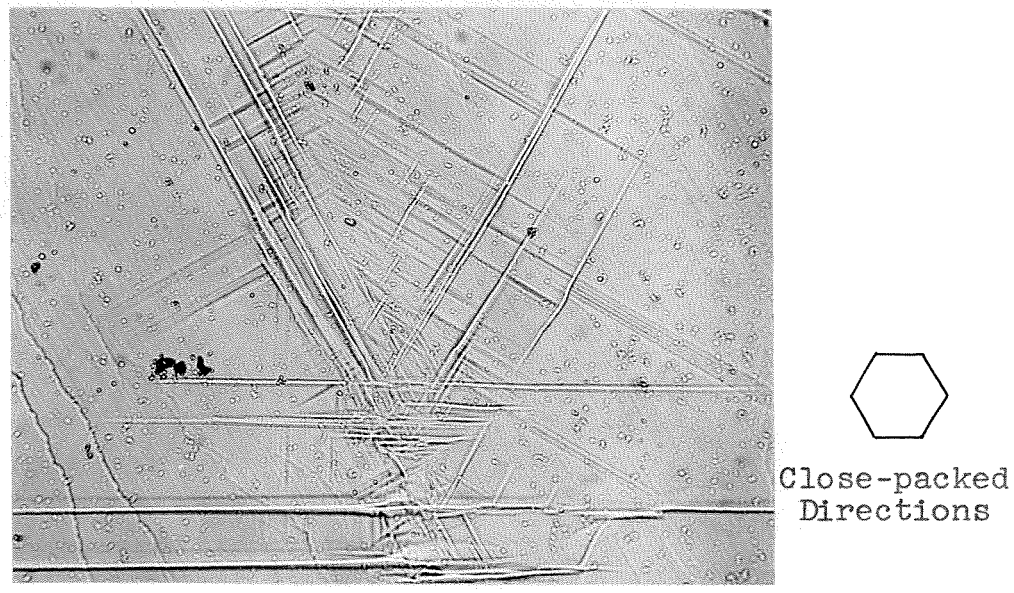

Fig. 18 Slip Lines and Twins on a Basal Surface of Zinc. 250 X

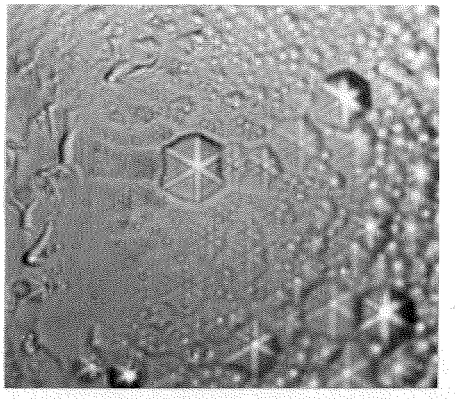

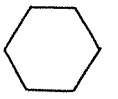

Close-packed
Directions

Fig. 19 Etch Pits on a Basal Surface of Zinc. 1000X

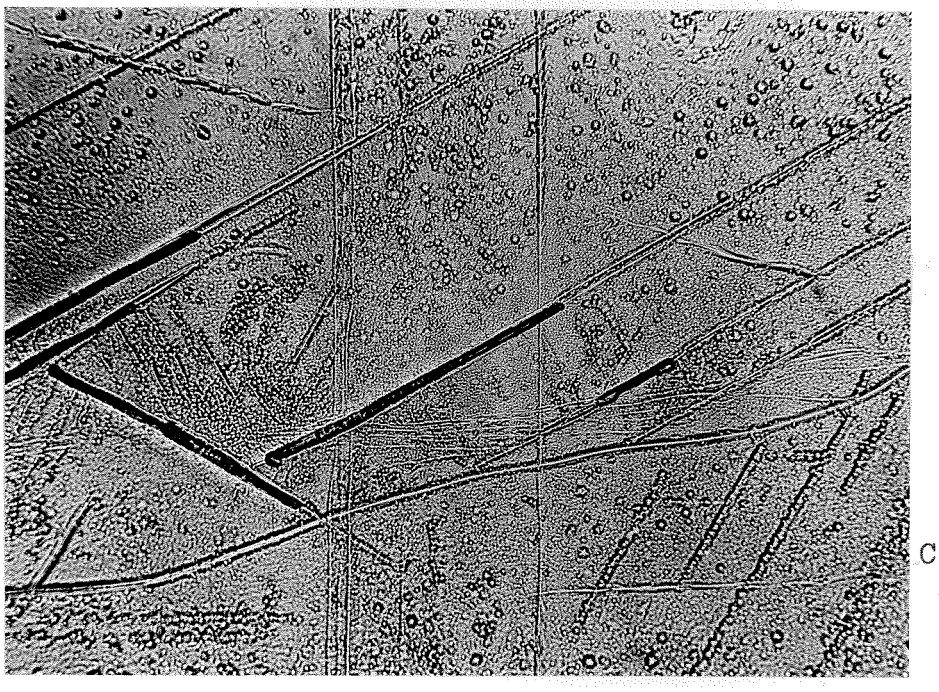

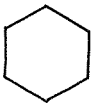

Close-packed
Directions

Fig. 20 Twins and Linear Arrays of Etch Pits on a Basal Surface of Zinc. 200 X

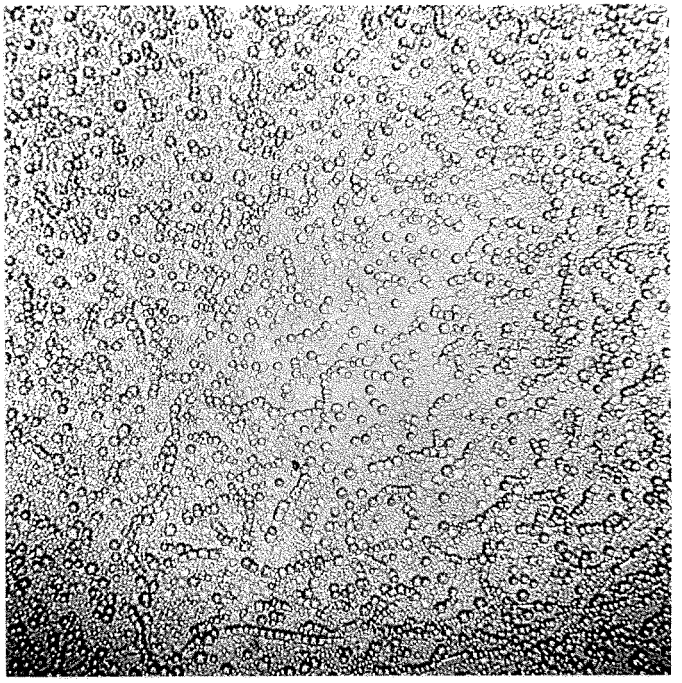

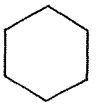

Close-packed
Directions

Fig. 21 Random Distribution of Etch Pits on a Basal Surface. 200 X

Fig. 29 Coarse Slip Bands Parallel to the Basal Planes of Zinc. 2.25 X

Fig. 31 Basal Fracture Surface Near a Solder Bond. 2X

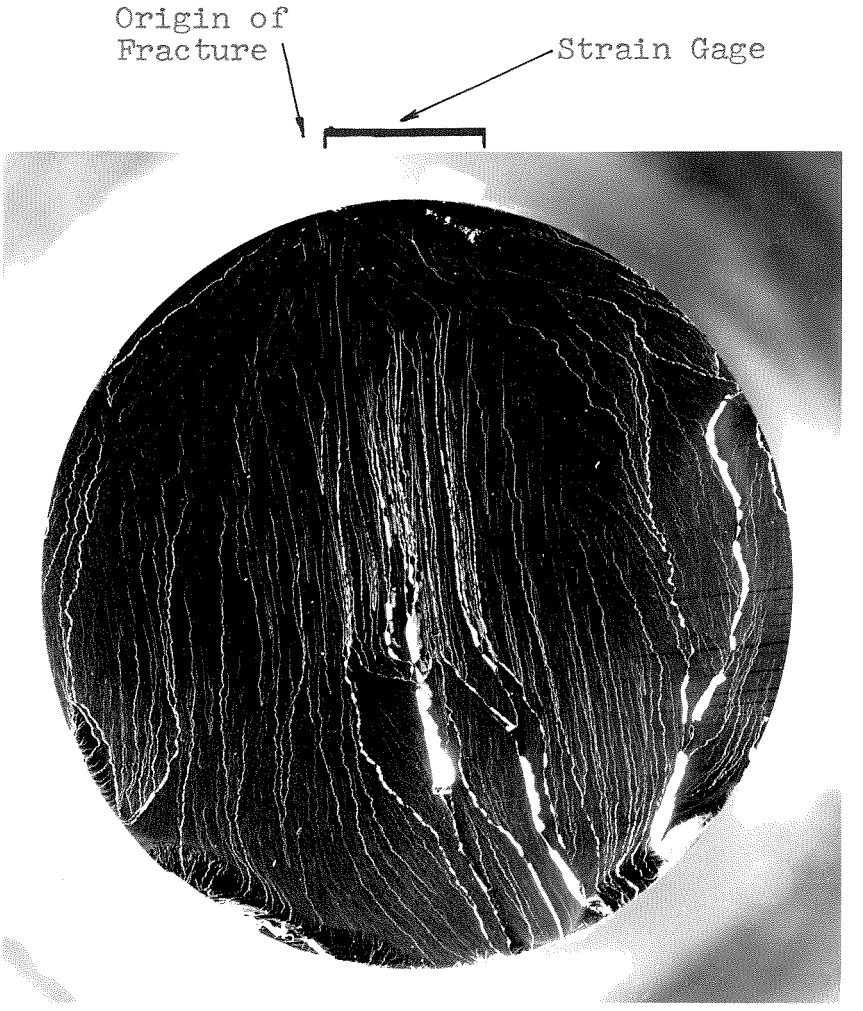

Fig. 32 Basal Fracture Surface Near a SR-4 Strain Gage. 7X

REFERENCES

1. F. Seitz and T. A. Read, "Theory of the Plastic Properties of Solids," Journal of Applied Physics (1941), Vol. 12, p. 472-486.

2. F. Zwicky, "Die Reissfestigkeit von Steinsalz," Physikalische Zeitschrift (1923), Vol. 24, p. 131-137.

3. M. Born and R. Furth, "The Stability of Crystal Lattices. III," Proceedings of the Cambridge Philosophical Society (1940), Vol. 36, p. 454-465.

4. J. Frenkel, "Zur Theorie der Elastizitatsgrenze und der Festigkeit Kristallinischer Korper," Zeitschrift fur Physik (1926), Vol. 37, p. 572-609.

5. P. B. Hirsch, "Direct Experimental Evidence of Dislocations," Metallurgical Reviews (1959), Vol. 4, No. 14, p. 101-140.

6. A. A. Griffith, "The Phenomena of Rupture and Flow in Solids," Philosophical Transactions of the Royal Society of London (1921), Series A, Vol. 221, p. 163-198.

7. G. T. Hahn, W. S. Owen, B. L. Averback and M. Cohen, Micromechanism of Brittle Fracture in Low-Carbon Steel," Welding Journal (1959), Vol. 38, p. 3675-3765.

8. N. J. Petch, "The Fracture of Metals," Progress in Metal Physics (1954), Vol. 5, p. 1-52.

9. C. Zener, "The Micro-mechanism of Fracture," Fracturing of Metals (1948), published by the American Society for Metals, Cleveland, Ohio, p. 3-31.

10. A. N. Stroh, "A Theory of the Fracture of Metals," Advances in Physics (1957), Vol. 6, p. 418-432.

11. A. N. Stroh, "The Cleavage of Metal Single Crystals," Philosophical Magazine (1958), Vol. 3, Eighth Series, p. 597-608.

12. A. H. Cottrell, "Theory of Brittle Fracture in Steel and Similar Metals," Transactions of the American Institute of Mining, Metallurgical and Petroleum Engineers (1958), Vol. 212, p. 192-203.

13. A. Deruyttere and G. B. Greenough, "The Criterion for the Cleavage Fracture of Zinc Single Crystals," Journal of the Institute of Metals (1956), Vol. 84, p. 337-345.

14. J. J. Gilman, "Fracture of Zinc Monocrystals and Bicrystals," Transactions of the American Institute of Mining, Metallurgical and Petroleum Engineers (1958), Vol. 212, p. 783-791.

15. J. J. Gilman, "Plastic Anistrophy of Zinc Monocrystals," Transactions of the American Institute of Mining, Metallurgical and Petroleum Engineers (1956), Vol. 206, p. 1326-1336.

16. E. Schmid and W. Boas, Plasticity of Crystals, with Special Reference to Metals (1950), F. A. Highes and Co. Ltd., London, p. 169, p. 241, p. 265.

17. Ibid., p. 152.

18. H. P. Stuwe, "Creep in Zinc Single Crystals at the Temperature of Liquid Nitrogen," Journal of Applied Physics (1959), Vol. 30, p. 450-451.

19. R. W. K. Honeycombe, "The Growth of Metal Single Crystals," Metallurgical Reviews (1959), Vol. 4, No. 13, p. 12.

20. R. Hill, The Mathematical Theory of Plasticity (1956), Oxford University Press, London, p. 94.

21. T. Vreeland, Jr. and R. Brandt, private communication.

22. E. H. Edwards, J. Washburn, and E. Parker, "Some Observations on the Work Hardening of Metals," Transactions of the American Institute of Mining, Metallurgical and Petroleum Engineers (1953), Vol. 197, p. 1525-1529.

23. K. Lucke, G. Masing and K. Schroeder, "Dehnversuche an Zink-Einkristallen," Zeitschrift fur Metallkunde, (1955), Vol. 46, p. 792-800.

24. R. L. Bell and R. W. Cahn, "The Dynamics of Twinning and the Interrelation of Slip and Twinning in Zinc Crystals," Proceedings of the Royal Society of London (1957), Vol. 239A, p. 494-521.

25. J. J. Gilman, "A Study of a New Mode of Deformation in Zinc Monocrystals," Transactions of the American Institute of Mining, Metallurgical and Petroleum Engineers (1955), Vol. 203, p. 206-214.

26. P. B. Price, "Pyramidal Glide and the Formation and Climb of Dislocation Loops in Nearly Perfect Zinc Crystals," The Philosophical Magazine (1960), Vol. 5, Eighth Series, p. 873-886.

27. J. J. Gilman, "Etch Pits and Dislocations in Zinc Monocrystals," Transactions of the American Institute of Mining, Metallurgical and Petroleum Engineers (1956), Vol. 206, p. 998-1004.

28. N. F. Mott, "A Theory of Work-hardening of Metal Crystals," The Philosophical Magazine (1952), Vol. 43, Seventh Series, p. 1151-1178.

29. A. H. Cottrell, Dislocations and Plastic Flow in Crystals, Oxford at the Clarendon Press (1953), p. 174.

30. A. Seeger, "The Mechanism of Glide and Work Hardening in Face-Centered Cubic and Hexagonal Close-Packed Metals," Dislocations and Mechanical Properties of Crystals (Editors: Fisher, Johnston, Thomson, and Vreeland) (1957), J. Wiley and Sons, Inc., New York, p. 271-277.

31. E. Orowan, Dislocations in Metals (Edited by M. Cohen) (1954), published by Amer. Inst. Min. and Metal. Engr., New York, p. 191.

32. J. Friedel, Les Dislocations (1956), Gauthier-Villars, Paris, p. 223-226.